

Investigation of Reactive Power Control and Compensation for HVDC Systems

By

Yi Zhang

A Thesis submitted to the Faculty of Graduate Studies of
The University of Manitoba
in partial fulfillment of the requirements for the degree of

Doctor of Philosophy

Department of Electrical and Computer Engineering
The University of Manitoba
Winnipeg, Manitoba, Canada

Copyright © by Yi Zhang 2011

Abstract

This thesis attempts to investigate the performance of various reactive power compensation devices, examine the mechanism of reactive power compensation for HVDC systems, and develop guidelines for the design of reactive power compensation schemes for HVDC systems. The capabilities of various reactive power compensators to enhance power system stability are compared in both steady and transient states. An understanding of the capabilities of these compensators provides a basis for further investigation of their performance in HVDC systems. The reactive power requirements of HVDC converters are studied. The voltage dependencies of the HVDC converters at different control modes are derived, which allow for predictions of how HVDC converters impact AC system voltage stability. The transient performance of reactive power compensation options for HVDC Systems is studied by comparing their behavior during DC fault recovery, Temporary Overvoltage (TOV), and commutation failure. How to quantify the system strength when reactive compensators are connected to the converter bus is investigated. A new series of indices are developed based on the Apparent Short Circuit Ratio Increase (ASCRI). The inertia of a synchronous condenser and its impact on the frequency stability of an AC/DC system are discussed. By modelling the inverter side AC system in greater detail, the frequency stability and rotor angle stability following fault transients is examined based on time domain simulation. Finally, a guideline for designing dynamic reactive power compensation for HVDC systems is proposed.

Acknowledgments

I gratefully acknowledge my advisor Prof. A. M. Gole for his excellent guidance. It has been a great opportunity for me to be a beneficiary of Prof. Gole's expertise in HVDC and power electronics.

I also gratefully acknowledge the advisory committee members Prof. U. D. Annakkage and Prof. R. Sri Ranjan for the suggestions they have given me, the discussions they have had with me, and the reviews of my research work they have carried out.

Special thanks to Amy Dario, Tracy Hofer and Erwin Dirks of the department of ECE for the great help they have given me during my studies.

Table of Contents

Chapter 1: Introduction	1
1.1 Background	1
1.2 Literature Survey	4
1.3 Scope of the Thesis	9
Chapter 2: Capability Comparison of Dynamic Reactive Power Compensation Devices	11
2.1 Introduction of Reactive Power Compensation Devices.....	11
2.2 Modelling of Reactive Power Compensation Devices.....	12
2.2.1 Modelling of Synchronous Condensers (SCs).....	12
2.2.2 Modelling of Static Var Compensators (SVCs).....	16
2.2.3 Modelling of Static Synchronous Compensators (STATCOMs)	17
2.3 Comparison of the Capability to Enhance Steady-State Voltage Stability	19
2.4 Comparison of the Capability to Enhance Steady-State Rotor Angle Stability.	26
2.5 Comparison of Dynamic Performances	32
2.5.1 Three-Phase Fault	34
2.5.2 Single-Phase Fault	35
2.5.3 Load Changing.....	36
2.5.4 Line Trip	37
2.5.5 Permanent Loss of Power	38
2.5.6 Short-Term Loss of Power.....	39
2.5.7 Short-Circuit Current Provided by Different Compensators	40
2.5.8 Summary of the Simulation Study	41
2.6 Chapter Conclusions	42
Chapter 3: Steady-State Analysis of Reactive Power Compensation of HVDC Systems	44
3.1 Introduction	44
3.2 Some Indices for AC/DC System Performance Studies	45
3.2.1 Short Circuit Ratio (SCR) and Effective Short Circuit Ratio (ESCR)	45
3.2.2 Maximum Power Curve (MPC) and Maximum Available Power (MAP) .	46
3.3 Nonlinear Load Characteristics of HVDC Converters.....	48
3.3.1 Control Mode 1: Constant P and Constant γ Control.....	49
3.3.2 Control Mode 2: Constant I and Constant γ Control	53
3.3.3 Control Mode 3: Constant α and Constant I Control	55
3.3.4 Considering the Capacitor and Filter at the Converter Bus	58

3.3.5	Summary of Non-linear Load Characteristics of HVDC Converters	63
3.4	Computation of MPC and MAP	63
3.4.1	Equations of the HVDC System with Reactive Power Compensation.....	64
3.4.2	Modelling of Reactive Power Compensators in the MPC Computation	65
3.4.3	Numerical Results of MPC with Reactive Power Compensators.....	67
3.4.4	Validation of the Analytical Algorithm	71
3.5	Chapter Conclusions	73
Chapter 4: Comparison of the Transient Performance of Reactive Power Compensation Options for HVDC Systems.....		75
4.1	Introduction	75
4.2	Study System and Reactive Compensators	76
4.3	Comparison of SCs and STATCOMs in Fault Recovery	80
4.3.1	Inverter Close-In Single Phase Fault	81
4.3.2	Inverter Close-In Three-Phase Fault.....	82
4.3.3	Inverter Remote Single-Phase Fault	83
4.3.4	Inverter Remote Three-Phase Fault	84
4.3.5	Rectifier Single-Phase Fault	85
4.3.6	Rectifier Three-Phase Fault	86
4.3.7	DC Temporary Fault.....	87
4.3.8	Summary of the Fault Recovery Studies	87
4.4	Comparison of SCs and STATCOMs in Suppressing Temporary Overvoltage (TOV).....	88
4.4.1	Rectifier Single-Phase Fault	89
4.4.2	Rectifier Three-Phase Fault	89
4.4.3	DC Temporary Fault.....	90
4.4.4	DC Permanent Block	91
4.4.5	Summary of the TOV Studies.....	91
4.5	Comparison of SCs and STATCOMs in Resisting Commutation Failure.....	92
4.5.1	Commutation Failure Immunity Index (CFII).....	93
4.5.2	Comparison of the Impact of the SC and the STATCOM on the CFII	94
4.5.3	Summary of Commutation Immunity Studies	96
4.6	Chapter Conclusions	97
Chapter 5: The Concept of System Strength when Dynamic Reactive Power Compensators are Connected to the Converter Bus		98
5.1	Introduction	98
5.2	Apparent Short Circuit Ratio Increase	100

5.3	Apparent Short Circuit Ratio Increase Based on MAP	101
5.4	Apparent Short Circuit Ratio Increase Based on the CFII	105
5.5	Apparent Short Circuit Ratio Increase based on Fault Recovery Time	108
5.6	Apparent Short Circuit Ratio Increase based on TOV	111
5.7	The Average ASCRI and Minimum ASCRI	114
5.8	Chapter Conclusions	116
Chapter 6: Consideration of Inertia for Design of Reactive Power Compensation Schemes		118
6.1	Introduction	118
6.2	Effects of Reactive Compensator Inertia on Frequency Stability	120
6.2.1	Inertia of Power Systems	120
6.2.2	Frequency Deviation in Multi-Machine AC/DC Systems	122
6.2.3	Inertia Requirement of AC/DC Power Systems	124
6.2.4	Effects of Synchronous Condensers on System Inertia	130
6.2.5	Selecting a Reactive Power Compensator Considering the Inertia	132
6.3	Simulation Studies.....	134
6.3.1	Simulation Case	134
6.3.2	Simulation Study Results	138
6.3.3	Discussion of the Simulation Results	149
6.4	Guideline on Considering Inertia in Designing Reactive Power Compensation	158
6.5	Chapter Conclusions	159
Chapter 7: Conclusions and Future Work.....		161
7.1	The Main Contributions of This Thesis	161
7.2	Conclusions	163
7.2.1	Comparison of Dynamic Reactive Power Compensators in Simple AC Systems	163
7.2.2	Steady State Analysis of Reactive Power Compensations for HVDC systems	164
7.2.3	Transient State Analysis of Reactive Power Compensations for HVDC systems	164
7.2.4	The Concept of System Strength when Dynamic Reactive Power Compensators are connected to Converter Bus	165
7.2.5	Consideration of Inertia for Design of Reactive Power Compensations ..	166
7.3	Future Work	167
REFERENCES		171

List of Figures

Figure 2.1: Synchronous Condenser Circuit and VI Characteristic.....	13
Figure 2. 2 Operation VI Characteristics of an SC	15
Figure 2. 3: Equivalent Circuit of an SC Connected to a System.....	16
Figure 2. 4: SVC Circuit and VI Characteristic	17
Figure 2. 5: STATCOM Circuit and VI Characteristic.....	18
Figure 2. 6: Reactive Power Compensation at the Load Side.....	19
Figure 2. 7: PV Curves When Reactive Power Compensation Increases.....	24
Figure 2. 8: The Relationship between the P_{max} and Compensator Size	25
Figure 2. 9: A Two-Machine System with Mid-Point Compensation	26
Figure 2. 10: Equivalent Circuit of SVC at Mid-point	28
Figure 2. 11: Equivalent Circuit of a STATCOM/an SC at the Mid-Point	28
Figure 2. 12: Phasor Diagram of a STATCOM/SC at Mid-Point.....	29
Figure 2. 13: Power-Angle Curve with Mid-Point Compensations.....	31
Figure 2. 14: Comparison of Power-Angle Curves with Different Compensators.....	32
Figure 2. 15: The Studied Simple Power System	33
Figure 2. 16: Three-Phase Fault.....	35
Figure 2. 17: Single-Phase Fault.....	36
Figure 2. 18: Load Increase	37
Figure 2. 19: Line Trip.....	37
Figure 2. 20: Voltage Decline When Power is Lost	39
Figure 2. 21: Transients of the Motor during Short-Term Tripping.....	40
Figure 2. 22: Fault Current Injections of Different Compensators.....	41
Figure 3. 1: The Converter Connected to an AC Bus.....	45
Figure 3. 2: Maximum Power Curve of HVDC Systems	47
Figure 3. 3: Voltage Dependence of the DC Current of Control Mode 1.....	50
Figure 3. 4: Voltage Dependence of Inverter Q of Control Mode 1.....	51
Figure 3. 5: Voltage Dependence of Rectifier Q of Control Mode 1	52
Figure 3. 6: Voltage Dependence of Inverter P of Control Mode 2	53
Figure 3. 7: Voltage Dependence of Inverter Q of Control Mode 2.....	54

Figure 3. 8: Voltage Dependence of Rectifier Q of Control Mode 2	55
Figure 3. 9: Voltage Dependence of Rectifier P of Control Mode 3	56
Figure 3. 10: Voltage Dependence of Rectifier Q of Control Mode 3	57
Figure 3. 11: Voltage Dependence of Rectifier Q of Control Mode 3	58
Figure 3. 12: Reactive Power Voltage Dependence of Control Mode 1	60
Figure 3. 13: Reactive Power Voltage Dependence of Control Mode 2	61
Figure 3. 14 Reactive Power Voltage Dependence of Control Mode 3.....	62
Figure 3. 15: MPC Computations without Reactive Compensation.....	68
Figure 3. 16: MPC Computations With ideal Reactive Compensation	69
Figure 3. 17: MPC Computations with Non-ideal Reactive Compensation.....	70
Figure 3. 18: MPC Computations by EMT Simulation	72
Figure 4. 1: CIGRE Benchmark Model for HVDC Control.....	77
Figure 4. 2: Special Modification on the VDCOL Control Loop.....	78
Figure 4. 3: The Excitation and AVR System of the SC	79
Figure 4. 4: Circuit of a STATCOM.....	79
Figure 4. 5: DQ Decoupled Control Diagram of a STATCOM	80
Figure 4. 6: DC Power during an Inverter Close-In Single-Phase Fault	82
Figure 4. 7: Inverter Bus Voltage during an Inverter Close-In Single-Phase Fault.....	82
Figure 4. 8: DC Power during an Inverter Close-in Three-Phase Fault.....	83
Figure 4. 9: Inverter Bus Voltage during an Inverter Close-in Three-Phase Fault.....	83
Figure 4. 10: DC Power during an Inverter Remote Single-Phase Fault.....	84
Figure 4. 11: Inverter Bus Voltage during an Inverter Remote Single-Phase Fault.....	84
Figure 4. 12: DC Power during an Inverter Remote Single-Phase Fault.....	85
Figure 4. 13: Inverter Bus Voltage during an Inverter Remote Single-Phase Fault.....	85
Figure 4. 14: DC Power during an Inverter Close-In Single-Phase Fault	86
Figure 4. 15: DC Power During an Inverter Close-In Single-Phase Fault.....	86
Figure 4. 16: DC Power during an Inverter Close-in Single-Phase Fault.....	87
Figure 4. 17: DC Power Recovery Time for Various Disturbances	88
Figure 4. 18: Inverter Bus Voltage during a Rectifier Single-Phase Fault	89
Figure 4. 19: Inverter Bus Voltage during a Rectifier Three-Phase Fault	90

Figure 4. 20: Inverter Bus Voltage during a DC Temporary Fault.....	90
Figure 4. 21 DC Permanent Block.....	91
Figure 4. 22: TOVs for Various Disturbances.....	92
Figure 4. 23: Illustration of CFII Computation.....	93
Figure 5. 1: MPC with different Compensator Capacity	102
Figure 5. 2: MPC with different SCR.....	102
Figure 5. 3: Correlations between Compensation Capacity and Equivalent SCR Increase	104
Figure 5. 4: Comparison of the ASCRI-M of different Reactive Power Compensators	105
Figure 5. 5: Relationships between the CFII and the SCR for a System without Compensation	105
Figure 5. 6: Relationships between CFII and STATCOM Capacity	106
Figure 5. 7: Comparison of the ASCRI-C of different Reactive Power Compensators .	107
Figure 5. 8: Recovery Time from a Three-Phase Fault	108
Figure 5. 9: Recovery Time and SCR for a System without Compensation	109
Figure 5. 10: Recovery Time and Reactive Power Compensator Capacity.....	110
Figure 5. 11: ASCRI based on Fault Recovery Time	111
Figure 5. 12: TOV and SCR for a System without Compensation.....	112
Figure 5. 13: TOV and Reactive Power Compensator Capacity	113
Figure 5. 14: TOV-based ASCRI.....	114
Figure 5. 15 Average ASCRI and Minimum ASCRI for a STATCOM.....	115
Figure 5. 16 Average ASCRI and Minimum ASCRI for a SC.....	115
Figure 6. 1: Circuit of an AC/DC System with Detailed AC Network at the Inverter Side	120
Figure 6. 2: The Relationship between Average H and Total MVA at the Sending End	126
Figure 6. 3: The Relationship between Average H and Frequency Deviation	127
Figure 6. 4: Relationship between H Constants and Total MVA at the Receiving End.	129
Figure 6. 5: Relationship between the H Constant and the MVA of a Synchronous Condenser	131

Figure 6. 6: Test Case to Show the Impact of Inertia	135
Figure 6. 7: Speed Changing when the DC is Blocked.....	136
Figure 6. 8: Rectifier Side Fault with High Inertia	140
Figure 6. 9: Inverter Side Close-in Fault with High Inertia.....	141
Figure 6. 10: Inverter Side Remote Fault with High Inertia.....	142
Figure 6. 11: DC Block with High Inertia	143
Figure 6. 12: Rectifier Side Fault with Low Inertia.....	144
Figure 6. 13: Inverter Side Close-in Fault with Low Inertia.....	146
Figure 6. 14: Inverter Side Close-in Fault with Slow Clearing	147
Figure 6. 15: Inverter Side Remote Fault with Low Inertia.....	148
Figure 6. 16: DC Block with Low Inertia.....	149
Figure 6. 17 Inverter Side Power System	152
Figure 6. 18 P-delta Characteritic of AC/DC Power Systems	154
Figure 6. 19 Equal Area Criterion for a Sending End Fault	156
Figure 6. 20: Equal Area Criterion for a Receiving End Fault	157

Chapter 1:Introduction

1.1 Background

Due to the significant progress in power electronics technology during the past two decades, the use of High Voltage Direct Current (HVDC) power transmission is becoming more and more attractive. HVDC transmission offers significant advantages for the transfer of bulk power over a long distance, for the transfer of power under water, and for the interconnection of two large systems with weak damping. As a result of the rapid increase in HVDC power transmission schemes, the behaviors of HVDC systems are playing ever greater roles in the performance of entire AC/DC power systems. It is important to thoroughly understand the mechanisms of the interactions between an HVDC system and an AC network so the HVDC scheme can be operated in a manner that enhances the stability and reliability of the entire power grid.

The purposes of the research discussed in this thesis are to investigate the performance of various reactive power compensation devices, to examine the mechanism of reactive power compensation for HVDC systems, and to develop guidelines for the design of reactive power compensation schemes for HVDC systems. Most of the HVDC systems operating today use conventional line commutated converters, which naturally absorb a large amount of reactive power in rectifier stations and inverter stations [1], [2], [3]. Effectively designing and operating the reactive power compensation system is necessary in order to achieve and maintain good overall performance of HVDC systems.

The interaction between the AC network and the HVDC link is one of the major concerns in AC/DC power systems [5], [6]. The significance of this interaction largely depends on the strength of the AC system at the converter bus. The strength of the AC system is demonstrated by its ability to maintain the voltage at the studied bus during various disturbances in the power system, such as faults and load changes. It should be noted that the strength of the system is shown by the strength of the bus voltage. It should also be noted that the system strength is a location-dependent concept as it is normally different for different buses even in the same AC network. A previous publication [8] discussed that the system strength at the converter bus is one of the most important factors to take into consideration when examining or predicting the interaction between the AC and HVDC systems. It is well-known that reactive power compensation is an effective and economical way to control the bus voltage so it naturally has the ability to improve system strength. Therefore, it is important to understand how reactive power compensation works and how to optimize its performance in AC/DC power systems.

The reactive compensation devices available today can be classified into three major categories: Synchronous Condensers (SCs), Static Var Compensators (SVCs), and Static Synchronous Compensators (STATCOMs).

SCs are the most mature technology, and they offer the additional advantage that they increase the system strength as they are real rotating machines. SCs help in maintaining the ac voltage at converter bus and hence make the ac system appear to be stronger to the

HVDC converter. They have been used successfully in several large HVDC systems, such as the Nelsen River Bipole Systems in Manitoba, Canada [5], [20], and the Itaipu HVDC System in Brazil [5].

Several researchers have suggested using power electronics based reactive power compensation, which is smaller and cheaper in some cases to achieve the same objective. Hydro Quebec's Châteauguay converter station uses a thyristor-based Static Var Compensator (SVC). Drawbacks of SVCs are that they do not increase the Short Circuit Ratio (SCR) and they lose their ability to compensate when the voltage drops significantly. Static Synchronous Compensators (STATCOMs) use gate-turnoff switches and are thus much more controllable and continue to provide reactive power even at very low voltages. Some preliminary investigations [17] indicate that they show promise for HVDC applications, and this aspect requires further investigation.

Another advantage with power-electronics-based compensators such as SVCs and STATCOMs is that they increase the ability to maintain the converter bus voltage without increasing the SCR. This raises the question of how to assess the system strength when such compensators are connected to the converter bus.

It has been argued that the mechanical inertia of the synchronous condensers provides some additional frequency stability; but it has also been argued that the mechanical stored energy is not really required because an HVDC system already provides a large source of real power for this purpose. However, when the dc is suddenly blocked, it creates a

significant disturbance to the system that causes voltage and frequency deviation. The inertia of SC helps to stabilize the frequency, and its exciter control helps stabilize the voltage. The STATCOM, on the other hand, can only stabilize the voltage, but no significant energy to provide frequency support. Now the questions is: “Can the STATCOM do the same job to compensate reactive power for HVDC system?” It is important to determine whether the frequency stability is a problem if a STATCOM is used as the reactive power compensator of the HVDC system.

The research in this thesis has been motivated by the issues raised in the preceding discussion of reactive power compensation in HVDC systems. It seeks to determine the advantages and disadvantages of various reactive power compensation schemes, mainly the two most promising options: the Synchronous Condenser (SC) and the STATCOM.

1.2 Literature Survey

Research into reactive power compensation for HVDC systems requires two types of knowledge: knowledge of the technology of reactive power compensation devices and knowledge of the technology of HVDC systems. A great deal of research work has been carried out in both areas, which provides a base for the research carried out in this thesis.

The SC is the most mature dynamic reactive power compensator, and it has been successfully used in several HVDC projects. The technical details of SCs are well-documented in Miller’s book [3] on reactive power control. Although there is not much direct discussion regarding SCs for HVDC applications, the principles and applications of

synchronous machines, of which the SC is an example, have been very well documented [2], [4]. Although many discussions have focused on more advanced reactive power compensators such as SVCs and STATCOMs, it should be noted that SCs are the only mature reactive power compensators, at least for older large HVDC systems. While SCs have been successfully used for many years in HVDC systems, more research on their behavior and their mechanism of operation is needed. For example, there does not seem to be a publication that clearly addresses the overload limits of SCs during faults and the impact of their inertia on overall system stability.

However, there are numerous publications on power-electronics-based compensators. Schauder et al [9] introduced vector control of STATCOM in the classic paper that ushered in a new era of reactive compensation based on Voltage Source Converter (VSC) technologies. The principles of STATCOMs and studies regarding their design have been covered in many books [1], [34], theses [18], and papers [16], [56]. Comparisons of different reactive compensators have been carried out by many researchers. Hammad et al [10], [42] analyzed the dynamic performance of different types of reactive power compensation devices from a transient voltage stability perspective. Larson et al [11] discussed the benefits of STATCOMs compared to those of SCs and SVCs. Canizares et al [28], [29] developed a new STATCOM model for voltage and angle stability and compared the ability of Power System Stabilizers (PSSs), SVCs, and STATCOMs to damp system oscillations. Teleke et al [12] recently presented a paper comparing the dynamic performance of SCs and SVCs. Happ et al [24] discussed static and dynamic var compensation in system planning. These papers covered quite a few important points

regarding the performance of STATCOMs. However, while a great deal of emphasis has been given to the fast response and improved compensating ability at low voltage of STATCOMs, very few discussions have focused on the effects of the low inertia. It was mentioned in [11] that if the energy storage is connected to a STATCOM, it may be operated as a real synchronous condenser. This thesis examines whether the performance of a STATCOM is adequate for HVDC systems when energy storage is not available, which is the case in most circumstances.

HVDC technologies have progressed a great deal in the past two decades. As many large HVDC projects have been put in operation there has been significant research in this area. Both the steady state and dynamic behavior of HVDC systems have been extensively investigated. Many publications have dealt with voltage stability, control stability, transient behavior, and commutation failure, which are related to the main purpose of this thesis on reactive power control and compensation. Canizares et al [31], [32], [33] presented algorithms for the calculation of the steady state voltage stability limits in large AC/DC systems. Andersson and his group have presented a significant number of results on AC/DC load flow [47], oscillation [48], voltage stability[49] and special studies for weak AC systems[46]. More recently, Lee and Andersson [25], [26], [27] studied the voltage and power stability of HVDC systems using modal analysis and reported many useful results; both steady state and dynamic approaches were used to investigate voltage and power stability. Another group of major contributors in this area are Hammad and his collaborators. Their contributions cover many aspects of research on HVDC systems, such as the voltage stability index [43], improvement of stability via control

modification [41], transient voltage stability [42], and special problems with AC/DC parallel configurations [40] and weak AC systems [46]. One adverse dynamic event in HVDC systems is commutation failure, which brings temporary interruption of HVDC power, and in some cases might induce more serious problems and longer power curtailment. Thio et al [7] introduced their investigation of commutation failure, which was based on the Nelsen River Bipoles. Recently, Rahami et al [52], [53] proposed a new index to quantify the ability of HVDC systems to resist commutation failure. Although reactive power compensation was not a major topic in the above papers, they provided many insights useful for the evaluation of reactive power compensation in this thesis.

A systematic description of reactive power compensation of HVDC can be found in the HVDC Handbook [19]. Chapter 9 describes the need for reactive power compensation and highlights both the traditional and unconventional schemes used to provide reactive power in HVDC converter stations. Both the steady state and the dynamic performance of the reactive compensation are discussed.

The influence of reactive power compensations to system strength is another interesting topic. IEEE Standard 1204 [5] provides a guideline for planning DC links that terminate at AC locations with low short-circuit capacities. It discusses many aspects of DC links, including reactive power compensation and its impact on the maximum available power (MAP). It is known that SCs increase the system SCR and, therefore, increase system strength and MAP [20], [21], [22]. It is also known that SVCs and STATCOMs increase the ability to maintain stable voltage [9], [24], whereas they do not decrease the equivalent system impedance. While it is recognized that SVCs do not increase the

system strength, there is no clear understanding of whether STATCOMs increase the SCR or system strength. For a system with a STATCOM, how the system strength is defined is still an open problem.

Comparisons of the dynamic performances of reactive power compensations for HVDC systems were studied by some researchers during late 80s and early 90s. Nyati et al [13] compared voltage control approaches for HVDC converter stations. Nayak et al [14] compared the performance of a fixed capacitor, an SC, and an SVC installed at a weak inverter station using an electromagnetic transient simulation. Menzies et al [16] and Zhuang et al [17] extended Nayak's work to STATCOMs. These papers have similar conclusions: SVCs are faster for light faults but SCs have better performance during serious faults. It was concluded in [17] that STATCOMs are the fastest devices and have a consistent advantage compared with SCs. It can, however, be noted that there is no STATCOM being used in a real HVDC system. In fact, the studies reported in those papers do not describe all problems of AC/DC interactions. Other system dynamics, such as commutation failure, have not been studied yet. The studied case in [17] was very simple and contained no rotating machine in the AC system. The dynamics of the AC system's frequency have, therefore, not yet been considered. Conclusions based on such a simple simulation case need further investigation to be generalized to real power systems.

1.3 Scope of the Thesis

The goal of this thesis is to develop an understanding of the reactive power control and compensation for HVDC systems and to propose a guideline for how to plan the reactive power compensation for an HVDC converter station. The organization of this thesis is as follows.

Chapter 1 (this chapter) provides an introduction to the thesis.

Chapter 2 discusses the capability of various reactive power compensators to enhance the stability in simple AC systems. The purpose is to obtain a clear understanding of the maximum capability of the compensators before they are integrated into a more complex HVDC transmission system. Both analytical study and numerical simulation are employed to investigate the steady state and dynamic behavior of the compensators.

Chapter 3 provides a study of steady state analysis of reactive power compensations in HVDC systems. Two important problems are addressed in this chapter. The first problem is to determine the reactive power requirements of HVDC converters. The voltage dependency of the HVDC converters is shown and this allows some predictions to be made regarding how HVDC converters impact AC system voltage stability. The second problem is to calculate the maximum power curve and the maximum available power when reactive power compensators are connected to the converter bus. A new algorithm that can accurately consider the reactive power limits and the characteristics of

compensators after the limits are reached is proposed. The algorithm is validated for correctness by an ElectroMagnetic Transient (EMT) simulation with PSCAD.

Chapter 4 compares the transient performance of reactive power compensation options for HVDC Systems. The performances of SCs and STATCOMs are intensively studied and compared based on EMT simulations using PSCAD. The simulation studies include a detailed comparison of three major transient performances: fault recovery time, temporary overvoltage (TOV), and commutation failure immunity index (CFII).

Chapter 5 investigates how to quantify system strength when dynamic reactive power compensators are connected to the converter bus. A new series of indices is developed based on Apparent Short Circuit Ratio Increase (ASCRI). The indices include the ASCRI-M based on MAP, the ASCRI-C based on CFII, the ASCRI-R based on fault recovery time, and the ASCRI-T based on TOV. As examples, the SC and STATCOM are tested and further compared using the new indices.

Chapter 6 investigates the effects of inertia in an AC/DC system based on time domain simulation. By modelling the inverter side AC system in more detail, it is possible to examine the frequency stability and rotor angle stability following fault transients. The performances of various compensators at an HVDC inverter bus are compared based on time domain simulation. The inertia and its impact on the frequency stability of the AC/DC system are discussed. The impacts of compensator inertia are investigated using both analytical and digital simulation methods.

Chapter 7 provides conclusions and outlines future work that could be carried out.

Chapter 2: Capability Comparison of Dynamic Reactive Power Compensation Devices

2.1 Introduction of Reactive Power Compensation Devices

This chapter presented a systematic introduction and discussion on the capability of dynamic reactive power compensation devices. The reactive compensation devices available today can be classified into three major categories: Synchronous Condenser (SC), Static Var Compensator (SVC), and Static Synchronous Compensators (STATCOM). It is important to understand the static and dynamic performances of these three types of compensators before investigating their potential applications in HVDC systems. In this chapter, the static capability of these three types of compensators to improve the voltage stability and rotor angle stability is compared in an analytical way. The purpose of this analytical study is to gain a precise understanding of the maximum capability of these devices. The dynamic performances of the compensators during transients are then examined using electromagnetic transient simulation with a simple test system. The analytical study and simulation in the simple system can provide a basis for fundamental understanding of these reactive power compensators. More detailed studies will be performed in the following chapters to investigate impact of these compensators in AC/DC power systems.

2.2 Modelling of Reactive Power Compensation Devices

Both the steady state and the dynamic performance of various reactive power compensators are investigated in this thesis. Analytical derivation and simple MATLAB/MATHECAD tools were used to study the steady state behavior of the compensators and ElectroMagnetic Transient (EMT) digital simulation tools were used to investigate the behavior of the compensators during transient period. This section describes how to model the reactive power compensators in steady state and in transients. Three types of reactive power compensators are discussed: Synchronous Condensers (SCs), Static Var Compensators (SVCs), and Static Synchronous Compensators (STATCOMs).

2.2.1 Modelling of Synchronous Condensers (SCs)

An SC is basically a synchronous generator with reactive power output only. Figure 2.1 shows a basic circuit diagram of an SC and its control. The reactive power exchanged between the SC and the connected power network is determined by the internal voltage, which is proportional to the excitation current. By changing the excitation voltage, the reactive power output of the SC can be varied to maintain the terminal bus voltage.

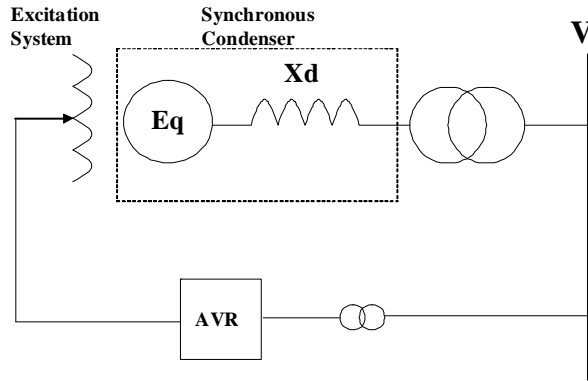


Figure 2.1: Synchronous Condenser Circuit and VI Characteristic

In steady state, the SC can be modelled as a controllable voltage source that keeps the bus voltage constant before its reactive power limit is reached. A “droop” is often introduced for voltage control coordination, which regulates the bus voltage in a slight slope with respect to reactive current. After its reactive power limitation is reached, the SC can be modelled as a current source. The current limit is normally imposed by the overcurrent protective relay. This modelling is reasonable in steady state because the relay will trip the SC if it is continuously operated with a very large current. During the transient period, the limit of current imposed by the overcurrent relay is no longer valid. This is because the overcurrent relay has a time delay and will not trip the device during a short transient period. It is the excitation ceiling that determines the synchronous condenser output during transients. In some cases, the output of the synchronous condenser can be significantly higher than its assigned steady state rating.

The above control philosophy is exhibited in Figure 2.2. It can be further explained using the equivalent circuit of an SC connected to a power system, as shown in Figure 2.3. The current from the SC to the system bus can be calculated as:

$$I = \frac{E_q - V}{X_d} \quad (2-1)$$

$$I = \frac{V - V_s}{X_s} \quad (2-2)$$

In which

E_q is the excitation voltage of the SC;

V is the SC terminal voltage;

V_s is the system voltage;

X_d is the equivalent impedance of the SC;

X_s is the impedance between the SC and the System.

Combining (2-1) and (2-2) we have:

$$E_q = V \left(1 + \frac{X_d}{X_s} \right) - \frac{X_d}{X_s} V_s \quad (2-3)$$

The basic principle of the SC operation is to maintain the terminal bus voltage V by changing E_q when V_s changes. It can be seen from (2-3) that E_q will increase when the system voltage V_s decreases and vice versa.

Assume the original operating point of the SC is A in Figure 2.2. When the system voltage decreases, the SC will increase E_q and output more reactive power by moving the operating point towards B. At point B, the current I_{cs} is the rated capacitive current and also the steady state limit of the SC. If the system voltage continues to decrease, the operating point will move towards C, at which the current will be larger than I_{cs} . The SC

can only work for a short period in this situation because the overcurrent protection will eventually trip it. If the system voltage drops further during a short period of time, the SC can still maintain the terminal bus voltage by increasing E_q until E_{qmax} at point D. We denote the current at this point as the capacitive transient current limit I_{ct} . Beyond D, the excitation voltage E_q has no more room to increase. If the system voltage still decreases, the terminal voltage V has to decrease to balance Equation (2-3) as at point E. Again, at any operation point beyond B, such as C, D, or E, the time that the SC can work is determined by the delaying time of the overcurrent protection. The behavior of the SC when it absorbs reactive power can be analyzed in a similar way. It is noticed in Figure 2-2 that the transient current limit of the SC could be significantly higher than the steady state current limit.

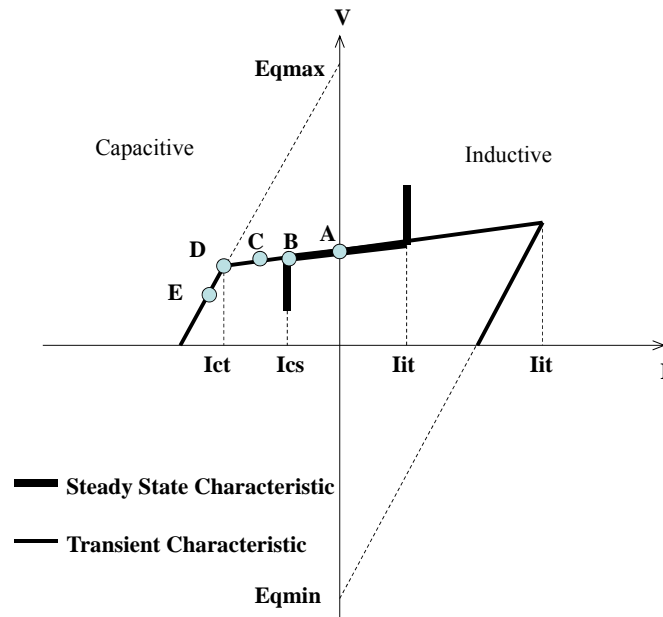


Figure 2. 2 Operation VI Characteristics of an SC

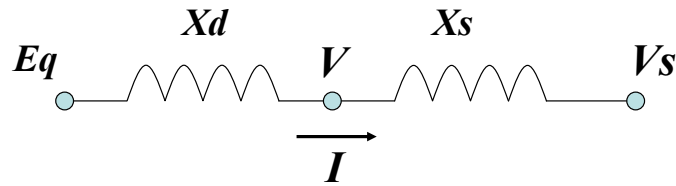


Figure 2. 3: Equivalent Circuit of an SC Connected to a System

2.2.2 Modelling of Static Var Compensators (SVCs)

The SVC is the most commonly used thyristor-controlled reactive power compensator. An SVC is usually a combined system that contains a thyristor controlled reactor (TCR), a Thyristor Switched Capacitor (TSC), and, sometimes, capacitor banks, as shown in Figure 2-4(a). The reactive power output limits of an SVC are determined by its maximum and minimum admittances. Unlike an SC, an SVC is basically a passive device that operates as a variable admittance. By controlling the firing angle of the thyristors, the admittance of the SVC changes from inductive to capacitive, so that the SVC can absorb or produce reactive power. The VI characteristic of an SVC is shown in Figure 2-4(b). When the reactive output of an SVC is within its control range, the SVC will maintain the bus voltage, and it behaves as a controllable voltage source in steady state. After the reactive power limit is reached, the SVC will behave as a constant impedance. Its reactive power output will be proportional to the square of the bus voltage. If the bus voltage is a great deal lower, the reactive power output will be significantly decreased. This characteristic tends to cause voltage collapse and is a major shortcoming of an SVC.

Unlike an SC, the limits of an SVC during a transient period and in steady state are set by the impedance limits. Therefore, there will be no large difference between the limits of an SVC during transient period and in steady state.

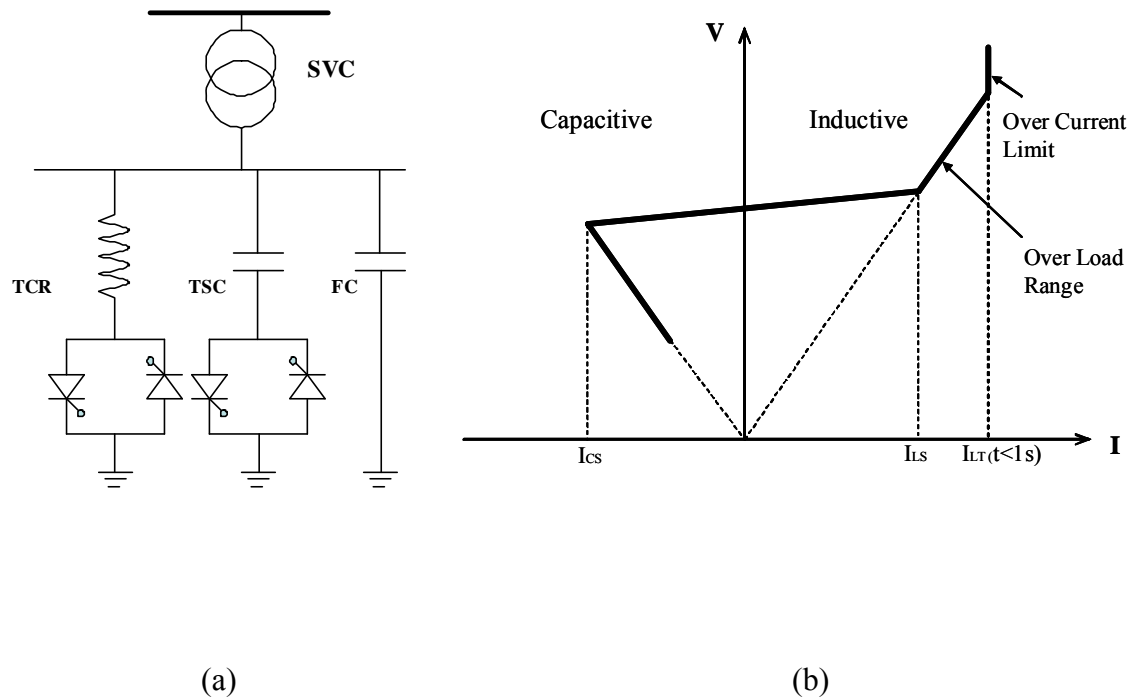


Figure 2. 4: SVC Circuit and VI Characteristic

2.2.3 Modelling of Static Synchronous Compensators (STATCOMs)

A STATCOM is a modern reactive power compensator that is based on the voltage source converter technology. Although it is made of power electronic circuits like an SVC, its behavior is more like that of an SC. It is actually a fully controllable active compensator, as shown in Figure 2-5 (a). A STATCOM works as a controllable voltage source that holds the bus voltage before its limits are reached. The limit of a STATCOM is the current limit that it allows to flow through its power electronic circuit. Figure 2-5 (b)

shows the voltage-current (VI) characteristics of a STATCOM. It should be noted that a STATCOM can provide its maximum current even if the voltage is dropped to a very low value. Its reactive power output beyond its controllable value is proportional to the bus voltage instead of proportional to the square of the bus voltage, as is the case with an SVC. This feature gives a STATCOM more capability to support the system voltage and improve the system voltage stability. The current limit of a STATCOM is normally imposed in the control system, for example limiting the I_q order in the DQ decoupling control. The current limits of the steady state and transient state are usually implemented with the same mechanism. Although they can be designed to allow a certain short-time overcurrent in some circumstances, the difference between the limits of the steady state and the transient state would not be very large.

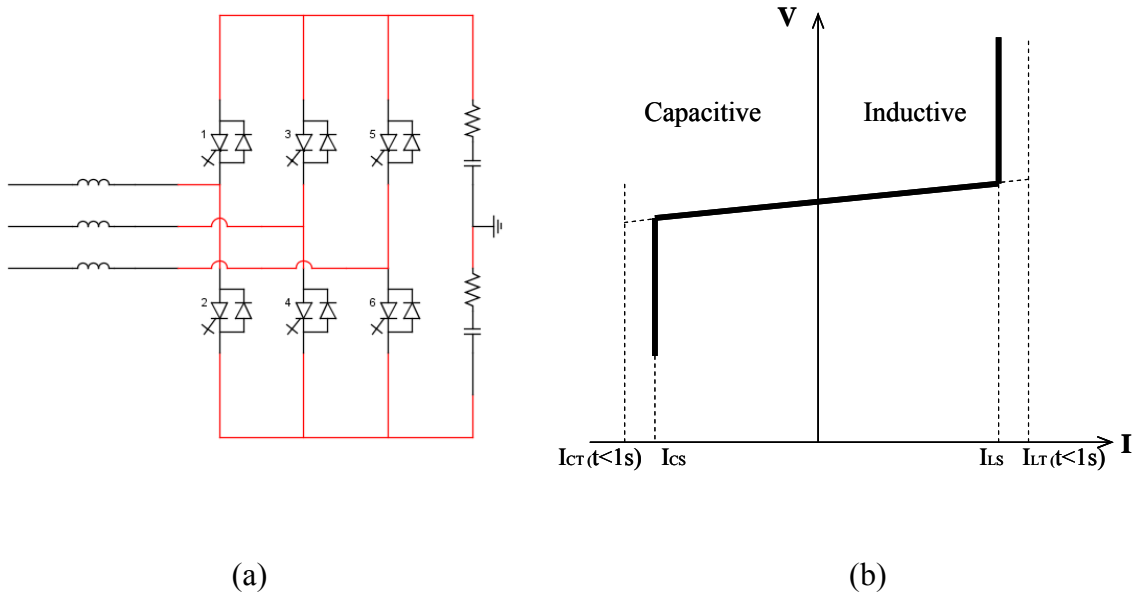


Figure 2. 5: STATCOM Circuit and VI Characteristic

2.3 Comparison of the Capability to Enhance Steady-State Voltage Stability

Reactive power compensation is widely used to improve voltage stability in the steady state or the transient state of power systems. In steady state voltage stability analysis, the maximum transfer capability P_{max} can be increased by reactive power compensation. The mechanism of how reactive power compensation increases P_{max} can be explained with a simple AC system, as shown in Figure 2.6.

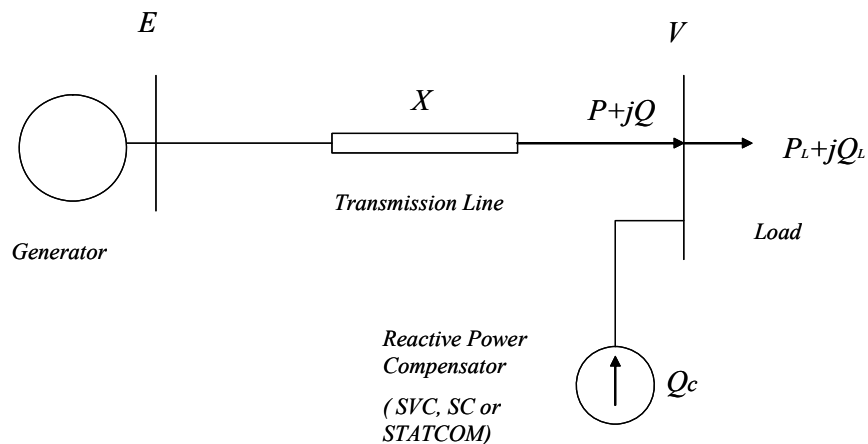


Figure 2. 6: Reactive Power Compensation at the Load Side

Having a controllable reactive power compensator with an output of Q_c at the load side, the voltage profile and the voltage stability of the power system can be significantly improved. The function of a dynamic reactive power compensator varies in two different stages. Before its reactive power limit is reached, the compensator controls the bus voltage to a constant value by adjusting its reactive power output. It is the reactive power

exchange between the load and the system that determines the bus voltage. After the reactive power limit is reached, the voltage setting cannot be held any longer. The reactive power output of the compensator will be limited by Q_{cmax} , I_{mmax} , or B_{cmin} , depending on the type of compensator used. It should be noted that, in steady state, before the reactive power limit is reached, all types of compensators will produce the same amount of reactive power for the same voltage order. After the reactive power limit is reached, different compensator types produce different amounts of reactive power even though the voltage orders are the same.

The P and Q at the receiving end of the transmission line can be written as:

$$P = \frac{EV}{X} \sin(\delta) \quad (2-4)$$

$$Q = \frac{EV}{X} \cos(\delta) - \frac{V^2}{X} \quad (2-5)$$

In which E and V are the voltage of the generator bus and the load bus, respectively, and X and δ are the impedance and phase angle difference between the generator bus and the load bus. When the reactive power output is within the limit of the compensator, the voltage of the load bus is controlled to the setting value. So we have:

$$\sin(\delta) = \frac{PX}{EV} \quad (2-6)$$

and

$$\cos(\delta) = \sqrt{1 - \frac{P^2 X^2}{E^2 V^2}} \quad (2-7)$$

Substitute (2-7) into (2-5) we can obtain:

$$Q = \frac{EV}{X} \sqrt{1 - \frac{P^2 X^2}{E^2 V^2}} - \frac{V^2}{X} \quad (2-8)$$

Assuming the load has the constant power factor angle φ , the relationship between P and Q at the load bus is:

$$Q + Q_c = Q_L = P_L \tan(\varphi) \quad (2-9)$$

When $Q_c < Q_{c \max}$, we have

$$Q_c = P_L \tan(\varphi) - Q \quad (2-10)$$

When $Q_c > Q_{c \max}$, the load bus voltage cannot be held and it will start to decline. The load bus voltage can be calculated in the following equation:

$$\frac{EV}{X} \sqrt{1 - \frac{P^2 X^2}{E^2 V^2}} - \frac{V^2}{X} = P \tan(\varphi) - Q_{c \max} \quad (2-11)$$

in which

$$Q_{c \max} = \begin{cases} Q_{c \max} & \text{For Ideal compensator} \\ V^2 B_{c \max} & \text{For SVC} \\ VI_{c \max} & \text{For STATCOM or Synchronous Condenser} \end{cases}$$

For an ideal compensator, the voltage can be solved from (2-11) directly. If we define

$$Y = X(P \tan(\varphi) - Q_{c \max}) \quad (2-12)$$

Substitute (2-12) into (2-11), we have:

$$(V^2 + Y)^2 = E^2 V^2 - P^2 X^2 \quad (2-13)$$

Define

$$Z = V^2 \quad (2-14)$$

We turn the problem into a second order equation of Z as following:

$$Z^2 + (2Y - E^2)Z + (Y^2 + P^2 X^2) = 0 \quad (2-15)$$

By defining

$$\Delta = (2Y - E^2)^2 - 4(Y^2 + P^2 X^2) \quad (2-16)$$

we can solve (2-15) as:

$$Z = \frac{-2Y + E^2 \pm \sqrt{\Delta}}{2} \quad (2-17)$$

The voltage can be obtained as:

$$V = \sqrt{Z} = \sqrt{\frac{-2Y + E^2 \pm \sqrt{\Delta}}{2}} \quad (2-18)$$

For an SVC, the reactive power output is proportional to the square of the bus voltage after the limit is reached. The Equation (2-11) becomes

$$\frac{EV}{X} \sqrt{1 - \frac{P^2 X^2}{E^2 V^2}} - \frac{V^2}{X} = P \tan(\varphi) - V^2 B_{\text{cmax}} \quad (2-19)$$

Equation (2-19) can be simplified as:

$$\sqrt{E^2 V^2 - P^2 X^2} = P \tan(\varphi) + (1 - B_{\text{cmax}}) V^2 \quad (2-20)$$

Define:

$$a = P \tan(\varphi) \quad (2-21)$$

$$b = 1 - B_{\text{cmax}} \quad (2-22)$$

$$Z = V^2 \quad (2-23)$$

We will again have a second order equation:

$$b^2 Z^2 + (2ab - E^2)Z + (a^2 + P^2 X^2) = 0 \quad (2-24)$$

By defining

$$\Delta = (2ab - E^2)^2 - 4b^2(a^2 + P^2 X^2) \quad (2-25)$$

we can solve (2-24) as

$$Z = \frac{-2ab + E^2 \pm \sqrt{\Delta}}{2b^2} \quad (2-26)$$

The voltage can be obtained as:

$$V = \sqrt{Z} = \sqrt{\frac{-2ab + E^2 \pm \sqrt{\Delta}}{2b^2}} \quad (2-27)$$

For compensators with limitations by maximum current, such as STATCOMs and SCs, the reactive power output is proportional to the bus voltage after the limit is reached. The equation (2-11) becomes

$$\frac{EV}{X} \sqrt{1 - \frac{P^2 X^2}{E^2 V^2}} - \frac{V^2}{X} = P \tan(\varphi) - VI_{\text{cmax}} \quad (2-28)$$

Equation (2-28) is the relationship between voltage and power, but it is difficult to separate the variables analytically as has been done in (2-18) and (2-27). However, it can be solved by a numerical method, and the solution of the voltage should lie between the results of (2-18) and (2-27).

It can be noted in (2-18) that the voltage has a real solution only when $\Delta \geq 0$. When P increases to a certain value of P_{max} , Δ will drop to zero so the voltage solution disappears. The corresponding P at this moment is the maximum power transfer that can be achieved by the transmission system. The relationship between the P and the V is the well-known PV curve widely used in voltage stability analysis.

Because we assume that the load has a constant power factor angle φ , the voltage and P_{max} at the nose point of the PV curve are functions of E , X , and Q_{cmax} . E and X are the operation and configuration parameters of the power network, which are not easy to vary. The Q_{cmax} is the limit or the capacity of the reactive compensator. The effect of Q_{cmax} on the PV curve is computed in the simple power system of Figure 2.6 and plotted in Figure 2.7. It can be seen that as the Q_{cmax} increases, the PV curve is expanded, which means more power can be transmitted by the assistance of reactive power compensations.

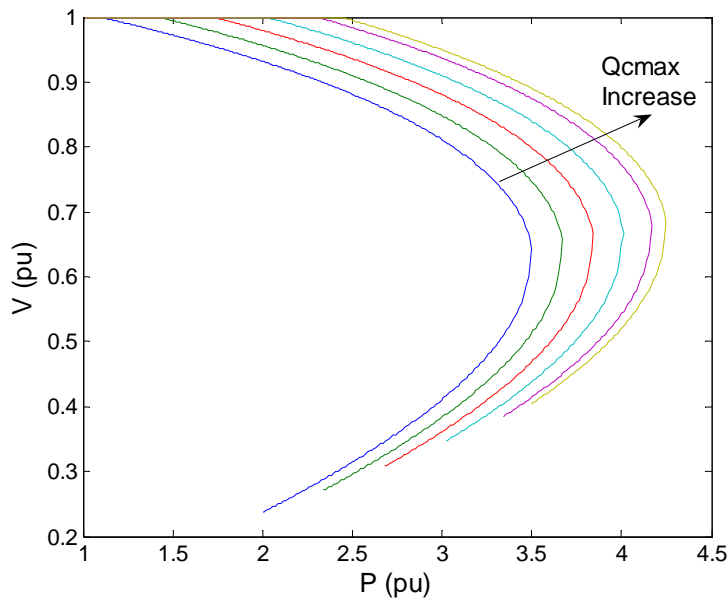


Figure 2. 7: PV Curves When Reactive Power Compensation Increases

The relationship between P_{max} and Q_{cmax} can be further derived in the following analytical form. The relationship for an ideal compensator and an ideal SVC can be obtained as in (2-29) and (2-30), respectively.

$$P_{\max} = \frac{1}{2X} \left(\sqrt{E^4 \tan^2(\phi) + E^4 + 4E^2 X Q_{c\max}} - E^2 \tan(\phi) \right) \quad (2-29)$$

$$P_{\max} = \frac{E^2 (\sqrt{\tan^2(\phi) + 1} - \tan(\phi))}{2X(1 - XB_{c\max})} \quad (2-30)$$

Unfortunately, there is no simple form of analytical solution for STATCOM, in which P_{\max} would be a function of $I_{c\max}$. However, it is believed that the solution can be obtained by numerical solution, which falls between (2-29) and (2-30). The relationship between P_{\max} and capacities of various reactive compensators is demonstrated in Figure 2.8. The curves in Figure 2.8 show that the maximum power transfer can be increased by reactive power compensation.

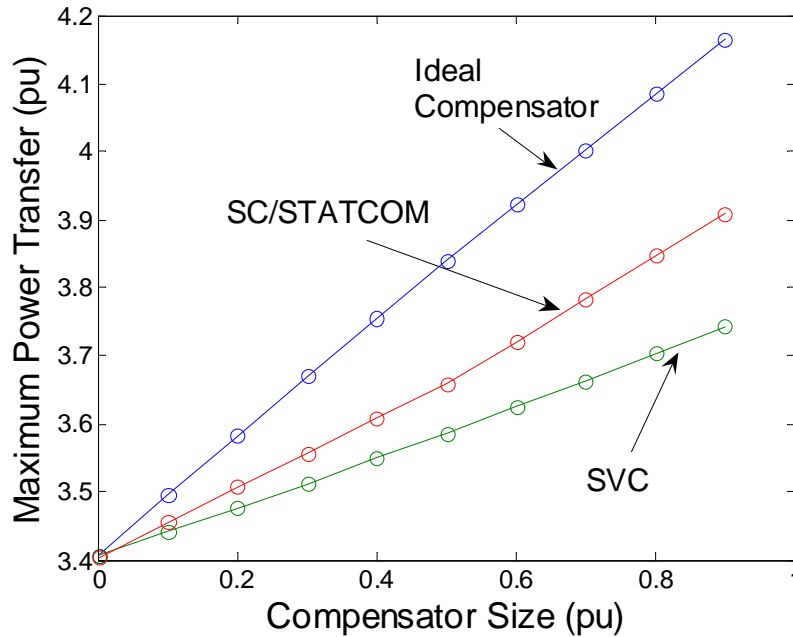


Figure 2. 8: The Relationship between the P_{\max} and Compensator Size

2.4 Comparison of the Capability to Enhance Steady-State Rotor Angle Stability

Reactive power compensators are often installed at the mid-point of a long transmission line to improve the power transfer capability. The term transfer capability here denotes the maximum power transfer between two AC systems, which is restricted by steady-state rotor angle stability. It is not the same as the transfer capability from system to load discussed in the previous section, which is mainly restricted by steady state voltage stability.

In the simple two-machine system in Figure 2.9, a reactive power compensator is installed at the mid-point of the transmission line. We assume the sending end voltage phasor to be $V/\underline{\delta/2}$ and the receiving end voltage phasor to be $V/-\underline{\delta/2}$.

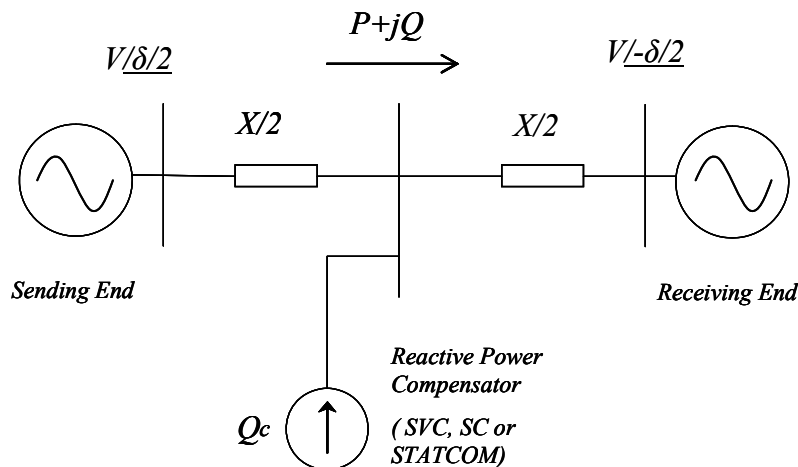


Figure 2. 9: A Two-Machine System with Mid-Point Compensation

When there is no compensation, the power transfer is:

$$P_0 = \frac{V^2}{X} \sin(\delta) \quad (2-31)$$

The maximum power transfer without compensation is:

$$P_{\max 0} = \frac{V^2}{X} \quad (2-32)$$

When a dynamic reactive compensator is installed, the mid-point voltage can be controlled to be constant, and then the power flow on the transmission line becomes:

$$P_c = \frac{2V^2}{X} \sin\left(\frac{\delta}{2}\right) \quad (2-33)$$

The transfer limit discussed above is in the background of a steady state. Before the reactive power limits are hit, the maximum power transfers are identical for all kinds of reactive power compensators, as in Equation (2.33). When the reactive power requirement exceeds the limit of the compensators, the mid-point voltage can no longer be maintained as a constant. Different compensators start to output different amounts of reactive power according to the reduced voltage. Therefore, the maximum power transfers will be different when different compensators are used.

An SVC behaves as a constant impedance (B_{\max}) when the reactive power limit is reached, as in Figure 2-10. By Y- Δ conversion, we can define the equivalent transfer impedance between the sending end and receiving end as:

$$X_{eq} = X - \frac{X^2 B}{4} \quad (2-34)$$

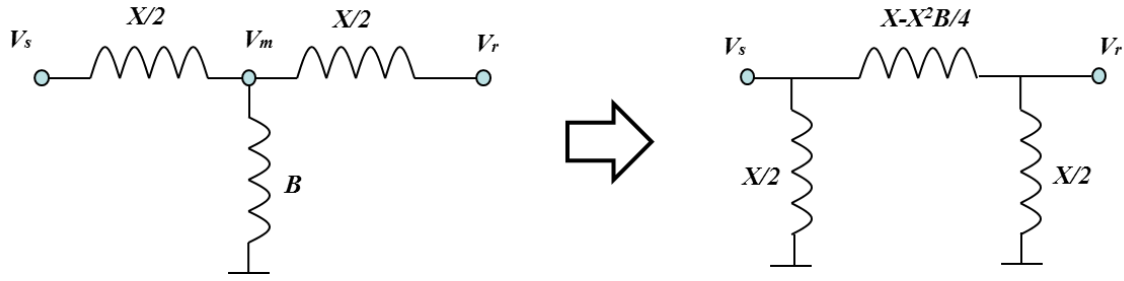


Figure 2. 10: Equivalent Circuit of SVC at Mid-point

Substitute (2-34) into (2-33), the maximum power transfer with an SVC at the mid-point becomes:

$$P_{svc} = \frac{V^2 / X}{1 - XB_{\max} / 4} \sin(\delta) \quad (2-35)$$

When a STATCOM and an SC reach their limit, as discussed in the previous section, they will become constant current sources (I_{max}). By Norton equivalence, we can get the equivalent circuits, as in Figure 2.11.

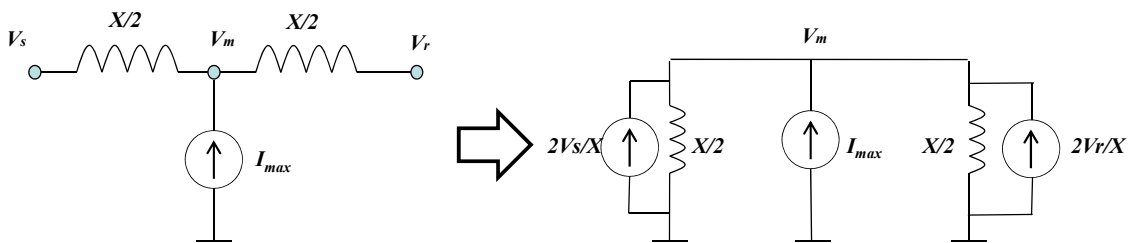


Figure 2. 11: Equivalent Circuit of a STATCOM/an SC at the Mid-Point

The mid-point voltage can be obtained by solving a nodal voltage equation:

$$\dot{V}_m = j \frac{X}{4} \dot{I}_{\max} + \frac{\dot{V}_s + \dot{V}_r}{2} \quad (2-36)$$

Assume the voltage magnitudes of the sending end and the receiving end are equal, and (2-36) can be presented in a clearer way in the phasor diagram, as shown in Figure 2-12.

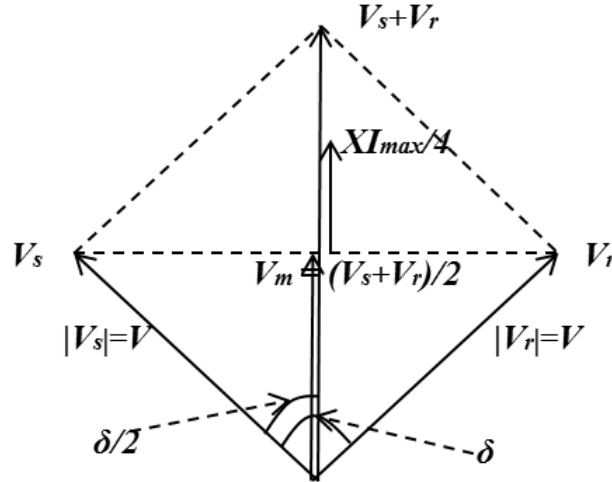


Figure 2. 12: Phasor Diagram of a STATCOM/SC at Mid-Point

The mid-point voltage magnitude can be obtained in the phasor diagram directly as:

$$V_m = \left| \frac{1}{2}(\dot{V}_s + \dot{V}_r) + j \frac{X}{4} \dot{I}_{\max} \right| = \frac{V}{2} \cos \frac{\delta}{2} + \frac{X}{4} I_{\max} \quad (2-37)$$

The power transfer can be represented as:

$$P_{ST} = \frac{V_s V_m}{X/2} \sin \frac{\delta}{2} \quad (2-38)$$

Substitute (2-37) into (2-38), and we get the power transfer as:

$$P_{ST} = \frac{V^2}{X} \sin \delta + \frac{VI_{\max}}{2} \sin \frac{\delta}{2} \quad (2-39)$$

In the simple two-machine system in Figure 2.9, when the power flow on the tie line increases, the angle difference increases, and the reactive compensator at the mid-point will also increase its output to maintain the voltage of the mid-point until the output exceeds the limit. We define the angle difference at this particular moment as δ_{cr} .

Knowing the maximum admittance B_{max} for the SVC and the maximum capacitive currents I_{max} for the STATCOM and the SC, we can calculate the angle difference δ_{cr} as the following:

For an SVC:

$$\delta_{cr} = 2 \cos^{-1} \left(\frac{4 - XB_{max}}{4X^2} \right) \quad (2-40)$$

For a STATCOM or an SC:

$$\delta_{cr} = 2 \cos^{-1} \left(1 - \frac{X}{4V} I_{max} \right) \quad (2-41)$$

Therefore, the power angle curve in the entire range from 0 degree to 180 degree can be represented as the following forms:

$$P_{svc} = \begin{cases} \frac{2V^2}{X} \sin \frac{\delta}{2} & \delta \leq \delta_{cr} \\ \frac{4V^2}{4X - X^2 B_{max}} \sin \delta & \delta > \delta_{cr} \end{cases} \quad (2-42)$$

$$P_{STSC} = \begin{cases} \frac{2V^2}{X} \sin \frac{\delta}{2} & \delta \leq \delta_{cr} \\ \frac{V^2}{X} \sin \delta + \frac{VI_{max}}{2} \sin \frac{\delta}{2} & \delta > \delta_{cr} \end{cases} \quad (2-43)$$

If we use the rated capacity S_N and the rated voltage V_N of the compensator to represent B_{max} and I_{max} , we have:

$$B_{max} = \frac{S_N}{V_N^2} \quad (2-44)$$

$$I_{max} = \frac{S_N}{\sqrt{3}V_N} \quad (2-45)$$

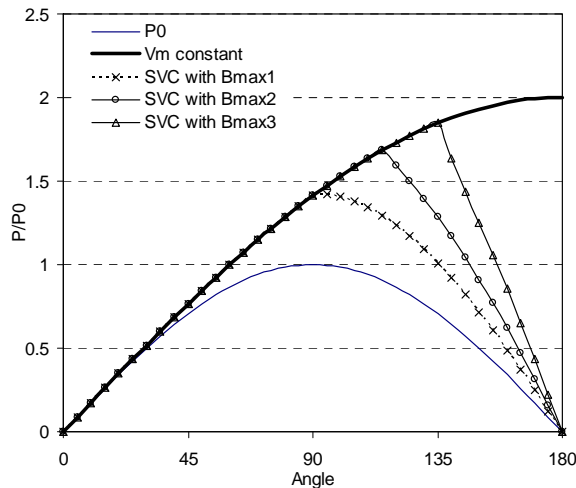
in which the P_{svc} denotes the power when an SVC is connected at the mid-point and P_{STSC} denotes the power when an SC or a STATCOM is connected at the mid-point.

Substitute (2-44) and (2-45) into (2-42) and (2-43), and we can get the power angle relationships as:

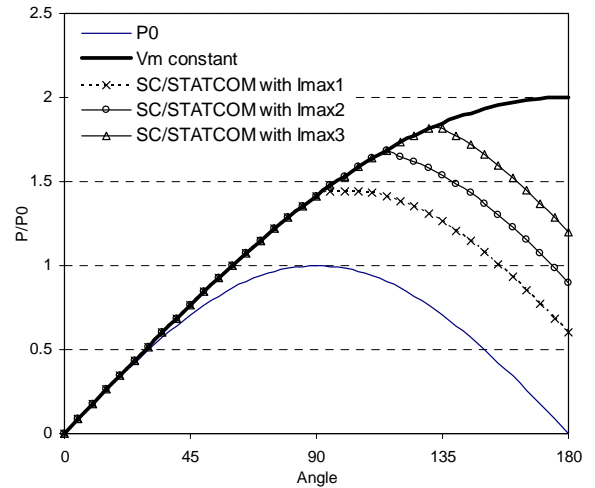
$$P_{svc} = \begin{cases} \frac{2V^2}{X} \sin \frac{\delta}{2} & \delta \leq \delta_{cr} \\ \frac{4V^2V_N^2}{4XV_N^2 - X^2S_N} \sin \delta & \delta > \delta_{cr} \end{cases} \quad (2-46)$$

$$P_{STSC} = \begin{cases} \frac{2V^2}{X} \sin \frac{\delta}{2} & \delta \leq \delta_{cr} \\ \frac{V^2}{X} \sin \delta + \frac{VS_N}{2\sqrt{3}V_N} \sin \frac{\delta}{2} & \delta > \delta_{cr} \end{cases} \quad (2-47)$$

The power angle curve with different compensators at the mid-point are plotted in Figure 2.13(a) and Figure 2.13(b). It should be noted that the compensation increases the maximum power transfer, and that the larger the compensator is, the more power can be transferred.



(a) SVC is Connected at the Mid-Point



(b) SC or STATCOM is Connected at the Mid-Point

Figure 2. 13: Power-Angle Curve with Mid-Point Compensations

Figure 2.14 demonstrates the comparison of different compensation schemes. It can be seen that for the same size of the compensators, the effects on power transfer are the same before the reactive power limits are reached. After the reactive power limits are reached, different compensators demonstrate different behaviors. A STATCOM and an SC can bring more power transfer than an SVC does. It is noticeable that even when the power angle is 180 degree the power transfer can still be positive with the help of a STATCOM or an SC.

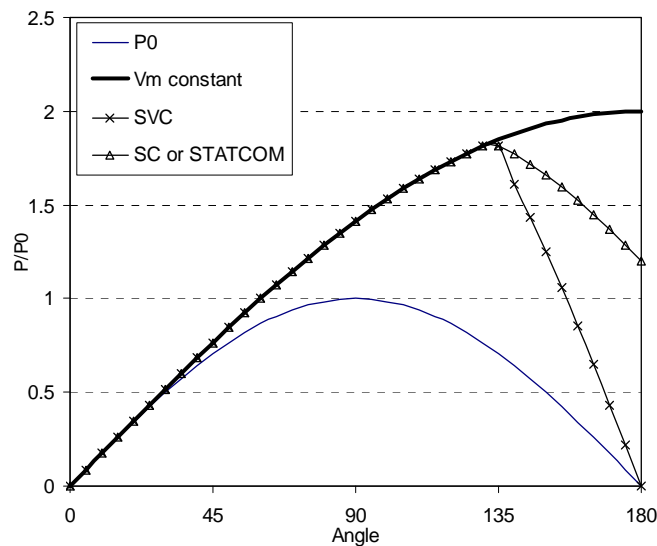


Figure 2. 14: Comparison of Power-Angle Curves with Different Compensators

2.5 Comparison of Dynamic Performances

The dynamic behaviors of various reactive power compensators are examined in this section using electromagnetic transient simulation. A simple power system, shown in

Figure 2.15, is used to compare the performances of an SC, an SVC, and a STATCOM. All studies were done on a Real Time Digital Simulator (RTDS).

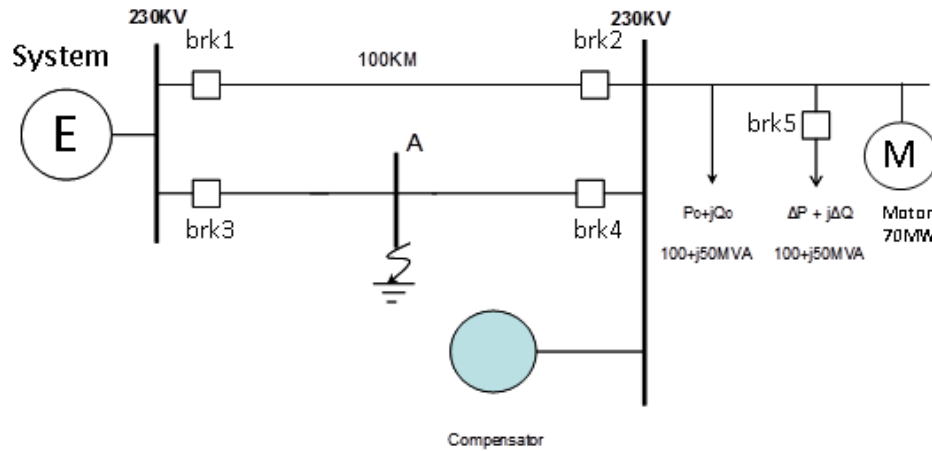


Figure 2. 15: The Studied Simple Power System

The dynamic performance of the reactive power compensators will be examined during the following faults/operation conditions:

- 1) Three-phase fault
- 2) Single-phase fault
- 3) Load increasing
- 4) Line trip
- 5) Permanent loss of power
- 6) Short term loss of power

2.5.1 Three-Phase Fault

To compare the dynamic performance of the three types of compensators, a three-phase fault was applied at the middle of one of transmission lines. The RMS voltage at the load bus is shown in Figure 2.16. It can be seen that the SVC and the STATCOM are equally fast to bring the voltage back to normal, and that the SC is slower to control the voltage and the voltage has oscillations. It can also be seen that during the fault, the bus voltage is highest with the SC, the second highest with STATCOM, and the lowest with the SVC. The reason is that the voltage is very low during the three-phase fault and the SC has largest short-term overvoltage capacity so it injects a large amount of reactive power when it is trying to control the voltage back to normal. In the meantime, the energy stored in its rotor is released to send some active power to the power system. These actions of the SC result in the highest bus voltage during the fault. The STATCOM has some overloading capability and it injects constant current when the voltage is very low. The SVC has no capacitive overcurrent ability and its reactive power output is proportional to the square of the voltage magnitude. Therefore, its contribution of reactive power during the fault is the lowest.

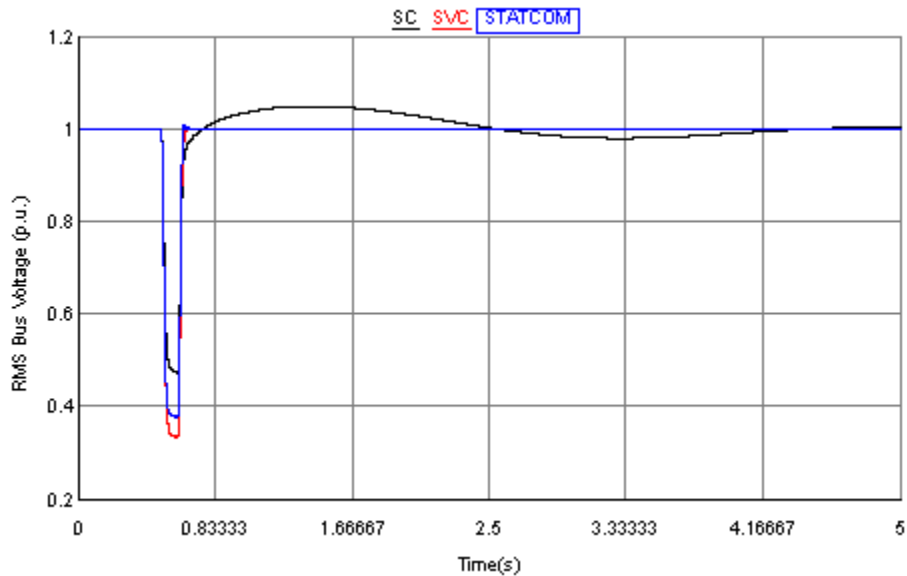


Figure 2. 16: Three-Phase Fault

2.5.2 Single-Phase Fault

The load bus voltage of a single-phase fault is shown in Figure 2.17. The STATCOM demonstrates better performance than the SVC and the SC in this case. A single-phase fault is an unbalanced fault and it is less severe than a three-phase fault; therefore it causes less voltage reduction. The STATCOM can quickly bring the voltage back to normal without reaching its reactive power limit. So the voltage dip is very small when the STATCOM is used. The SVC also has fast response speed, but it has largest voltage dip during the fault. The SC has a slow response time and the voltage appears to have oscillations, which is likely caused by the swing of the SC's rotor. Figure 2.17 shows that the STATCOM has a better capability to control the voltage for unbalanced faults.

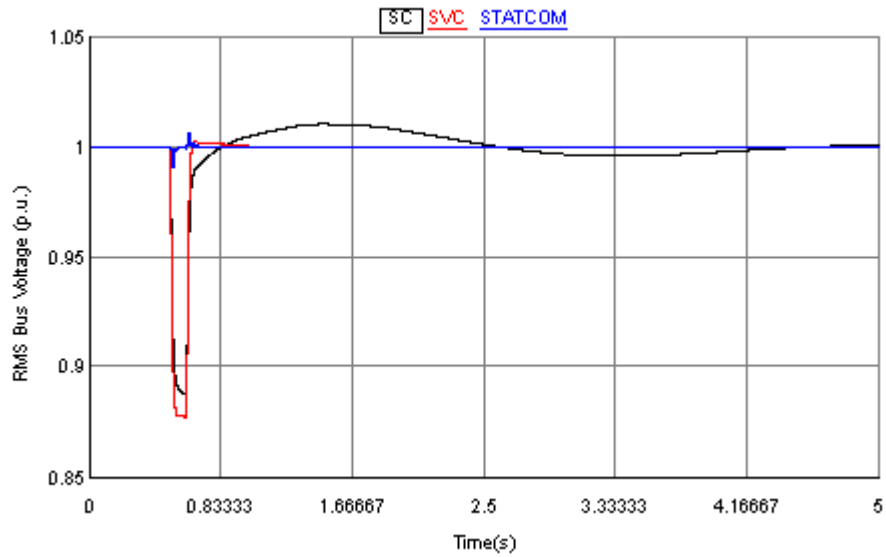


Figure 2. 17: Single-Phase Fault

2.5.3 Load Changing

The bus voltage under a sudden load increase is shown in Figure 2.18. The STATCOM demonstrates the best performance for this large load switching disturbance. The response time of the STATCOM is much faster and more accurate when the load is switched on than the response times of the other compensators. The SC responses much slower and brings some bus voltage oscillation.

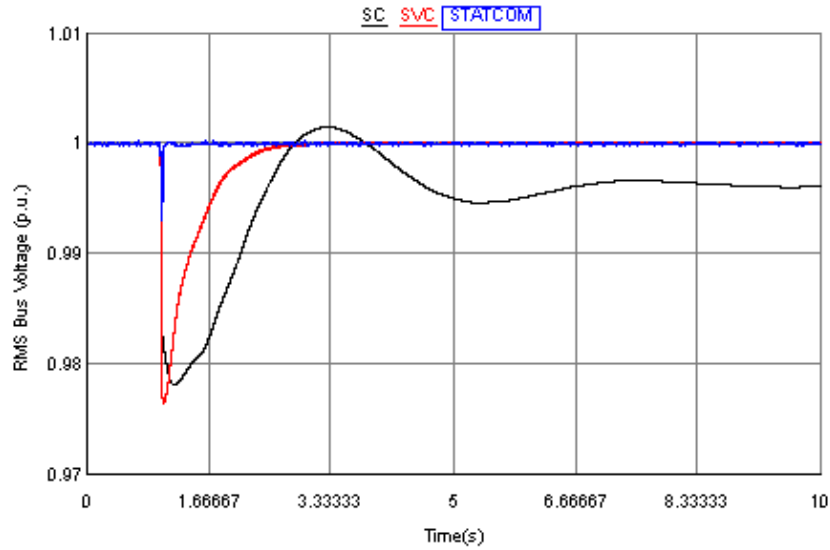


Figure 2. 18: Load Increase

2.5.4 Line Trip

This test shows the bus voltage changing when one of the transmission lines is tripped. The results are shown in Figure 2.19. Again, the STATCOM demonstrates the fastest ability to regulate the load bus voltage.

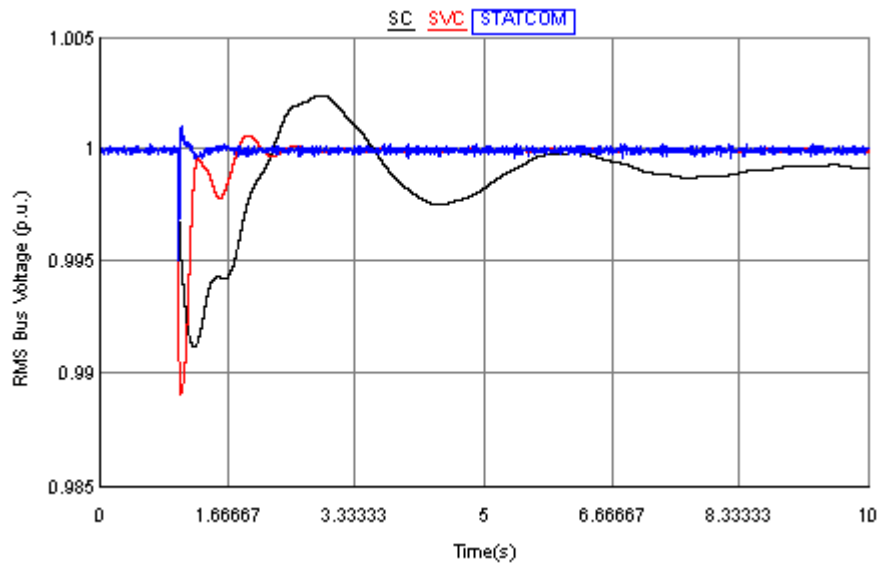


Figure 2. 19: Line Trip

2.5.5 Permanent Loss of Power

Figure 2.20 shows how the bus voltage declines when power is lost by tripping both of the transmission lines. The reason for this test was to determine how the inertia of different reactive compensators influences dynamics of the whole network. The results show that the voltage can be held longer when the SC is used. If both lines trip and the SC is used, the voltage takes about 2.0 seconds to decline to 0.5 per unit. This indicates that if fast backup or reclosure are available to put power back, it would be very helpful if an SC is installed because the SC would help the motors to start. This result also means the transient voltage stability can be greatly improved by using SCs.

Such an effect of the inertia might indicate a situation in the HVDC receiving end; if the HVDC is shut down and then started up again, the SC might be able to hold the voltage for certain time and consequently improve the transient voltage stability. The voltage stability might depend on the total inertia of the receiving end. However, if there is no other inertia in the receiving end, the SC would be a good option there. Further investigation in detail will be undertaken in Chapter 6.

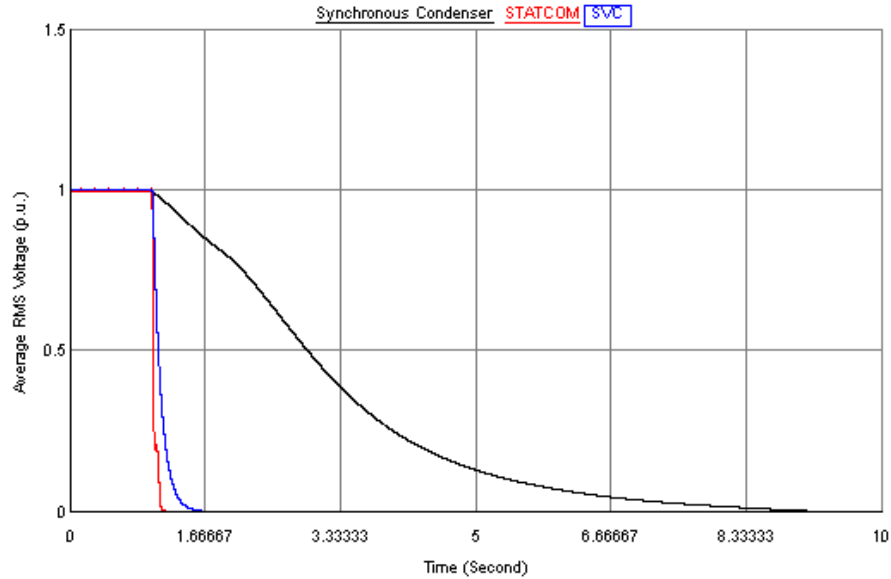


Figure 2. 20: Voltage Decline When Power is Lost

2.5.6 Short-Term Loss of Power

The inductive motor at the converter bus can manifest the frequency dynamics of the industrial load and the impact of the system inertia. When one of the transmission lines is out of service, if the remaining line experiences any temporary outage of three cycles, the load will experience three cycles of a no power situation. Figure 2.21 shows the real power and the speed of the motor when different compensators are used. The results demonstrate that the motor becomes unstable when a STATCOM or an SVC is used, but remains stable when an SC is used. The results indicate the inertia of the SC is playing an important role when no synchronous generator is available during the isolating circumstance. At the moment the load bus is isolated from the power network, the speed of the motor will decline. The SC has some energy stored in its rotor; therefore, it helps

to hold the system frequency so the motor remains stable. This result also implies the SC can provide some advantage if the inertia of the system is not sufficient.

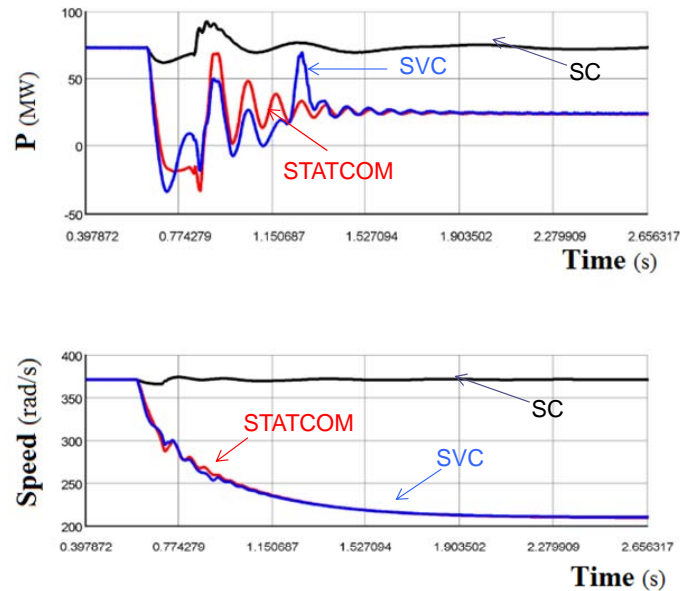


Figure 2. 21: Transients of the Motor during Short-Term Tripping

2.5.7 Short-Circuit Current Provided by Different Compensators

This section addresses the question of whether the reactive power compensators provide short-circuit current. Figure 2.22 shows the fault currents contributed by various reactive power compensators. Only SCs contribute significant amount of short-circuit current. The STATCOM and the SVC are not electrical machines. There is not much energy stored in those power electronics devices except for the capacitor charging energy. Although it is true that an ideal fault consumes zero power, in reality fault impedance and resistive losses in the lines and equipment do create a power loss. As the SVC and STATCOM have very limited energy storage in the form of charged capacitor, they very quickly

dissipate their energy and cannot sustain the fault current for long. On the other hand, SC is a real synchronous machine so it can provide significant amount of short circuit current during any faults and disturbances. Therefore, the short-circuit MVA will be increased by an SC, but not by a STATCOM or an SVC. However, the SVC and STATCOM provide the voltage support for the AC bus. In fact, the SVC and the STATCOM provide faster voltage regulating than SC in most cases. This result indicates that the traditional short-circuit MVA cannot precisely quantify the system strength when modern power electronics compensators are used in the electrical power system.

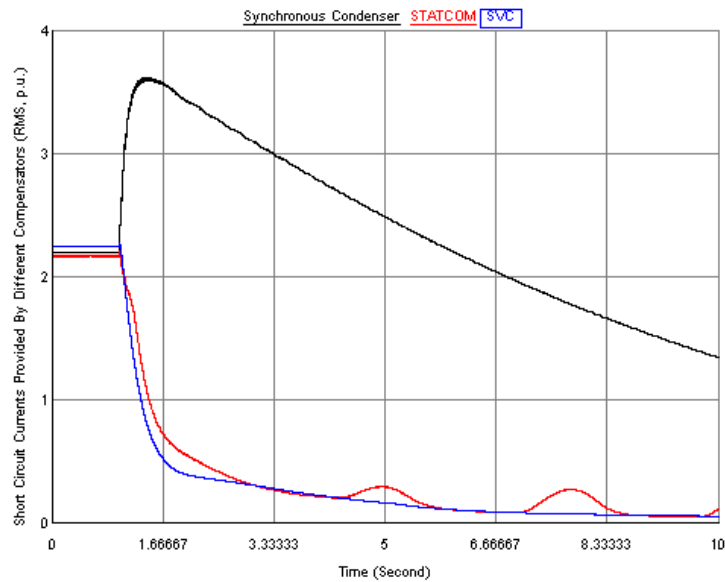


Figure 2. 22: Fault Current Injections of Different Compensators

2.5.8 Summary of the Simulation Study

The EMT-type simulation study in this section demonstrated that the STATCOM has better performance in voltage recovery from faults. The simulation results also confirm

that the SC is the only compensator that has the ability to add inertia and provide short-circuit current. The study in this section also suggests the system strength after adding a STATCOM or an SVC should not be quantified with short-circuit MVA.

2.6 Chapter Conclusions

This chapter investigated the steady state and dynamic capabilities of various reactive compensation schemes. The conclusions from this chapter can be summarized as follows:

1. The modelling approaches for reactive power compensation devices were discussed. The limits of the compensators in steady state and transients were obtained.
2. The ability of reactive power compensation to enhance voltage stability in a simple transmission system was discussed. The analytical relationship between the amount of reactive power compensation and the capability of maximum power transfer was obtained.
3. The impact of reactive power compensation upon rotor angle stability was discussed. The analytical form of the power and angle equations that considers mid-point compensation was derived.
4. The performances of reactive power compensators during transients in a simple AC system were studied using numerical simulation. The results showed that the STATCOM offers the best performance in most of the cases and that the SC has an advantage when the system inertia is not sufficient.

Although we are discussing an old and fundamental topic which has been discussed in many publications, the following original contributions are made through this chapter:

- The analytical relationship between the voltage stability maximum power transfer and the size of reactive power compensator in a simple ac transmission system was derived.
- In a simple ac power system, the impact of reactive power compensator inertia on system stability was revealed by EMT simulation. It was demonstrated that the only SC could help the motor to recovery from temporary islanding operation in case no other generators were available in the isolated power network.

Chapter 3: Steady-State Analysis of Reactive Power Compensation of HVDC Systems

3.1 Introduction

The steady-state problems of the reactive power compensation of HVDC systems are investigated in this chapter. Two problems associated with the reactive power requirement and compensation of HVDC systems are studied and discussed, which can be considered as parts of the contributions of this thesis. The first problem is to determine the voltage dependence of HVDC converters as a load. The solution to this problem helps with understanding the impact of HVDC systems on the voltage stability of the AC/DC system. The second problem is to calculate the maximum available power (MAP) of HVDC systems when reactive compensators are installed. The MAP is an important index used to measure the transfer capability of HVDC systems. The solution to this problem helps with understanding the effects of reactive power compensation on enhancing the strength of AC systems and improving the power stability of HVDC systems.

3.2 Some Indices for AC/DC System Performance Studies

3.2.1 Short Circuit Ratio (SCR) and Effective Short Circuit Ratio (ESCR)

The strength of an AC system is measured in terms of the Short Circuit Ratio (SCR) or the Effective Short Circuit Ratio (ESCR). The SCR and ESCR indicate the relative strength of an AC system with respect to the rated DC power.

The SCR is defined as the ratio of the short-circuit MVA of the AC system at the AC busbar with the DC blocked and the AC voltage re-adjusted to its nominal voltage V_L , to the rated DC power P_{dc} at that bus.

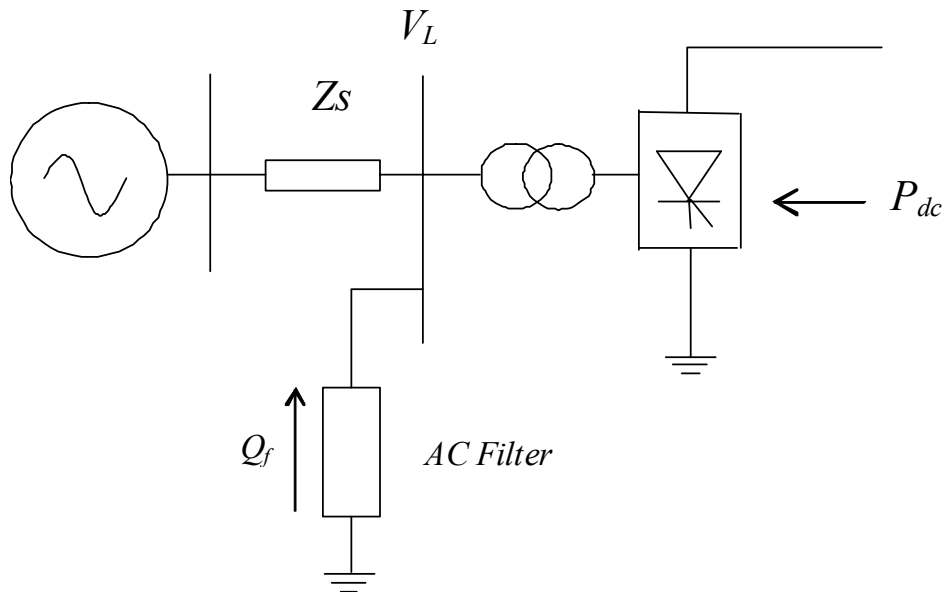


Figure 3. 1: The Converter Connected to an AC Bus

Using Figure 3-1, we can calculate SCR as:

$$SCR = \frac{SMVA}{P_{dc}} = \frac{V_L^2 / Z_s}{P_{dc}} \quad (3-1)$$

Here, the Thevenin impedance is given by Z_s , the DC power by P_{dc} , and the rated line voltage is V_L . More often, the index of Effective Short Circuit Ratio (ESCR), as shown in (3-2), is used.

$$ESCR = \frac{SMVA - Q_f}{P_{dc}} = \frac{V_L^2 / Z_s - Q_f}{P_{dc}} \quad (3-2)$$

The ESCR takes into account the reactive power generation Q_f due to AC filters, which increases the susceptibility to overvoltage. The ESCR is thus smaller in magnitude than the SCR. Note that, strictly speaking, the SCR is a complex number that is inversely proportional to Z_s . However, as Z_s is usually highly inductive, the SCR is almost all imaginary. Hence, the phase of the SCR (or ESCR) is often ignored and only its magnitude is referred to.

3.2.2 Maximum Power Curve (MPC) and Maximum Available Power (MAP)

The Maximum Power Curve (MPC) shows the power that can be injected into the AC system at the inverter bus of HVDC system versus the DC current. In the basic equation of DC voltage:

$$V_d = \frac{3\sqrt{2}}{\pi} V_L \cos \gamma - \frac{3}{\pi} X_c I_d \quad (3-3)$$

The DC voltage tends to decrease if the DC current increases. The DC power injection is:

$$P_d = -\frac{3}{\pi} X_c I_d^2 + \frac{3\sqrt{2}}{\pi} V_L I_d \cos \gamma \quad (3-4)$$

The DC power (P_d) is a second order nonlinear function of DC current (I_d), which defines the MPC as shown in Figure 3.2. The maximum value on the MPC is the largest power that can be injected from the DC inverter into the AC system, which is called the Maximum Available Power (MAP). MAP is an index commonly used to quantify the power transfer capability of an HVDC system.

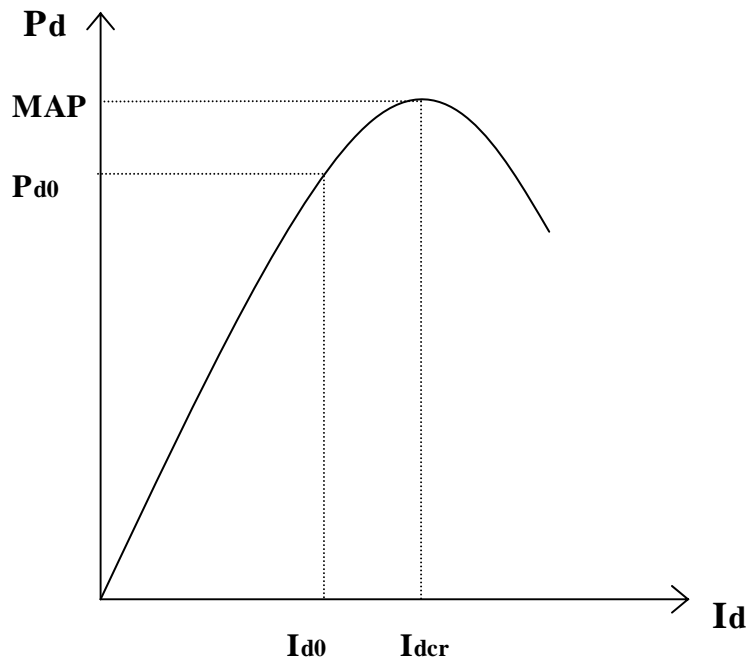


Figure 3. 2: Maximum Power Curve of HVDC Systems

3.3 Nonlinear Load Characteristics of HVDC Converters

For different HVDC control modes the P and Q exchanges between an HVDC converter and the connected AC system are different. Consequently, the voltage stability of the AC/DC system will differ depending on the utilized HVDC control mode. A rectifier is similar to a nonlinear load at the converter bus. If a DC rectifier is a load from the AC side, the load is voltage-dependent, and its characteristics are different for different HVDC control modes. Similarly, an inverter acts as a generator with a leading power factor that injects real power into the AC system and absorbs reactive power from the AC system. It is a common property that the rectifier and the inverter consume a large amount of reactive power. Part of the reactive power will be balanced by the filters at the converter stations. The rest of the reactive power needs to be supplied either by the AC system or by extra compensation devices at the converter station. For the purpose of voltage stability assessment, it is important to understand the voltage-dependent characteristics of the active and reactive powers of the DC converters. Developing this understanding is the intention of this section.

The following three typical HVDC control modes are investigated in this section:

Control mode 1: constant P at the rectifier side, constant γ at the inverter side

Control mode 2: constant I at the rectifier side, constant γ at the inverter side

Control mode 3: constant α (or α_{min}) at the rectifier side, constant I at the inverter side

A simple back-back DC transmission scheme [36] [64] is used for demonstration purposes in this chapter. The inverter is operated in the constant extinction angle control mode with $\gamma=15$ degrees. The scheme is rated at 142 kV, 500 MW. The converter transformer is rated at 605 MVA, 120 kV / 120 kV, $X_c =15\%$. The AC system has a short-circuit ratio of 2.5 (purely inductive) and the filters are rated at 250 Mvar (purely capacitive) at the fundamental frequency. It should be noted that, although the curves are plotted based on this system, the equations and algorithms developed in this chapter should be valid for general HVDC systems.

3.3.1 Control Mode 1: Constant P and Constant γ Control

In control mode 1, the real power P is a constant value, so it does not change with the AC voltage. This is similar to the constant power load in AC power systems. The reactive power consumed by the HVDC system can be calculated based on the basic DC operation equations as follows.

The DC power P_d is a second order function of the DC current as in Equation (3.4). When P_d is constant, we can solve I_d as:

$$I_d = \frac{3\sqrt{2}V_L \cos(\gamma) - \sqrt{18V_L^2 \cos^2(\gamma) - 12\pi X_c P_d}}{6X_c} \quad (3-5)$$

The power factor of the inverter station is:

$$\cos(\phi) = \cos(\gamma) - \frac{X_c I_d}{\sqrt{2}V_L} \quad (3-6)$$

The reactive power consumed by the inverter can be calculated according to (3-6):

$$Q_d = P_d \tan(\phi) = P_d \frac{\sqrt{1 - \left(\cos(\gamma) - \frac{X_c I_d}{\sqrt{2} V_L} \right)^2}}{\left(\cos(\gamma) - \frac{X_c I_d}{\sqrt{2} V_L} \right)} \quad (3-7)$$

Substitute (3-5) into (3-7) and we can get Q_d as a function of the AC bus voltage V_L :

$$Q_d = P_d \frac{\sqrt{1 - \left(\cos(\gamma) - \frac{3V_L \cos(\gamma) - \sqrt{9V_L^2 \cos^2(\gamma) - 6\pi X_c P_d}}{6V_L} \right)^2}}{\left(\cos(\gamma) - \frac{3V_L \cos(\gamma) - \sqrt{9V_L^2 \cos^2(\gamma) - 6\pi X_c P_d}}{6V_L} \right)} \quad (3-8)$$

Figure 3.3 shows the relationships between the DC current and the AC voltage. Figure 3.4 shows the reactive power consumed by the DC system and the AC voltage.

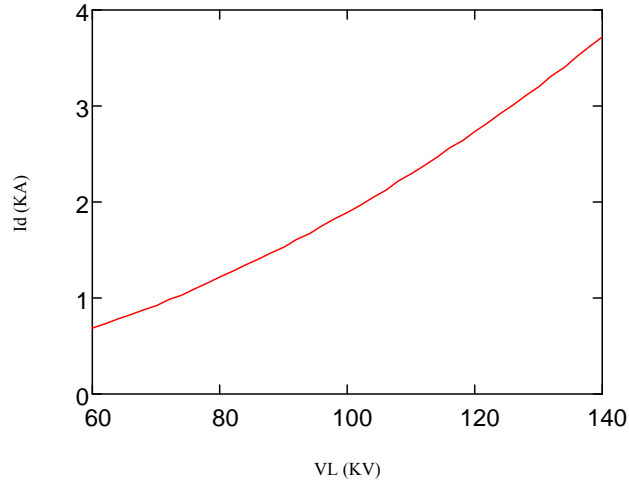


Figure 3. 3: Voltage Dependence of the DC Current of Control Mode 1

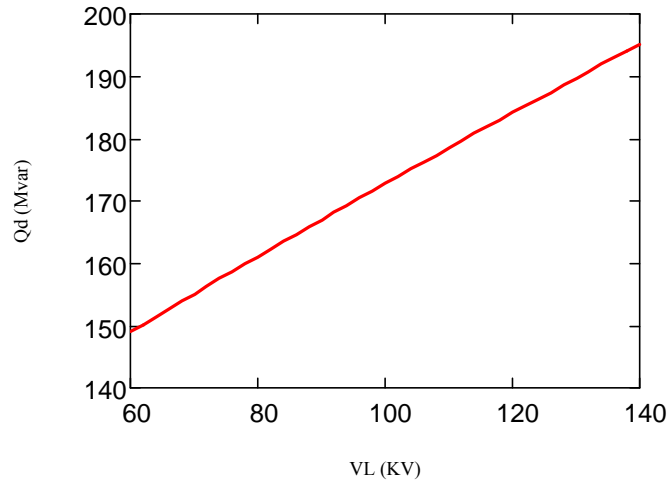


Figure 3. 4: Voltage Dependence of Inverter Q of Control Mode 1

For the rectifier side:

$$P_d = -\frac{3}{\pi} X_{cr} I_d^2 + \frac{3\sqrt{2}}{\pi} V_{Lr} \cos(\alpha) I_d \quad (3-9)$$

Also, we have the power factor of the rectifier side:

$$\cos(\phi) = \cos(\alpha) - \frac{X_{cr} I_d}{\sqrt{2} V_{Lr}} \quad (3-10)$$

Solve $\cos(\alpha)$ from (3-9), we have:

$$\cos(\alpha) = \frac{P_d - \frac{3}{\pi} X_{cr} I_d^2}{\frac{3\sqrt{2}}{\pi} V_{Lr} I_d} \quad (3-11)$$

Substitute (3-11) into (3-10), we have:

$$\cos(\phi) = \frac{P_d - \frac{3}{\pi} X_{cr} I_d^2}{\frac{3\sqrt{2}}{\pi} V_{Lr} I_d} - \frac{X_{cr} I_d}{\sqrt{2} V_{Lr}} = \frac{P_d}{\frac{3\sqrt{2}}{\pi} V_{Lr} I_d} = \frac{P_d}{\left(\frac{3\sqrt{2}}{\pi} V_{Lr} \frac{3\sqrt{2} V_L \cos(\gamma) - \sqrt{18 V_L^2 \cos^2(\gamma) - 12 \pi X_c P_d}}{6 X_c} \right)} \quad (3-12)$$

Therefore, the reactive power of the rectifier side can be calculated as:

$$Q_{dr} = P_{dr} \tan(\phi_r) = P_d \sqrt{1 - \left(\frac{P_d}{\frac{3\sqrt{2}}{\pi} V_{Lr} \frac{3\sqrt{2} V_{Li} \cos(\gamma) - \sqrt{18 V_{Li}^2 \cos^2(\gamma) - 12 \pi X_{ci} P_d}}{6 X_{ci}}} \right)^2} \quad (3-13)$$

Figure 3.5 shows the relationship between the reactive power consumed by the DC system and the AC voltage at the rectifier side.

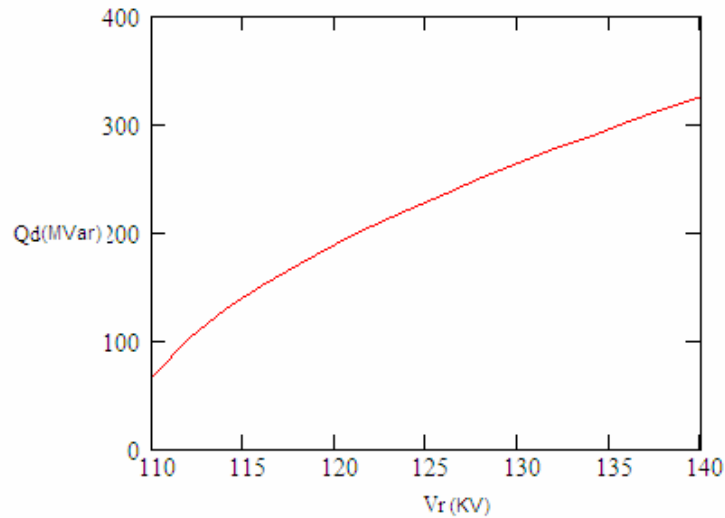


Figure 3. 5: Voltage Dependence of Rectifier Q of Control Mode 1

3.3.2 Control Mode 2: Constant I and Constant γ Control

If the DC system is controlled in constant current mode,

$$P_d = -\frac{3}{\pi} X_{ci} I_d^2 + \frac{3\sqrt{2}}{\pi} V_{Li} \cos(\gamma) I_d \quad (3-14)$$

This indicates that the DC real power P_d is linearly dependent on the AC voltage at the inverter side. The reactive power of the inverter side can be derived as:

$$Q_{di} = P_d \tan(\phi_i) = \left(-\frac{3}{\pi} X_{ci} I_d^2 + \frac{3\sqrt{2}}{\pi} V_{Li} \cos(\gamma) I_d \right) \frac{\sqrt{1 - \left(\cos(\gamma) - \frac{X_{ci} I_d}{\sqrt{2} V_{Li}} \right)^2}}{\left(\cos(\gamma) - \frac{X_{ci} I_d}{\sqrt{2} V_{Li}} \right)} \quad (3-15)$$

Figure 3.6 and Figure 3.7 show the relationships between inverter side active/reactive power and the AC voltage, respectively.

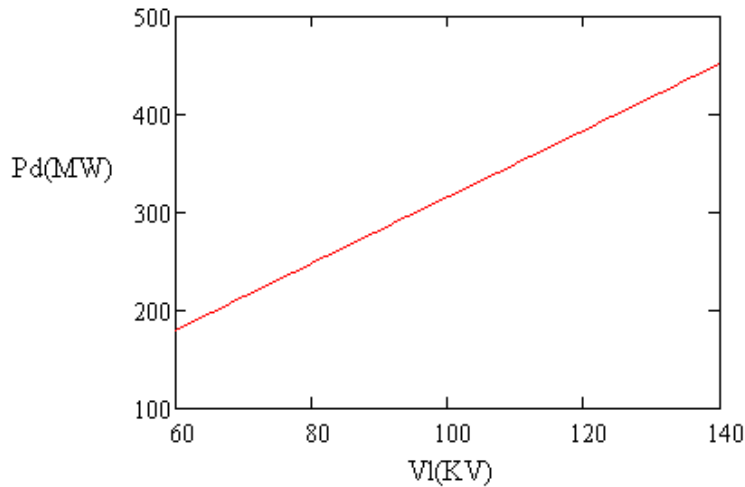


Figure 3. 6: Voltage Dependence of Inverter P of Control Mode 2

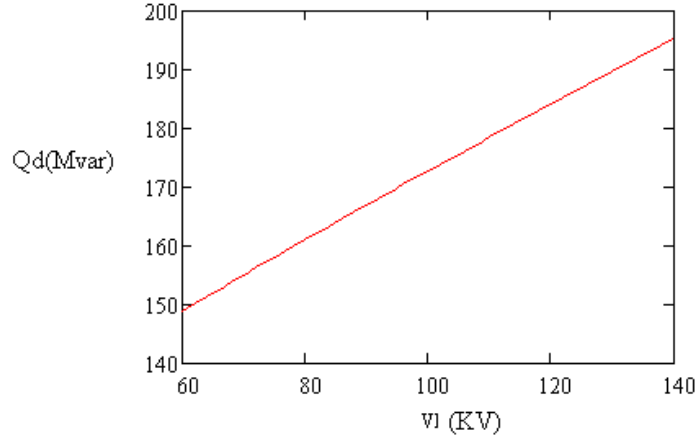


Figure 3. 7: Voltage Dependence of Inverter Q of Control Mode 2

The power factor of the rectifier side is:

$$\cos(\phi_r) = \cos(\alpha) - \frac{X_{cr} I_d}{\sqrt{2} V_{Lr}} \quad (3-16)$$

The DC voltage can be represented by the variables either at the rectifier or inverter side:

$$V_d = \frac{3\sqrt{2}}{\pi} V_{Lr} \cos(\alpha) - \frac{3}{\pi} X_{cr} I_d = \frac{3\sqrt{2}}{\pi} V_{Li} \cos(\gamma) - \frac{3}{\pi} X_{ci} I_d \quad (3-17)$$

Solve $\cos(\alpha)$ from (3-17), we have:

$$\cos(\alpha) = \frac{\sqrt{2} V_{Li} \cos(\gamma) - X_{ci} I_d + X_{cr} I_d}{\sqrt{2} V_{Lr}} \quad (3-18)$$

Substitute (3-18) into (3-16) we obtain:

$$\cos(\phi_r) = \frac{\sqrt{2} V_{Li} \cos(\gamma) - X_{ci} I_d}{\sqrt{2} V_{Lr}} \quad (3-19)$$

Therefore, the reactive power of the rectifier side can be calculated as:

$$Q_{dr} = P_d \tan(\phi_r) = \left(-\frac{3}{\pi} X_{ci} I_d^2 + \frac{3\sqrt{2}}{\pi} V_{Li} \cos(\gamma) I_d \right) \frac{\sqrt{1 - \left(\frac{\sqrt{2} V_{Li} \cos(\gamma) - X_{ci} I_d}{\sqrt{2} V_{Lr}} \right)^2}}{\left(\frac{\sqrt{2} V_{Li} \cos(\gamma) - X_{ci} I_d}{\sqrt{2} V_{Lr}} \right)} \quad (3-20)$$

Figure 3.8 shows the relationship between rectifier side reactive power and AC voltage.

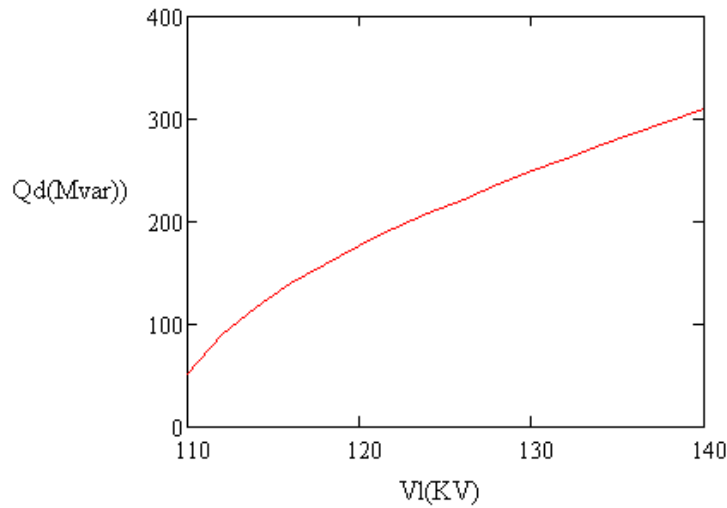


Figure 3. 8: Voltage Dependence of Rectifier Q of Control Mode 2

3.3.3 Control Mode 3: Constant α and Constant I Control

This unlikely control mode only applies when the rectifier is at α_{\min} control. When the rectifier side AC voltage decreases to a certain level, the DC system will be automatically adjusted to a new operating point at which the rectifier controls the firing angle α (called α_{\min} Control) and the inverter controls the current. In this case the DC voltage is linearly determined by the AC voltage as:

$$V_d = \frac{3\sqrt{2}}{\pi} V_{Lr} \cos(\alpha) - \frac{3}{\pi} X_{cr} I_d \quad (3-21)$$

The DC power is a second order function of the DC current:

$$P_d = -\frac{3}{\pi} X_{cr} I_d^2 + \frac{3\sqrt{2}}{\pi} V_r \cos(\alpha) I_d \quad (3-22)$$

The power factor of the rectifier side can be calculated as:

$$\cos(\phi_r) = \cos(\alpha) - \frac{X_{cr} I_d}{\sqrt{2} V_{Lr}} \quad (3-23)$$

The reactive power consumed at the rectifier side can be calculated as:

$$Q_{dr} = P_d \tan(\phi_r) = P_d \frac{\sqrt{1 - \left(\cos(\alpha) - \frac{X_{cr} I_d}{\sqrt{2} V_{Lr}} \right)^2}}{\left(\cos(\alpha) - \frac{X_{cr} I_d}{\sqrt{2} V_{Lr}} \right)} \quad (3-24)$$

Figure 3.9 and Figure 3.10 show the relationships between the rectifier side active power and the AC voltage and the reactive power and the AC voltage, respectively.

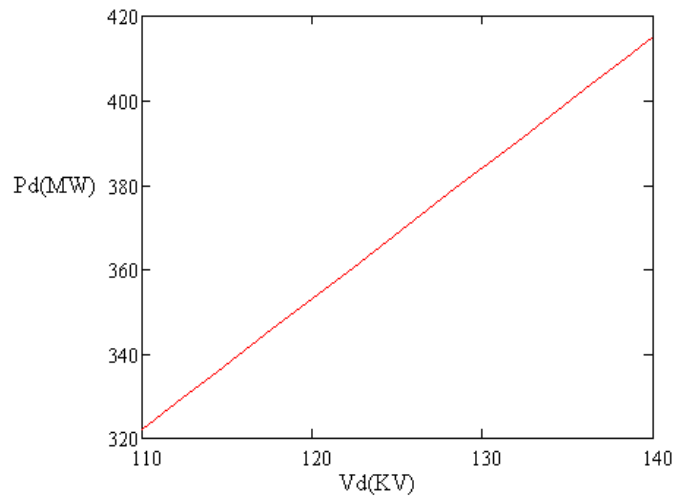


Figure 3. 9: Voltage Dependence of Rectifier P of Control Mode 3

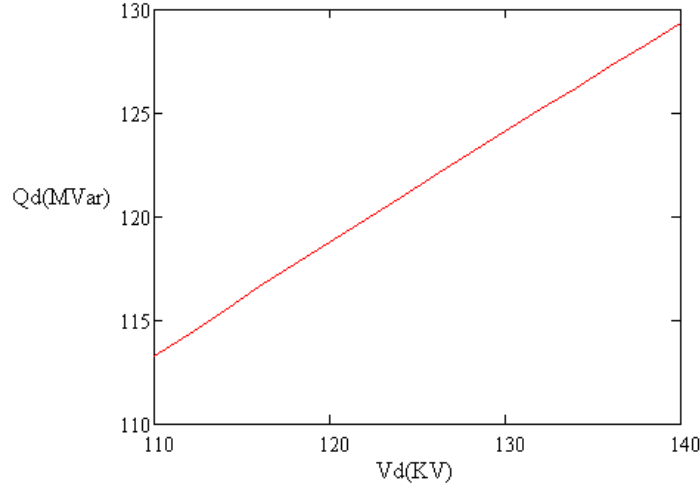


Figure 3. 10: Voltage Dependence of Rectifier Q of Control Mode 3

The power factor of the inverter side is:

$$\cos(\phi_i) = \cos(\gamma) - \frac{X_{ci} I_d}{\sqrt{2} V_{Li}} \quad (3-25)$$

Solve $\cos(\gamma)$ from Equations (3-21) and (3-25):

$$\cos(\gamma) = \frac{\sqrt{2} V_{Lr} \cos(\alpha) + X_{ci} I_d - X_{cr} I_d}{\sqrt{2} V_{Li}} \quad (3-26)$$

The reactive power of the inverter side then becomes:

$$Q_{di} = P_d \tan(\phi_i) = P_d \frac{\sqrt{1 - \left(\frac{\sqrt{2} V_{Lr} \cos(\alpha) - X_{cr} I_d}{\sqrt{2} V_{Li}} \right)^2}}{\left(\frac{\sqrt{2} V_{Lr} \cos(\alpha) - X_{cr} I_d}{\sqrt{2} V_{Li}} \right)} \quad (3-27)$$

Figure 3.11 shows the relationship between inverter side reactive power and the AC voltage.

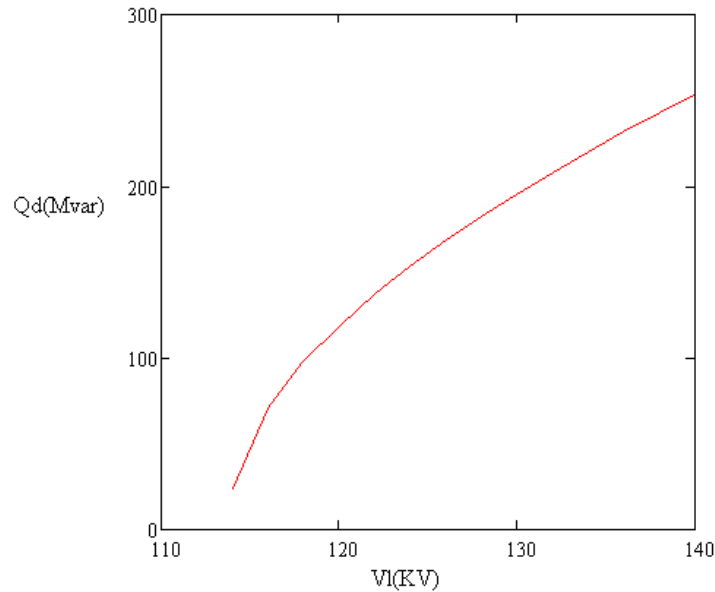


Figure 3. 11: Voltage Dependence of Rectifier Q of Control Mode 3

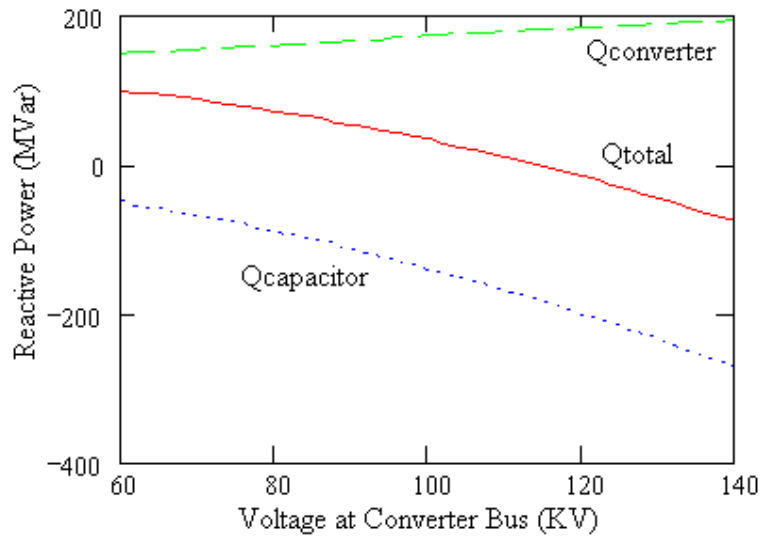
3.3.4 Considering the Capacitor and Filter at the Converter Bus

The results in Figure 3.3 -3.11 show the voltage dependences of the HVDC converters of various control modes. However, the amount of reactive power consumption of an HVDC converter is large, at about 60% of its real power rating. This large amount of reactive power is provided either by the AC system or by the local capacitor or filters. Sometimes most of the reactive power of the HVDC converter is supplied by the local capacitors and filters at the converter bus. Those capacitors and filters are designed specifically to supply reactive power for the HVDC converter. Therefore, it is necessary to consider the HVDC converter and the capacitive equipment as an integral when its impact on AC system voltage stability is examined.

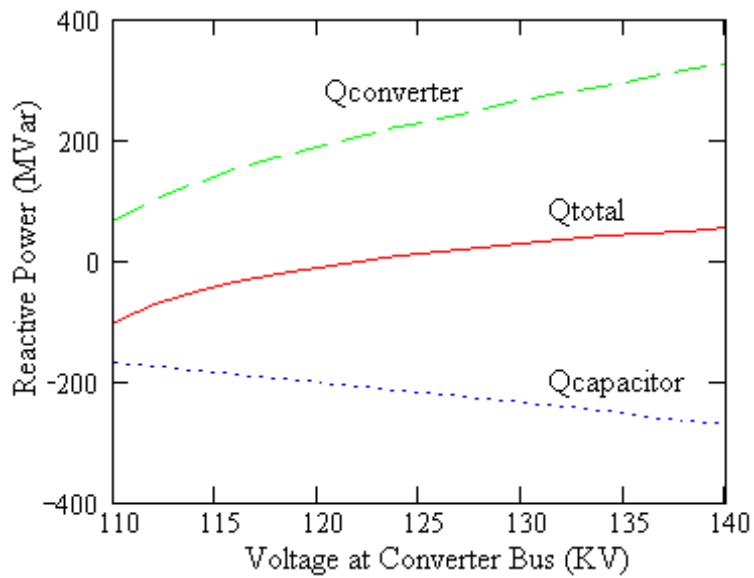
In the worst condition, that all reactive power $Q_{F0}(\approx 60\%P_d)$ is supplied by the capacitors and filters, is assumed, the total reactive power requirement of the converter station can be represented as:

$$Q_{total}(V_L) = Q_d(V_L) - Q_{F0} \left(\frac{V_L}{V_{L0}} \right)^2 \quad (3-28)$$

Equation (3-28) is still a function of AC bus voltage V_L , in which $Q_d(V_L)$ can be in different forms depending on the different control modes and the type of the converter (rectifier or inverter). Figures 3.12 to 3.14 demonstrate the reactive power voltage dependence of HVDC converters in three typical control modes. The curves give some indications of how the converter response would matter from a voltage stability point of view. For example, consider the inverter characteristics of constant γ control at the inverter side and either constant power or constant current control at the rectifier side in Figure 3.12(a) and Figure 3.13(a), it is noted that the Q of the converter by itself drops (become less inductive) as V drops. On the other hand, the total Q of the converter station increases (become more inductive) as the voltage drops. This is unfavorable from a voltage stability point of view.



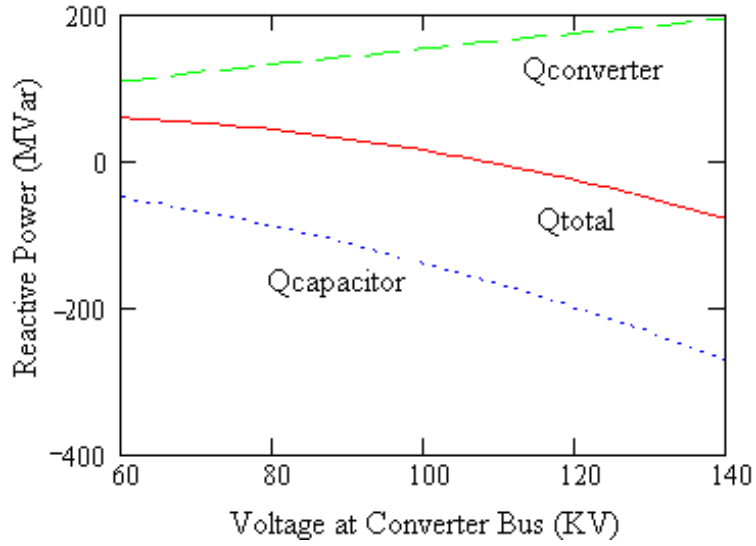
(a)



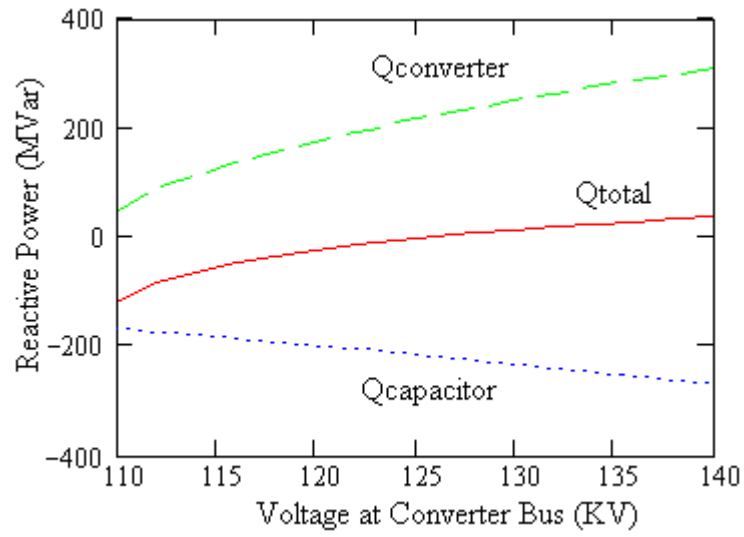
(b)

Figure 3. 12: Reactive Power Voltage Dependence of Control Mode 1

(a) Reactive Power of the Inverter Side (b) Reactive Power of the Rectifier Side



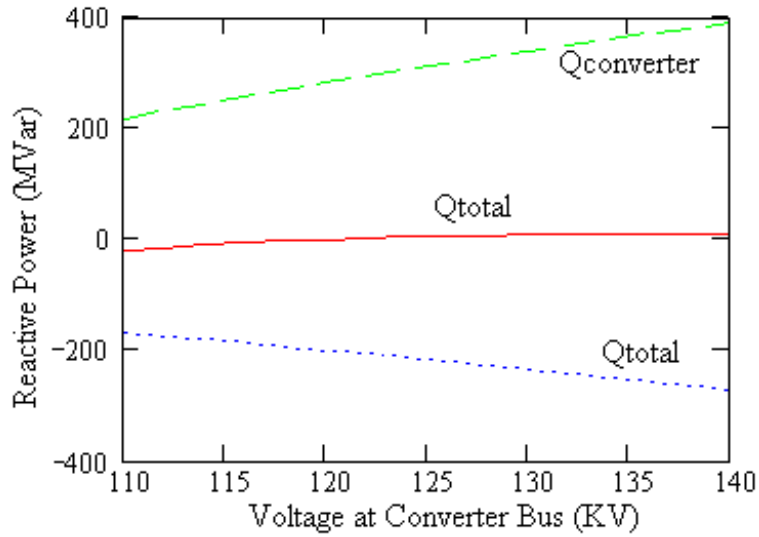
(a)



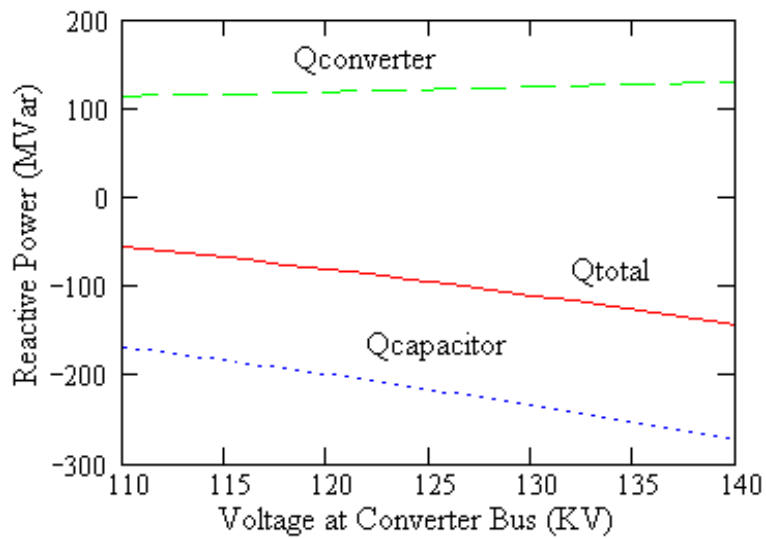
(b)

Figure 3. 13: Reactive Power Voltage Dependence of Control Mode 2

(a) Reactive Power of the Inverter Side (b) Reactive Power of the Rectifier Side



(a)



(b)

Figure 3. 14 Reactive Power Voltage Dependence of Control Mode 3

(a) Reactive Power of the Inverter Side (b) Reactive Power of the Rectifier Side

3.3.5 Summary of Non-linear Load Characteristics of HVDC Converters

The investigation of the reactive power requirement of HVDC converters helps with the understanding of the effects of HVDC converters on AC system voltage stability. It provides a reference for voltage stability prediction in AC systems with HVDC links.

The results of this section can be summarized as the following:

- For some of the operating modes, the total Q increases and the converter station becomes more inductive as voltage drops. This is an unfavorable effect as far as voltage stability is concerned.
- The inverter at control modes 1 and 2, and the rectifier at the control mode 3, demonstrated worse load characteristics than in other control modes in terms of AC system voltage stability.
- The results indicate that the converter that controls the firing angle or the extinction angle experiences a worse situation than the converter that controls power or current.
- The results obtained in this section can be used as HVDC load models and can be included in a load flow or voltage stability program to improve the accuracy of the load modelling of HVDC converters.

3.4 Computation of MPC and MAP

Maximum Power Curve (MPC) and Maximum Available Power (MAP) are widely used in evaluating the transfer capability of HVDC links. Most of the earlier treatments of

MPC and MAP were carried out without including the properties of reactive power compensators. This section investigates the methodology and algorithm for how to properly consider the effects of reactive power compensators in MPC and MAP.

3.4.1 Equations of the HVDC System with Reactive Power Compensation

The Maximum Power Curve (MPC) can be obtained by solving the steady state equations of HVDC systems.

$$V_t = \frac{\sqrt{2}X_c I_d}{T(\cos(\gamma) + \cos(\alpha_L))}$$

$$\cos(\phi) = \frac{\cos(\alpha) - \cos(\gamma)}{2}$$

$$V_d = \frac{3\sqrt{2}}{\pi} V_t \cos(\gamma) - \frac{3}{\pi} X_c I_d \quad (3-28)$$

$$P_d = V_d I_d$$

$$P_d = -\frac{E_s V_t}{X_s} \sin(\delta)$$

$$Q_{comp} = \frac{V_t^2}{X_s} - \frac{E_s V_t}{X_s} \cos(\delta) + P_d \tan(\phi) - \frac{V_t^2}{X_f}$$

Where the variables are defined as:

V_t : Line to line voltage at the AC busbar

X_c : Commutation impedance

I_d : DC current

T : Transformer turns ratio

α : Firing angle of inverter

γ : Extinction angle

φ : Power factor angle of converter AC current

V_d : DC voltage

P_d : DC power

X_f : Impedance of AC filters

E_s : Source voltage of system equivalent

δ : Angle of system equivalent voltage

X_s : System impedance equivalent

Q_{comp} : Reactive power of the compensator

3.4.2 Modelling of Reactive Power Compensators in the MPC Computation

Several approaches can be taken to consider the effects of reactive power compensators on the MPC. The simplest method is to parallel the internal impedance of the compensator to the system equivalent impedance. This modification will reduce the total system impedance so that the SCR increases and the system becomes stronger. Consequently, the MAP will increase. This method has a very clear physical meaning and is very easy to be implemented. However, it ignores the restraining condition that the compensator can only provide reactive power.

In [41] and [45] an improvement was made by adding an extra equation to represent the SC. An extra variable of E_{fd} was included to represent the field winding voltage of the machine. This treatment forces the compensator to inject reactive power only. However,

it does not reflect the fact that the compensator is controlling the V_t to a constant value until its output limits are reached. So the resulting MPC will not depict the same steady state operation curve as that which occurs in the real world.

The approach taken in this section is similar to the PV bus algorithm in load flow computation. At the initial state, the V_t is set to a constant value and Q_{comp} is calculated. If Q_{comp} is within the output limits of the compensator:

$$Q_{min} < Q_{comp} < Q_{max}$$

then V_t is maintained at the set value and the solution continues.

If Q_{comp} is beyond the output limit, for instance

$$Q_{comp} > Q_{max}$$

then Q_{comp} will be set to Q_{max} , and V_t is changing from a constant value (its setting) to a new unknown variable of the equations. In fact, if the compensator reaches its limit, it loses the ability to control the AC bus voltage; therefore, V_t starts to decline. This transition depicts the actual behavior of a compensator in an AC/DC system, which should be represented in the analysis program [46], [47].

After the output limit is reached, a Static Var Compensator (SVC) will become a constant impedance but a Static Condenser (STATCOM) and a Synchronous Condenser (SC) will become constant current sources. The details of this difference can be represented by modifying the Q_{comp} to a voltage-dependent reactive power injection.

For SVCs, the last equation of (3-28) will become

$$\frac{V_t^2}{X_{svc}} = \frac{V_t^2}{X_s} - \frac{E_s V_t}{X_s} \cos(\delta) + P_d \tan(\phi) - \frac{V_t^2}{X_f} \quad (3-29)$$

For STATCOMs and SCs, the corresponding equation will be:

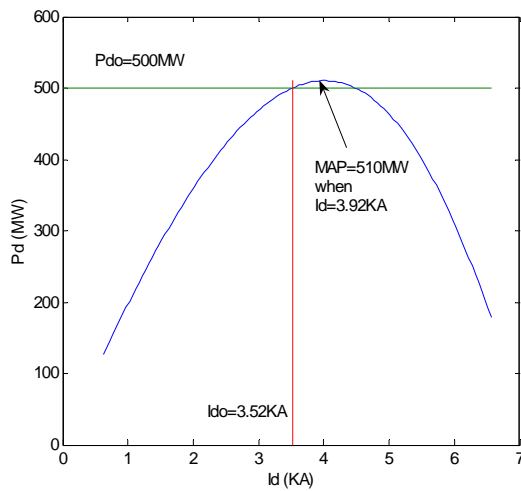
$$V_t I_{comp} = \frac{V_t^2}{X_s} - \frac{E_s V_t}{X_s} \cos(\delta) + P_d \tan(\phi) - \frac{V_t^2}{X_f} \quad (3-30)$$

3.4.3 Numerical Results of MPC with Reactive Power Compensators

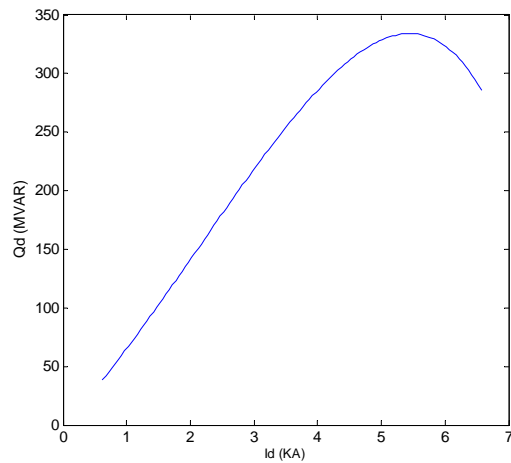
The above algorithm was implemented as a MATLAB program and was tested in a sample back-to-back DC transmission scheme, which is described in Section 3.3. Figure 3.15(a) shows the Maximum Power Curve (MPC) when no compensator is available at the converter bus, and Figure 3-15(b) to Figure 3-15(d) show the corresponding changes of reactive power, AC bus voltage, and DC voltage. The MAP is about 510 MW and it occurs when the DC current is 3.92 KA. It is noted that the operation point with DC current being 3.52 KA and DC power being 500 KW is pretty close to the MAP.

Figure 3.16(a) to Figure 3.16(d) demonstrate the results when a 200 Mvar ideal reactive power compensator is installed at the HVDC converter bus. The MPC in Figure 3.16(a) suggests that the MAP of the HVDC system increases significantly when the reactive power compensator is used. Figure 3.16(b) is the reactive power demand of the HVDC system. Figure 3.16(c) and 3.16(d) represent the transition when the limit of the reactive power compensator is reached. The voltage at the converter bus is kept constant until the output of the compensator increases up to 200 Mvar. In the meantime, the reactive power

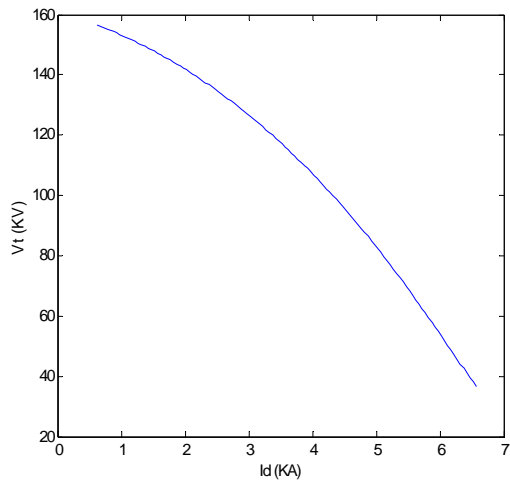
output of the compensator keeps increasing until it reaches 200 Mvar, and then it remains constant at this value. This is the situation of an ideal compensator. In fact, the reactive power of real compensators such as SVCs, STATCOMs, or SCs will decrease along with the bus voltage after the reactive power limits are reached.



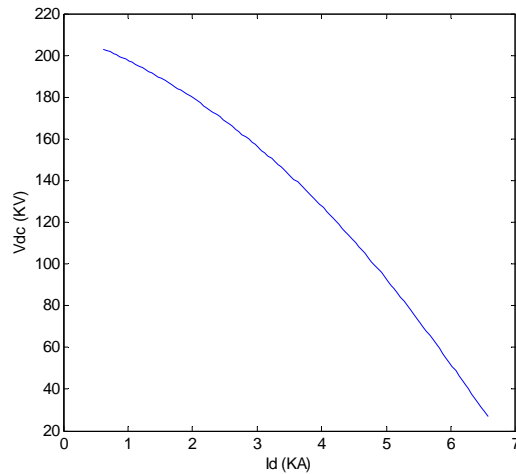
(a) DC Real Power



(b) DC Reactive Power

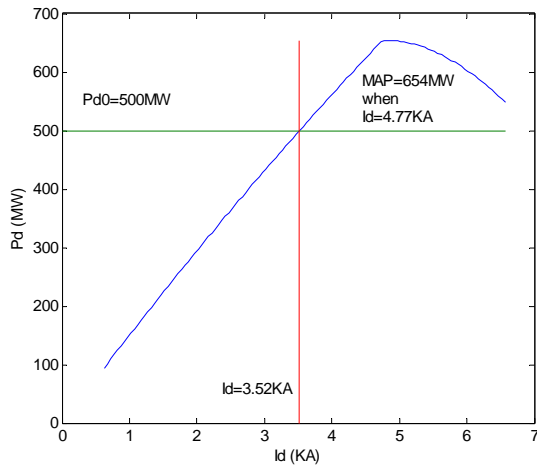


(c) AC Bus Voltage

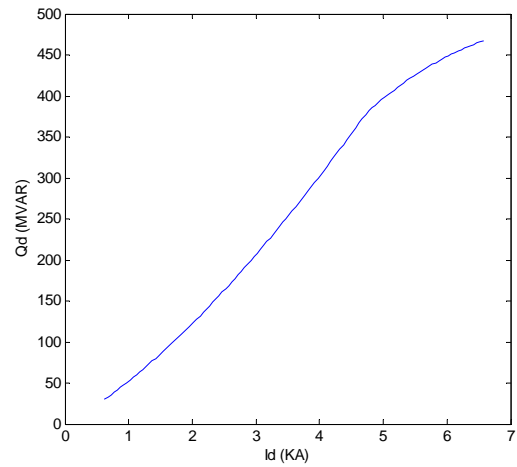


(d) DC Voltage

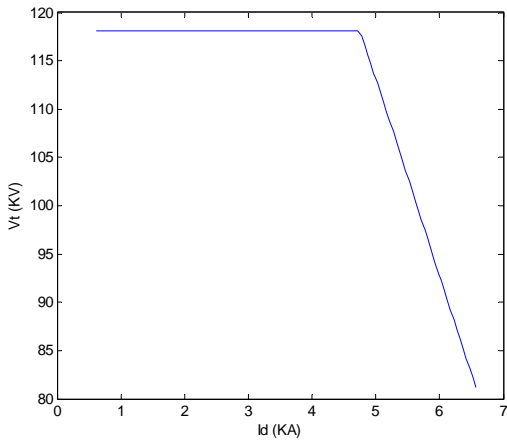
Figure 3. 15: MPC Computations without Reactive Compensation



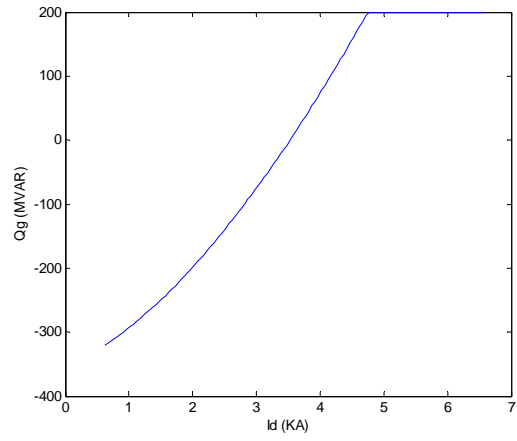
(a) DC Real Power



(b) DC Reactive Power



(c) AC Voltage at Converter Busbar

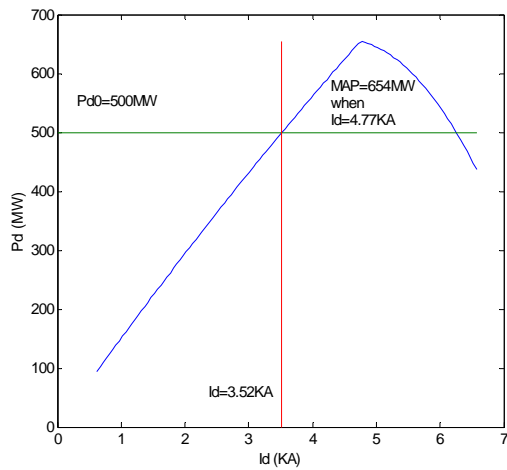


(d) Reactive Power of The Compensator

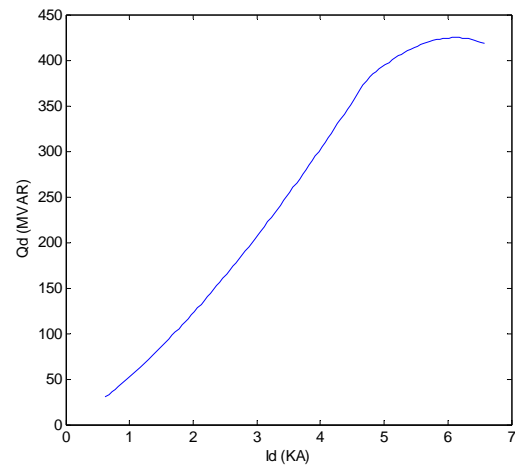
Figure 3. 16: MPC Computations With ideal Reactive Compensation

Figure 3.17(a) to Figure 3.17(d) demonstrate the results when a non-ideal current-limit-type reactive power compensator, either an SC or a STATCOM, is installed at the HVDC converter bus. The results in Figure 3.17 and Figure 3.16 are identical until the reactive power limits of the compensators are reached. Figure 3.17(d) shows that the reactive power output of the compensator declines after the turning point at the reactive power limit, which means the reactive power contribution of the compensator will reduce after

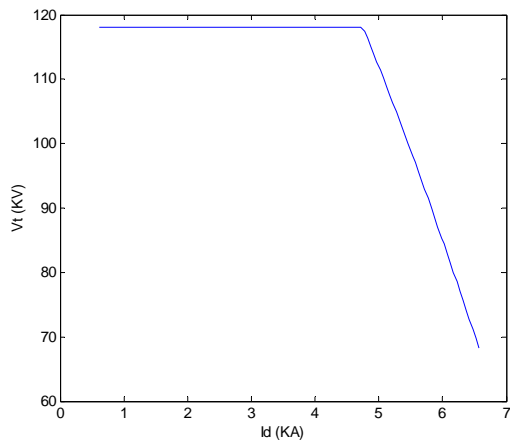
the turning point. This is because the SC and the STATCOM become current sources after they reach the reactive power limit. Therefore, the reactive power output will decline linearly with the decreased voltage. In the meantime, the reduction of reactive power accelerates the reduction of the voltage in a mutually-developing process. As a consequence, the AC bus voltage in Figure 3.17(c) declines faster than in Figure 3.16(c).



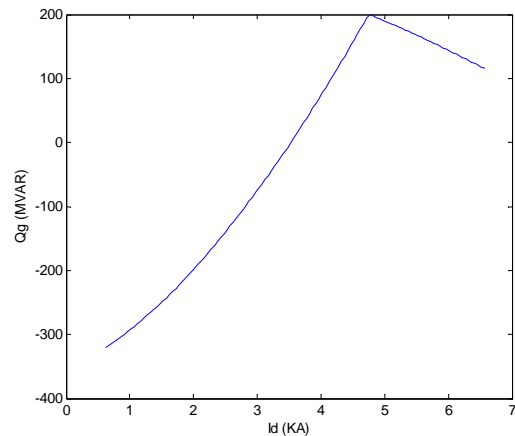
(a)DC Real Power



(b)DC Reactive Power



(c) AC Voltage at Converter Busbar

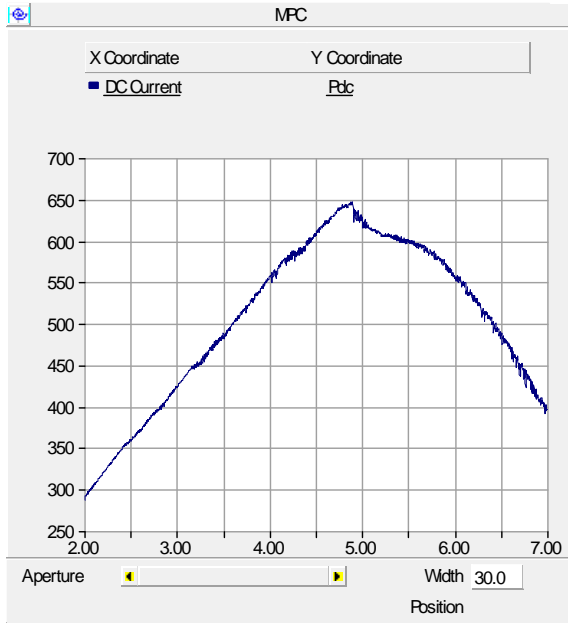


(d) Reactive Power of The Compensator

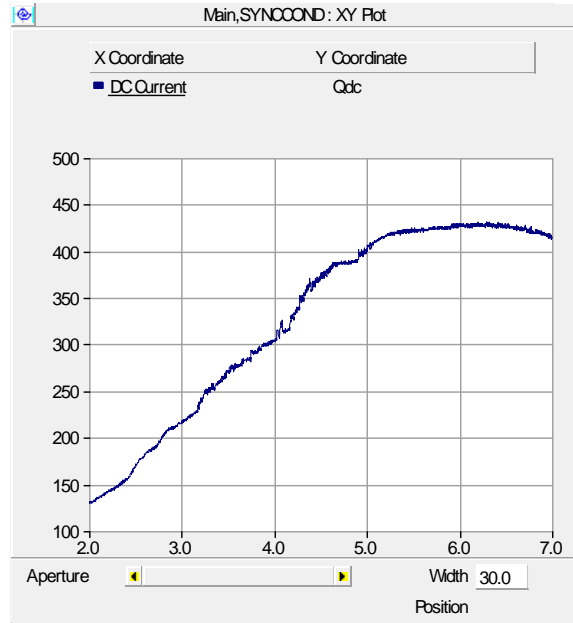
Figure 3. 17: MPC Computations with Non-ideal Reactive Compensation

3.4.4 Validation of the Analytical Algorithm

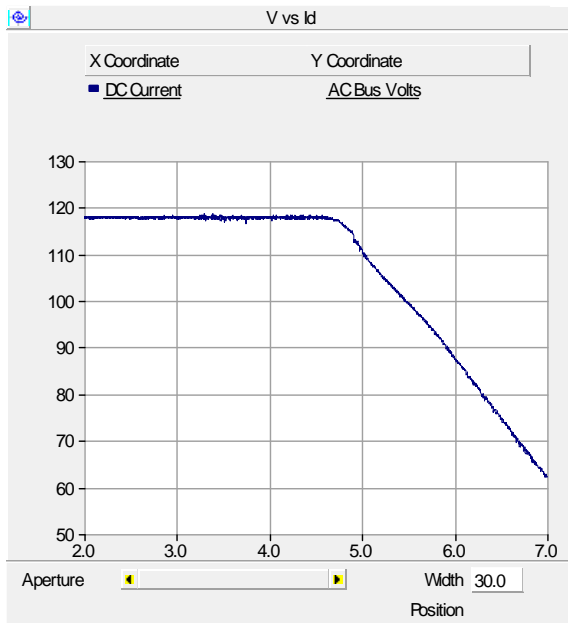
The EMT digital simulation was used to verify the algorithm of MPC and MAP proposed in this section. A simulation case with the same parameters in which a 200 MVA STATCOM was installed at the inverter bus was set up on PSCAD. By gradually increasing the DC current, the DC power, AC voltage, and reactive power of the compensators could be obtained, as in Figure 3.18. The agreement between the results in Figure 3.17 and Figure 3.18 demonstrates that the proposed algorithm in this section is able to calculate the MPC and MAP correctly, as in real AC/DC systems.



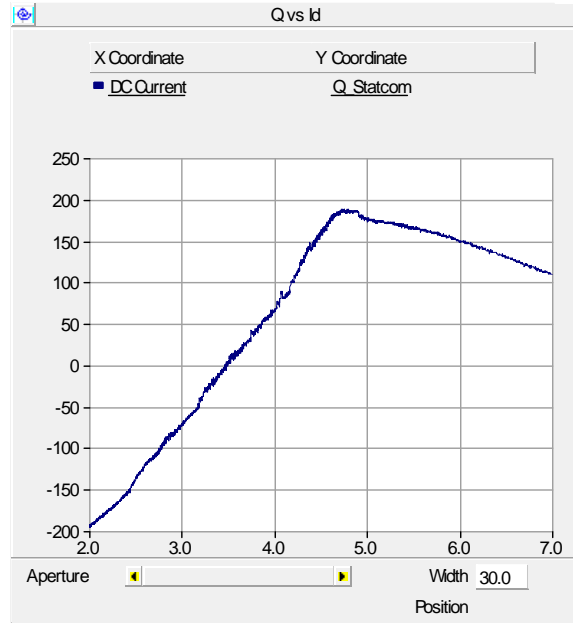
(a) DC Real Power



(b) DC Reactive Power



(c) AC Voltage at Converter Busbar



(d) Reactive Power of The Compensator

Figure 3. 18: MPC Computations by EMT Simulation

3.5 Chapter Conclusions

This chapter investigated the steady state characteristics of reactive power compensation for HVDC systems. The conclusions from this chapter can be summarized as follows:

1. The voltage dependency of the HVDC converter was derived. Understanding the voltage dependency of HVDC systems allows for predictions to be made regarding how HVDC converters impact the AC system voltage stability.
2. An algorithm to calculate the MAP that takes into consideration the reactive power compensation was developed and implemented in MATLAB. The principle of the algorithm is keeping the converter bus voltage to be constant until the reactive power compensators reach their var limits. After the var limits, the different equations are used to model of various reactive power compensators.
3. The computation results in an example case showed the reactive power compensations can significantly increase the MAP. The proposed algorithm was validated by the detail EMT digital simulation on PSCAD.

The following new contributions were made in this chapter:

- The reactive power requirement of HVDC converter station as a function of ac bus voltage was derived.

- The algorithm to calculate the Maximum Power Curve (MPC) and Maximum Available Power (MAP) to including the contribution of dynamic reactive power compensation was developed and the validation of the proposed algorithm was performed by EMT simulation.

Chapter 4: Comparison of the Transient Performance of Reactive Power Compensation Options for HVDC Systems

4.1 Introduction

This chapter investigates the transient performance of different reactive power compensation schemes for HVDC systems. In Chapter 2, the static and dynamic capabilities of various compensators in a simple power system were reviewed. In this chapter, the detailed simulation study is extended to a power system with an HVDC link. This problem has attracted significant interest in the past few decades [14], [16], [17], [50], [51], [41]. Nayak et al [14] investigated the dynamic performance of Synchronous Condensers (SCs) and Static Var Compensators (SVCs) at an HVDC inverter bus in a very weak AC system and obtained results that demonstrated the SCs were preferable to the SVCs in most of the situations examined. This is because of the unfavorable constant impedance property of SVCs after they hit their reactive power limits. Zhuang et al [16], [17] expanded the research of Nayak et al to a nine-level Static Synchronous Compensator (STATCOM). The conclusion was that the STATCOM consistently had equal or better performance under all conditions investigated. More than 10 years have passed since the publication of [14], [16], [17], and it is well-accepted today that advanced compensators based on power electronics devices have much faster response times than conventional SCs. However, to the best of this writer's knowledge,

no STATCOM is being used in a major HVDC system. The understanding of the transient performance of a STATCOM is still limited. The investigation in this chapter attempts to extend the research work of Nayak [14] and Zhuang [17]; more detailed and general studies are conducted to examine the transient behavior of reactive power compensation options for HVDC systems. A more general STATCOM model and the advanced DQ decoupled vector control algorithm are used in the simulation study. In addition, the impacts of reactive power compensations on commutation failures are investigated based on the recently-developed algorithm of commutation failure immunization evaluation [52].

Because the conclusion that an SC is better than an SVC for reactive power compensation at an HVDC converter bus has been clearly made in previous research [14], [16], [17], SVCs will not be included in this chapter. This chapter will focus on a comparison between SCs and STATCOMs only.

4.2 Study System and Reactive Compensators

The study system shown in Figure 4.1 was developed on PSCAD/EMTDC based on the CIGRE benchmark model [54]. In a similar manner to what was done in [14] and [17], the SCR of the inverter side was changed from 2.5 to 1.5 to obtain a situation of a very weak AC system in which more transient problems are potentially arising. The performances of reactive power compensators during fault recovery and temporary

overvoltage (TOV) were studied in the background of an HVDC system connected to a very weak AC system.

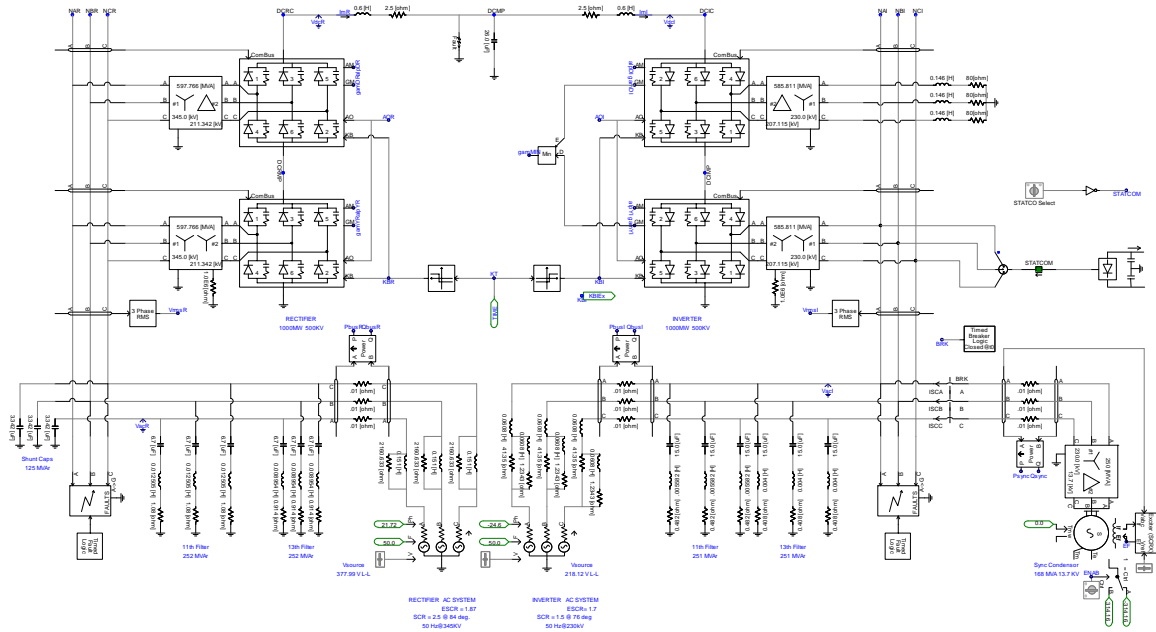


Figure 4. 1: CIGRE Benchmark Model for HVDC Control

A special modification was made in the HVDC control system to insure the proper operation of the control system in the very weak AC system, as shown in Figure 4.2. A ramping rate limit was added in the Voltage Dependent Current Order Limit (VDCOL). This change significantly increases the fault recovery capability of the HVDC system. It also helps in system starting, especially when the connected AC system is very weak.

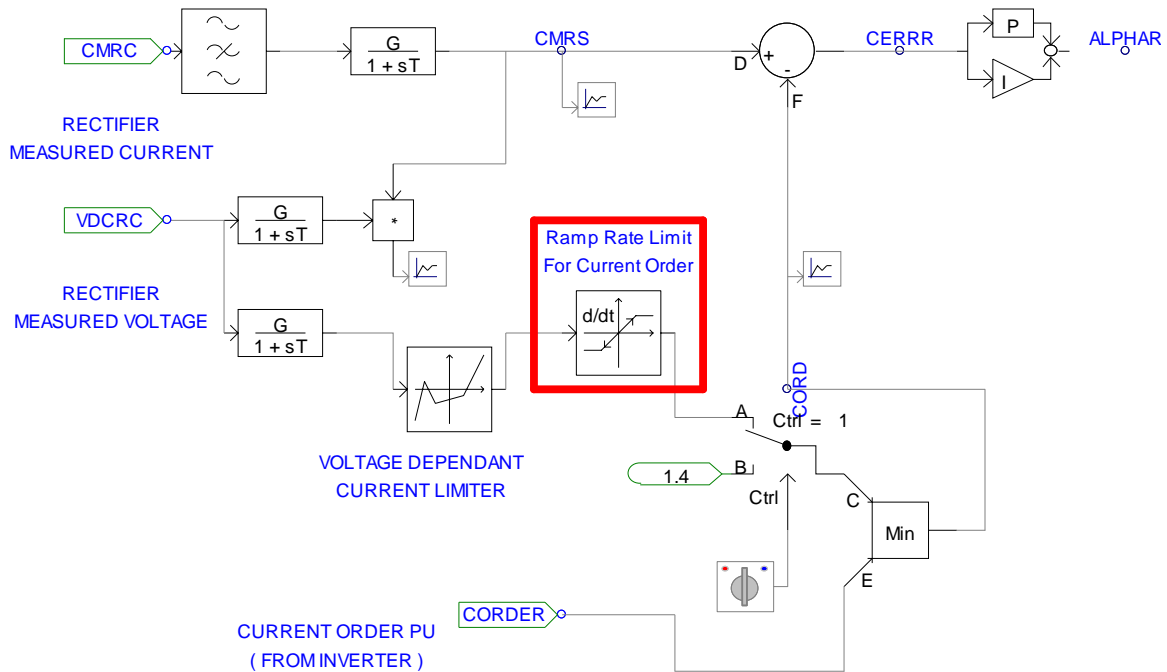


Figure 4. 2: Special Modification on the VDCOL Control Loop

The studies of commutation failure were performed in the CIGRE benchmark system with both the original SCR (2.5) and the modified SCR (1.5).

Both the SC and the STATCOM have a rating of +300/-300 MVA. The SC uses the solid static excitation system, as in Figure 4.3. The ceiling excitation voltage is +6.0/-6.0 per unit.

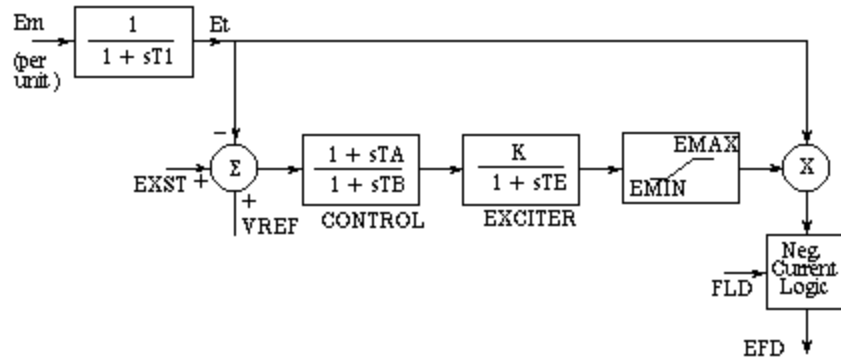


Figure 4. 3: The Excitation and AVR System of the SC

A general Voltage Source Converter (VSC) was used to model the STATCOM in the simulation studies. Its circuit is shown in Figure 4.4. The principle of the STATCOM is to control the terminal voltage by creating a voltage source in phase with the terminal voltage. The in and out of the reactive power is regulated by adjusting the magnitude of the voltage source.

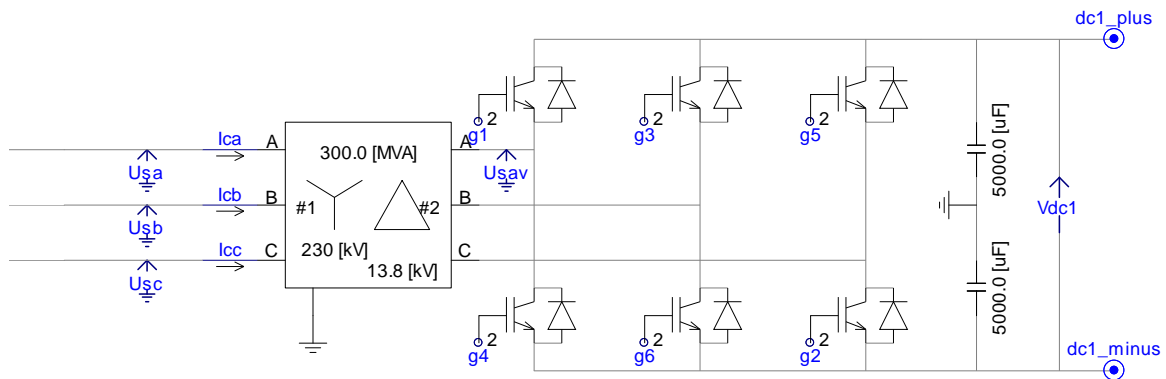


Figure 4. 4: Circuit of a STATCOM

The STATCOM in the simulation studies utilizes a *dq* decoupled control method [9], as shown in Figure 4.5, in which the active power and reactive power are controlled

independently. The PI loop of I_q regulates the capacitor voltage to a constant value by charging and discharging the capacitor voltage. The real power is basically controlled in this loop. The PI loop of I_d regulates the voltage of the controlled bus; in fact, it is the main control loop of the STATCOM. The bus voltage is controlled by adjusting the reactive current order. The limits of the STATCOM can be included by setting the output limit of the PI regulator of the I_d control.

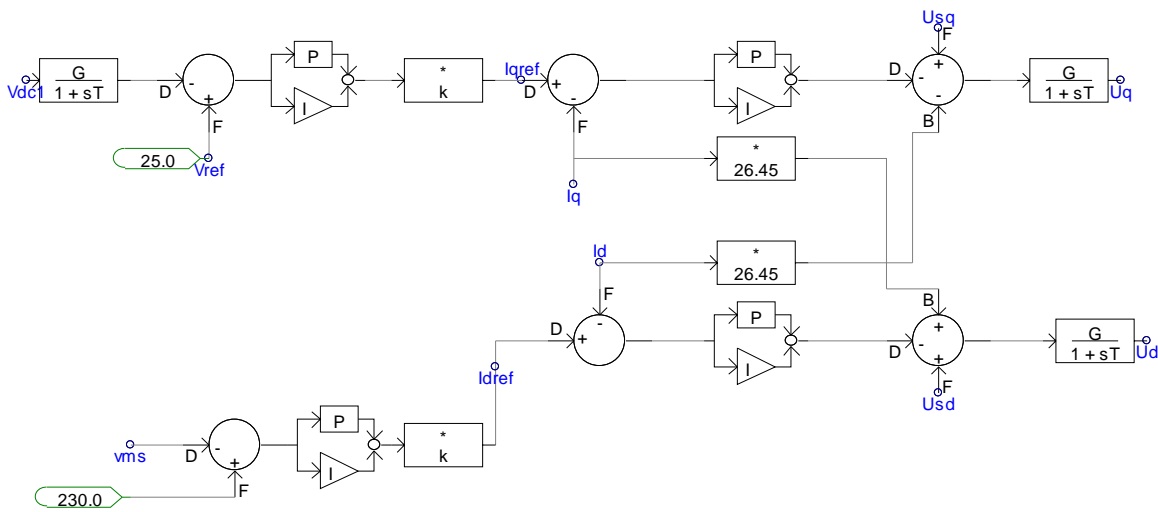


Figure 4. 5: DQ Decoupled Control Diagram of a STATCOM

4.3 Comparison of SCs and STATCOMs in Fault Recovery

The following faults are studied in this section. For the purposes of easy comparison, an identical fault duration of 5 cycles (100ms) was used for all faults.

- Inverter close-in single-phase fault
- Inverter close-in three-phase fault

- Inverter remote single-phase fault
- Inverter remote three-phase fault
- Rectifier single-phase fault
- Rectifier three-phase fault
- DC temporary-fault

DC power recovery time is the time it takes for the DC power to recover to 80% of the pre-fault power after the fault is cleared. The DC power recovery time is often used to evaluate the recovery ability of a DC system during system disturbances. It can also be used to examine the capability of reactive power compensators to improve DC system recovery.

4.3.1 Inverter Close-In Single Phase Fault

Figure 4.6 shows the DC power during a single-phase fault on the inverter bus. The DC power recovery times to 80% of pre-fault power are approximately 0.19 seconds for the STATCOM and 0.23 seconds for the SC. The STATCOM brings a little faster recovery time. Figure 4.7 shows the inverter bus voltage during the faults. The STATCOM controls the voltage back to normal quickly, while SC brings more oscillations and takes much longer to settle down.

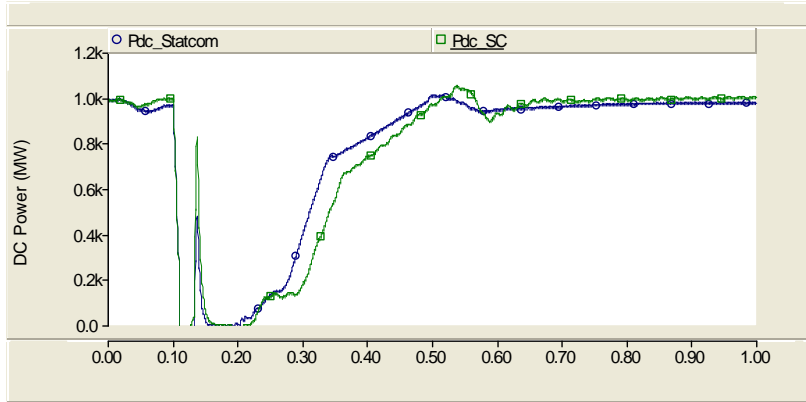


Figure 4. 6: DC Power during an Inverter Close-In Single-Phase Fault

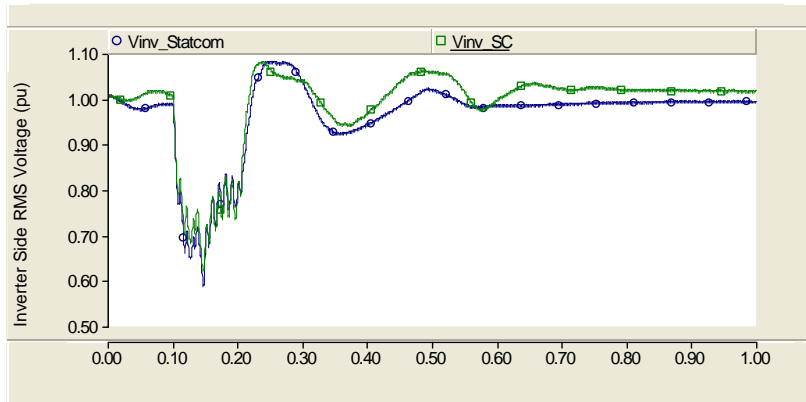


Figure 4. 7: Inverter Bus Voltage during an Inverter Close-In Single-Phase Fault

4.3.2 Inverter Close-In Three-Phase Fault

Figure 4.8 shows the DC power during a three-phase fault on the inverter bus. The DC power recovery time is almost the same for the STATCOM and the SC. When the SC is used the DC power passes the 80% line very slightly faster than when the STATCOM is used, but it exhibits larger oscillations. Figure 4.9 shows that the STATCOM maintains the AC voltage much more effectively than the SC.

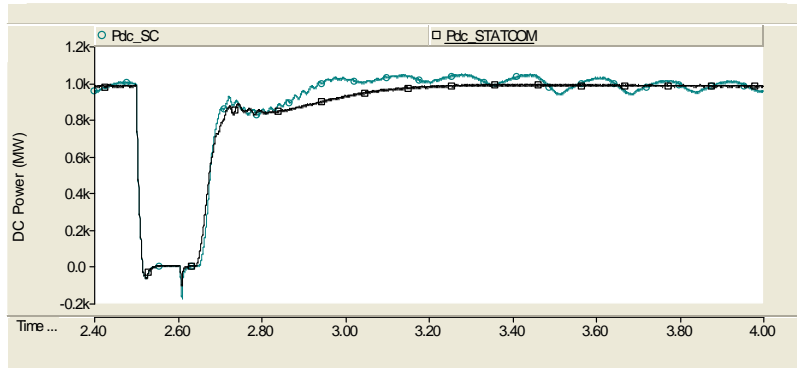


Figure 4. 8: DC Power during an Inverter Close-in Three-Phase Fault

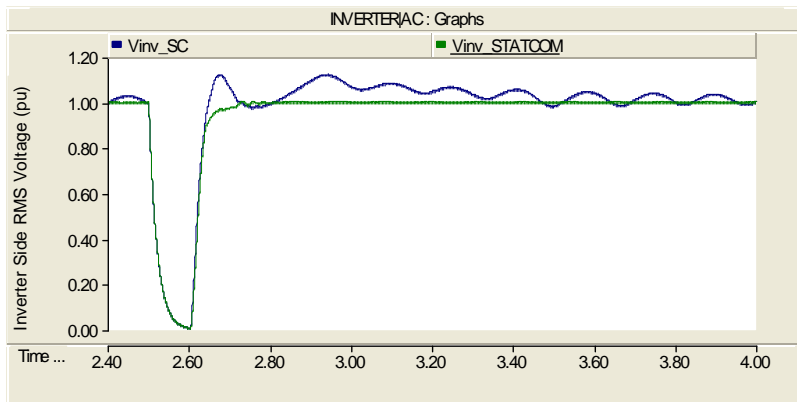


Figure 4. 9: Inverter Bus Voltage during an Inverter Close-in Three-Phase Fault

4.3.3 Inverter Remote Single-Phase Fault

Figure 4.10 shows that the DC power recovery times are about 0.20 seconds for the STATCOM and about 0.23 seconds for the SC. The STATCOM brings about a slightly faster recovery time. Figure 4.12 shows that the STATCOM controls the AC voltage noticeably better than the SC - faster and more accurate.

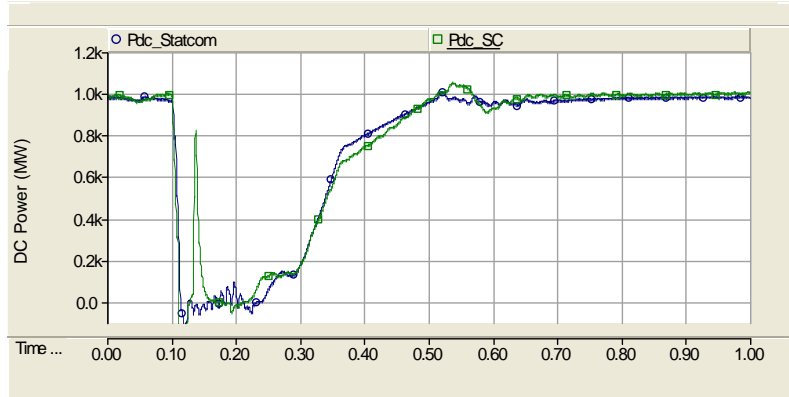


Figure 4. 10: DC Power during an Inverter Remote Single-Phase Fault

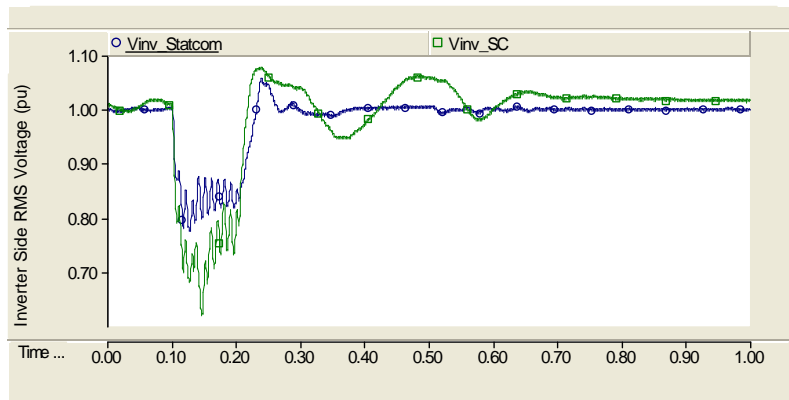


Figure 4. 11: Inverter Bus Voltage during an Inverter Remote Single-Phase Fault

4.3.4 Inverter Remote Three-Phase Fault

The results of remote three-phase faults are very similar to those of close-in three-phase faults. The DC power recovery time is almost identical for the SC and the STATCOM, as shown in Figure 4.12. The STATCOM again demonstrates superior capability in AC voltage control, as shown in Figure 4.13.

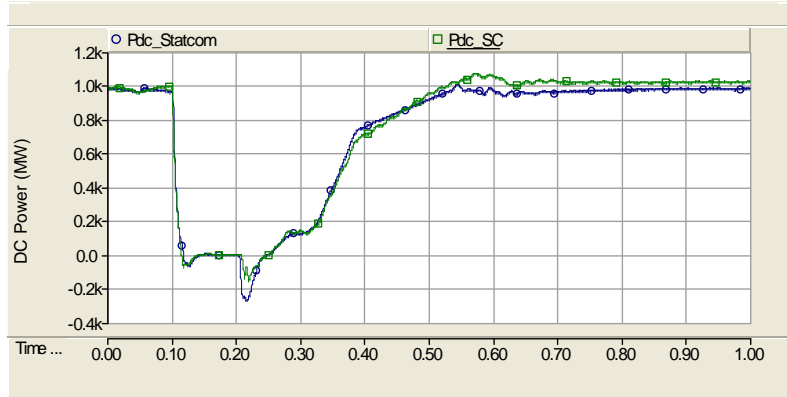


Figure 4. 12: DC Power during an Inverter Remote Single-Phase Fault

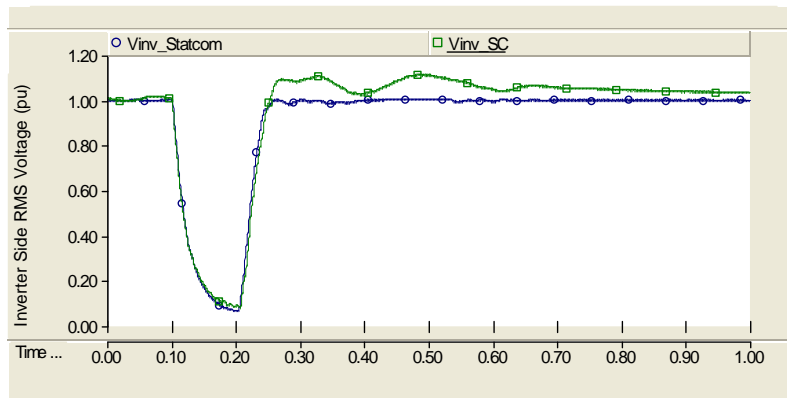


Figure 4. 13: Inverter Bus Voltage during an Inverter Remote Single-Phase Fault

4.3.5 Rectifier Single-Phase Fault

Figure 4.14 shows that the STATCOM and the SC bring about almost identical DC power recovery time. A single-phase fault is not as severe as other faults so the recovery is very fast., The DC power has much less oscillation when a STATCOM is used, which is similar to what occurred during other faults. The rectifier faults and the DC line fault

also cause some Temporary Overvoltage (TOV) problems, which will be discussed in the next section.

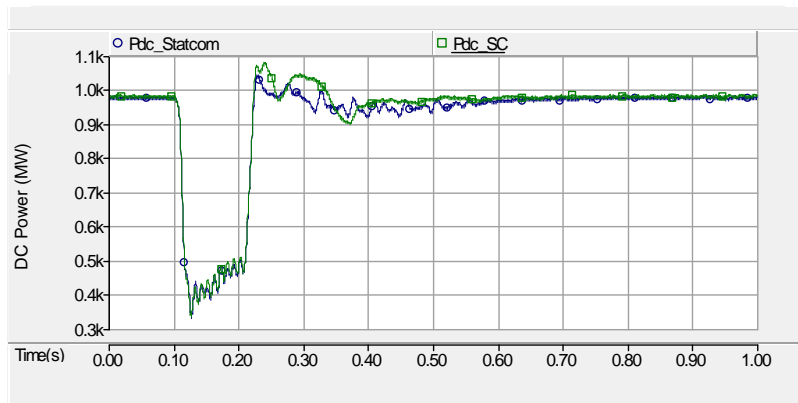


Figure 4. 14: DC Power during an Inverter Close-In Single-Phase Fault

4.3.6 Rectifier Three-Phase Fault

The results of a rectifier three-phase fault are shown in Figure 4.15. The STATCOM exhibits a little advantage over the SC in recovery, but the DC power recovery times to the rectifier-side faults are very similar for both reactive power compensators.

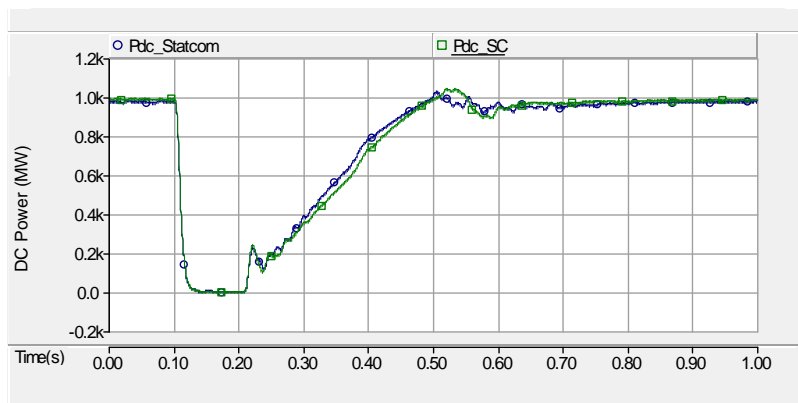


Figure 4. 15: DC Power During an Inverter Close-In Single-Phase Fault

4.3.7 DC Temporary Fault

Figure 4.16 shows the DC power recovery times are approximately 0.27 seconds for the STATCOM and 0.29 seconds for the SC. The performances of the SC and the STATCOM are very close during recovery from a DC temporary fault.

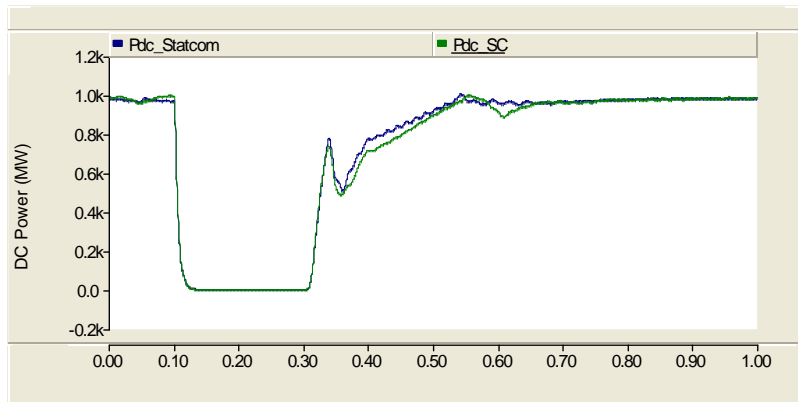


Figure 4. 16: DC Power during an Inverter Close-in Single-Phase Fault

4.3.8 Summary of the Fault Recovery Studies

The performances of the SC and the STATCOM during fault recovery are compared in this section. The simulation results demonstrate that the STATCOM has performance better than or equal to the SC for all the faults studied. The chart in Figure 4.17 shows the DC power recovery times of all the faults for the two compensators, basically summarizing the simulation results presented in this section.

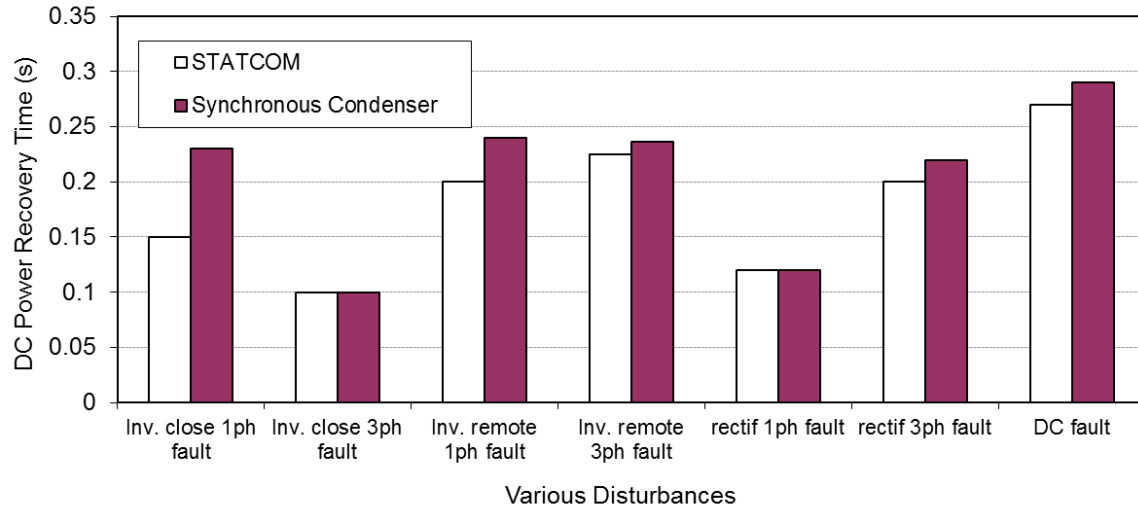


Figure 4. 17: DC Power Recovery Time for Various Disturbances

4.4 Comparison of SCs and STATCOMs in Suppressing Temporary Overvoltage (TOV)

Temporary overvoltage usually happens when disturbances occur on the DC line or at the rectifier side. There are a large number of RLC-based filters at the inverter side that supply a large part of the reactive power of the inverter. If the DC is blocked and the inverter side has no fault, the reactive power of those filters will flow into the AC system, which often causes TOV. When voltage control equipment is not available at the inverter side, the TOV could be very high and could damage the insulation of the equipment. A comparison of the ability of the STATCOM and the SC to suppress TOV will be carried out in this section.

The following disturbances are studied in this section. As in the previous section, identical fault durations of 5 cycles (100 ms) are used for all faults.

- Rectifier single phase fault
- Rectifier three phase fault
- DC temporary fault
- DC permanent block

4.4.1 Rectifier Single-Phase Fault

The inverter side AC RMS voltages during a rectifier-side single-phase fault are shown in Figure 4.18. Both the STATCOM and the SC can keep the voltage pretty low. The highest RMS voltage for the SC was 1.06 and the highest RMS voltage for the STATCOM was 1.02. Basically, there is no TOV issue to be concerned for this type of fault.

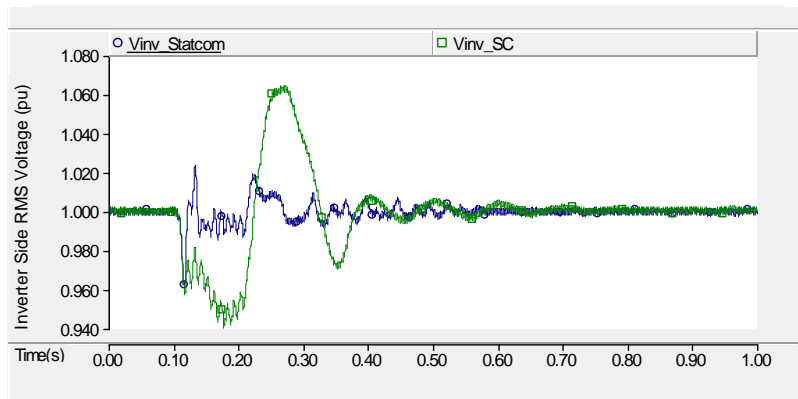


Figure 4. 18: Inverter Bus Voltage during a Rectifier Single-Phase Fault

4.4.2 Rectifier Three-Phase Fault

The TOV during a rectifier three-phase fault is a little more severe, as shown in Figure 4.19. The high RMS voltages are 1.16 p.u. for the SC and 1.09 p.u. for the STATCOM. The STATCOM again demonstrates its advantage in voltage control.

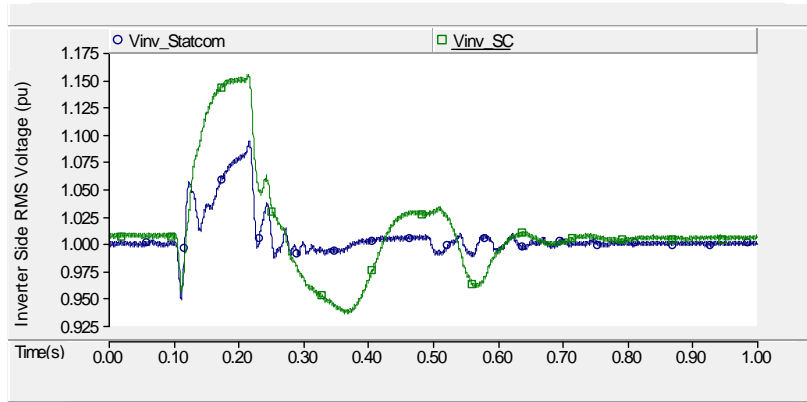


Figure 4. 19: Inverter Bus Voltage during a Rectifier Three-Phase Fault

4.4.3 DC Temporary Fault

A DC line fault will cause the DC to be blocked for a short period of time. As shown in Figure 4.20, the levels of TOV with the SC and the STATCOM are similar to those that occur during rectifier-side three-phase faults. The STATCOM demonstrated better ability than the SC in controlling TOV.

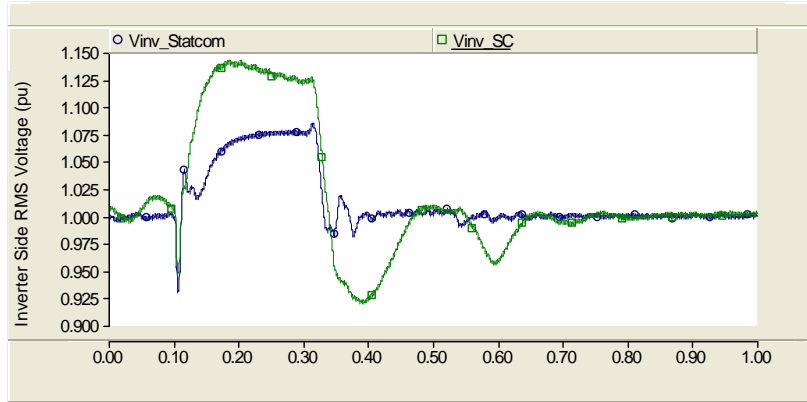


Figure 4. 20: Inverter Bus Voltage during a DC Temporary Fault

4.4.4 DC Permanent Block

A DC permanent block is the most severe case regarding TOV. Figure 4.21 shows that the highest RMS voltages reach 1.12 p.u. with the SC and 1.06 p.u. with the STATCOM. The STATCOM again demonstrated its excellent voltage control ability.

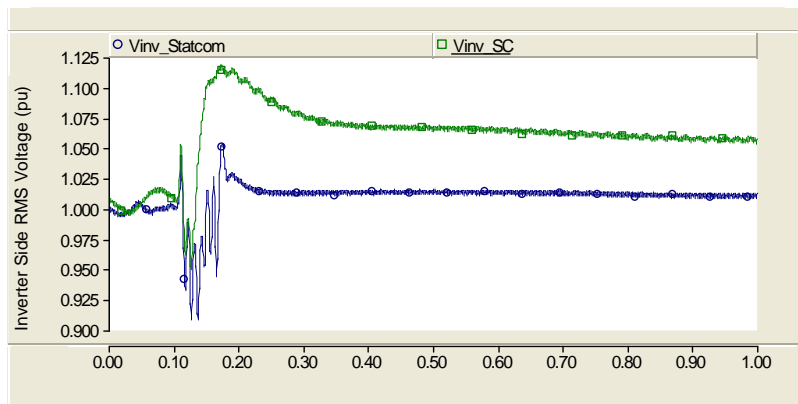


Figure 4. 21 DC Permanent Block

4.4.5 Summary of the TOV Studies

The comparison of the ability of the SC and the STATCOM to suppress TOV is summarized in Figure 4.22. The results support the conclusion that both are able to limit the overvoltage significantly, but the STATCOM is better at voltage control.

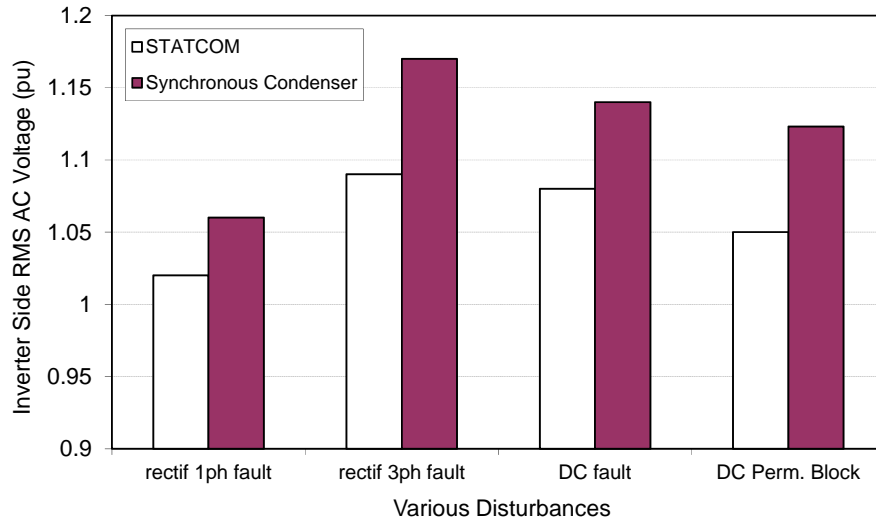


Figure 4. 22: TOVs for Various Disturbances

4.5 Comparison of SCs and STATCOMs in Resisting Commutation

Failure

A commutation failure is a typical adverse dynamic event in an HVDC system. It is most often caused by ac fault induced voltage reduction. The consequences of a commutation failure can be interruption of power transmission, stresses on the valve equipment, or triggering of more severe transients, such as system resonances that can lead to a longer duration of power curtailment. Therefore, it is important to increase the ability of HVDC systems to resist commutation failures.

4.5.1 Commutation Failure Immunity Index (CFII)

A previous publication [52] proposed an index to quantify the capability to resist commutation failure called the Commutation Failure Immunity Index (CFII). As shown in Figure 4.23, the CFII is calculated by applying three-phase inductive faults at the inverter bus with electromagnetic transient simulation.

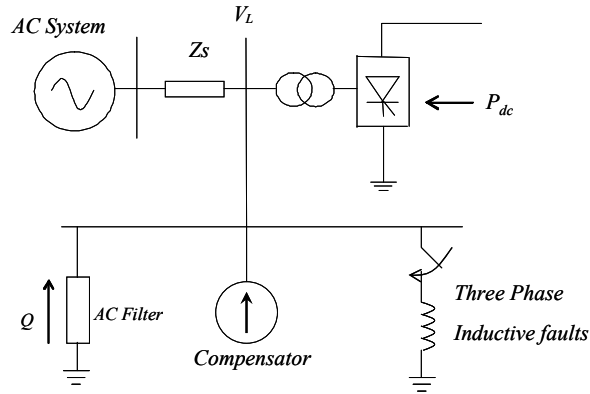


Figure 4. 23: Illustration of CFII Computation

By varying the value of the fault inductance using the multiple run function in PSCAD, the smallest possible fault inductance L_{\min} that does not result in a commutation failure can be obtained, regardless of the point on wave when the fault was applied. CFII has been defined as given in (4-1):

$$CFII = \frac{\text{Worst Critical Fault MVA}}{P_{dc}} \cdot 100 = \frac{V_{ac}^2}{\omega \cdot L_{\min} \cdot P_{dc}} \cdot 100 \quad (4-1)$$

Under this definition, the CFII for the CIGRÉ benchmark system with the SCR of 2.5 is calculated to be 13.3%.

The implementation of the CFII computation is through the multiple runs function of PSCAD. Two variables are changed during the simulation: the size of fault inductance and the fault point on wave, For instance, we can change the inductance from 12.5% to 20% and change the point-on-wave from 0 to 180 degree, and carry out a total of 6000 simulation runs. The multiple runs can record the fault inductance MVA and a 1/0 index for whether or not the fault causes a commutation failure. By observing the fault inductance with the smallest value that does not cause a commutation failure, the CFII can be determined.

A byproduct of multiple runs is the mean value of all the 1/0 indices for commutation failure, which reflects the probability of commutation failure among all the 6000 computation cases. It is natural to think the smaller mean value indicates the lesser chance of commutation failure in all possible fault conditions. Rahimi et al [53] introduced an index of commutation failure probability that is referred to here as the Commutation Failure Probability Index (CFPI). The definition of CFPI is given in (4-2), and it will be used as an auxiliary index together with the CFII to investigate the commutation failure problem.

$$CFPI = \frac{\text{Number of case with commutation failure}}{\text{Total Number of Case in The Multiple Run}} \quad (4-2)$$

4.5.2 Comparison of the Impact of the SC and the STATCOM on the CFII

The algorithm to calculate the CFII was implemented on PSCAD. Two test cases were used to compare the impact of an SC and a STATCOM on the CFII. The index of CFPI

was also calculated to provide more information for the comparison. The results of the multiple-run simulation are as follows.

4.5.2.1 Case 1- CIGRE Benchmark Case with a Normal SCR (2.5)

The original CIGRE benchmark case was modified by adding an SC and a STATCOM, each rated at 300 MVA. The SCR of the case was 2.5, which is often considered to indicate a strong system. The simulation results are listed in Table 4.1. The results of fixed capacitor compensation are also listed as a reference for comparison. The CFII result of fixed capacitor compensation is consistent with the result in [52], which validates the basic setting of the simulation case. The results show that the SC and the STATCOM increase the resistance of the HVDC system against commutation failures. The SC brings a slightly larger CFII while the STATCOM brings a smaller CFPI. This means the SC is a little stronger than the STATCOM in helping the immunity of the HVDC system against commutation failure, but there is very little difference between the two compensators. The STATCOM is better than the SC in reducing the probability of commutation failure in the overall range of all test cases.

Table 4. 1: Comparison of an SC and a STATCOM in a Normal AC/DC System

Various Compensation Options	CFII	CFPI
Fixed Capacitor	13.25	0.6172
Synchronous Condenser	16.75	0.2812
STATCOM	16.25	0.1549

4.5.2.2 Case 2 - CIGRE Benchmark Case with a Lower SCR (1.5)

The SCR of the CIGRE benchmark case was changed to 1.5 to create the situation of an HVDC system connected to a very weak AC system. The same calculation was carried out. The results listed in Table 4.2 are similar as those of case 1. The CFII is identical for the SC and the STATCOM while the SC is slightly better in decreasing the CFPI.

Table 4. 2: Comparison of an SC and a STATCOM in a Very Weak AC/DC System

Various Compensation Options	CFII	CFPI
Fixed Capacitor	8.5	0.4855
Synchronous Condenser	13.25	0.1103
STATCOM	13.25	0.1146

4.5.3 Summary of Commutation Immunity Studies

The general impression is that the SC and the STATCOM can increase the capability of the HVDC system against commutation failure, and that the performance difference between these two compensation options is not significant. This is in contrast to the SVC, which was reported in [14] to have poor performance against commutation failures.

4.6 Chapter Conclusions

This chapter investigated the transient performances of reactive power compensation options for HVDC systems based on the simulation of the CIGRE Benchmark HVDC System. The conclusions from this chapter can be summarized as the following:

1. The STATCOM has performance equal to or slightly better than the SC in improving HVDC system fault recovery
2. The STATCOM has significantly better performance than the SC in suppressing TOV
3. Both the SC and the STATCOM can increase the capability of the HVDC system to resist commutation failures, but the difference between the two compensation options is not significant.

The following contribution is made in this chapter:

- The performance of the SC and the STATCOM in reducing commutation failure susceptibility of HVDC systems was compared based on EMT simulation study. The results showed that the capabilities of the SC and the STATCOM in preventing commutation failure are very similar.

Chapter 5: The Concept of System Strength when Dynamic Reactive Power Compensators are Connected to the Converter Bus

5.1 Introduction

The interaction between the AC and the HVDC is one of the major concerns in AC/DC power systems. The significance of the interaction is largely dependent on the strength of the AC system at the converter bus. The strength of an AC/DC power system is a useful index to predict the interaction between the AC and HVDC systems.

Short Circuit Ratio (SCR) is the index most widely used to describe the strength of an AC/DC power system. It is defined as the short circuit MVA expressed in per unit of DC power. SCR has been successfully used to quantify the strength of power systems without dynamic reactive power compensators at the HVDC converter bus. In earlier work, the concept of Effective Short Circuit Ratio (ESCR) was used when filters were considered. The SCR and the ESCR are good indicators of system performance for systems without dynamic reactive power compensators. However, the definitions in (3.1) and (3.2) are not directly applicable for power electronic based reactive power devices as they only consider the system impedance and filter impedance. As we described in chapter 1, there

are several types of reactive compensation devices, which can be classified into three major categories; Synchronous Condensers (SCs), Static Var Compensators (SVCs), and Static Synchronous Compensator (STATCOMs). The SC is the most mature, most widely-used reactive power compensator. It offers the additional advantage in increasing the Short Circuit Ratio (SCR) because it is a real rotating machine. It is fairly straightforward to consider the contribution of the SC to the SCR by paralleling the X_d' or X_d'' with the system equivalent impedance [20]. By forcing the active power output to zero, the effects of the SC on the SCR can be represented in a more accurate way [45]. When an SVC or a STATCOM is connected to the converter bus, it provides extra support to the bus voltage and makes the AC system stronger [14], [17]. However, these devices are not rotating machines so they do not increase the short-circuit level at the converter bus. If a conventional SCR is used to evaluate the AC system strength, the contribution of these compensators will be missed. Therefore, new indices are required to quantify the strength of an AC/DC system that uses those modern reactive power compensators.

This chapter investigates the contributions of dynamic reactive power compensators and develops a new concept for system strength. The system is considered 'strong' when MAP is high, the load rejection voltage at the converter bus is low, commutation failure probability is low, and recovery from faults is fast. Indices that capture the above behaviors are, therefore, derived instead of simply one SCR. The steady-state and dynamic performances of reactive power compensators in HVDC systems have been studied in Chapter 3 and chapter 4 of this thesis. In this chapter a series of new indices

will be developed based on the results obtained in the previous chapters. It is hoped that the new indices can be used as a new evaluation methodology to quantify the system strength that gives proper consideration of dynamic reactive power compensators. The new evaluation method will be demonstrated by the example cases described in Section 3.4 and Section 4.1.

5.2 Apparent Short Circuit Ratio Increase

In order to consider the contribution of dynamic reactive power compensators to the system strength, a new evaluation system needs to be developed to replace the traditionally-used index, the SCR. In previous chapters it was proved that the dynamic reactive power compensators can significantly increase the Maximum Available Power (MAP) and the Commutation Failure Immunity Index (CFII), and decrease Fault Recovery Time and Temporary Overvoltage (TOV). It is known that the compensators can make a weaker system with a lower SCR behave as a stronger system with a higher SCR would. However, the higher SCR is not a real physical concept; we call it Apparent SCR. The difference between the actual SCR and the apparent SCR is an interesting concept that indicates the contribution of the dynamic reactive power compensator to system performance. We define this difference as the Apparent Short Circuit Ratio Increase (ASCRI) and will use it as new index to quantify the system strength change brought about by reactive power compensators.

It should be noticed that ASCRI is an index based on the system performance. There are different types of performance of HVDC systems during different operating and fault circumstances. Depending on which performance index is considered, the ASCRI could be different. For instance, a certain type of compensator may be very strong in increasing CFII but not very strong in Maximum Available Power (MAP). Therefore, unlike a single index such as SCR, the ASCRI should be evaluated based on various conditions.

The following performance indices are used to evaluate the ASCRI in this chapter:

- Maximum Available Power (MAP)
- Commutation Failure Immunity Index (CFII)
- Fault Recovery Time
- Temporary Over-Voltage (TOV)

5.3 Apparent Short Circuit Ratio Increase Based on MAP

The computation of MPC and MAP when reactive power compensators are connected on the inverter bus has been discussed in Section 3.4. From Equations (3-28), (3-29), and (3-30), we know the MAP is affected by several factors, such as the size of the reactive power compensator and the system short circuit ratio (SCR). If the capacity of the compensator increases, the ability to support the AC bus voltage will increase accordingly. Thus the MAP will increase, as shown in Figure 5.1. System short circuit ratio (SCR) is another factor that can be used to determine the MAP. If the system SCR

increases, the system becomes stronger, and apparently the MAP will increase. The changing of MAP versus the changing of SCR is displayed in Figure 5.2.

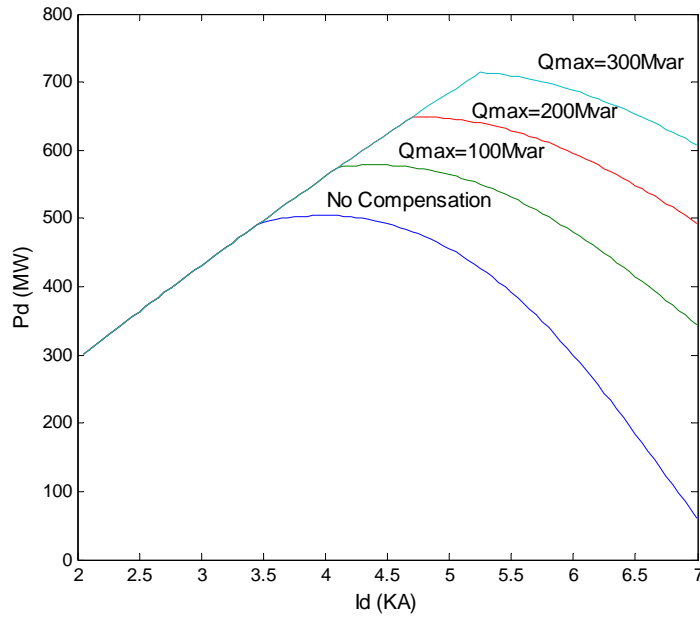


Figure 5. 1: MPC with different Compensator Capacity

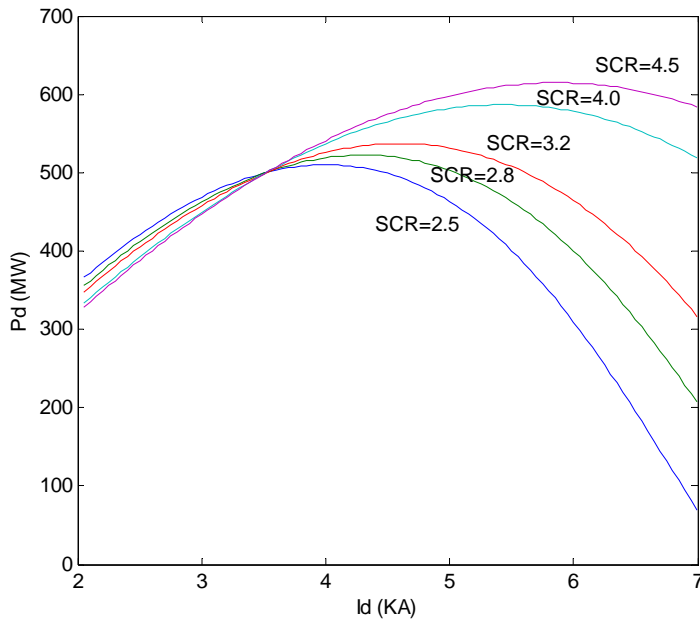


Figure 5. 2: MPC with different SCR

Figure 5.1 and Figure 5.2 demonstrate the relationship between MAP, SCR, and compensation capacity. It is likely that there are correlations between those three variables. Regarding achieving a higher MAP, installing the compensator has a similar function as increasing the SCR. In other words, by installing the reactive power compensator the weaker system can deliver the same power as the stronger system. In a sense, reactive power compensators do strengthen the system.

It would be very interesting if we can quantify the effects of reactive power compensation based on the results of MAP. By employing a number of mathematical treatments, we find the relationship between the ideal compensation capacity and the MAP-based Apparent SCR Increase (ASCRI) to be that shown in Figure 5.3. We call this new index ASCRI-M. The horizontal axis is the compensation capacity and the vertical axis is the ASCRI-M, which indicates the amount of SCR increase that brings the same amount of MAP increase by the compensator. This curve tries to answer an interesting question: How can the SCR be calculated when a reactive power compensator is installed? ASCRI-M reflects the contribution of reactive power compensation to AC system strength quantified by the maximum available power of the HVDC system.

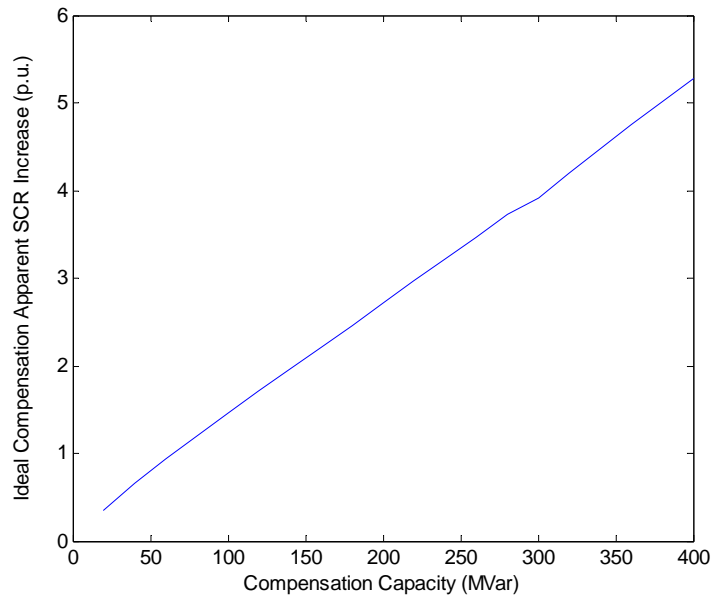


Figure 5. 3: Correlations between Compensation Capacity and Equivalent SCR Increase

The ASCRI-M of non-ideal compensators can be obtained by using similar methods. The effects of increasing SCR by the use of different compensators can be compared by plotting the curves together, as in Figure 5.4. The results show that the differences of the three types of compensators are visible but not significant. This phenomenon indicates that regarding the steady state stability issue, the performances of different types of compensators are very close. The studies in this section indicate that steady-state performance should not be a major concern when choosing a reactive compensator for an HVDC system.

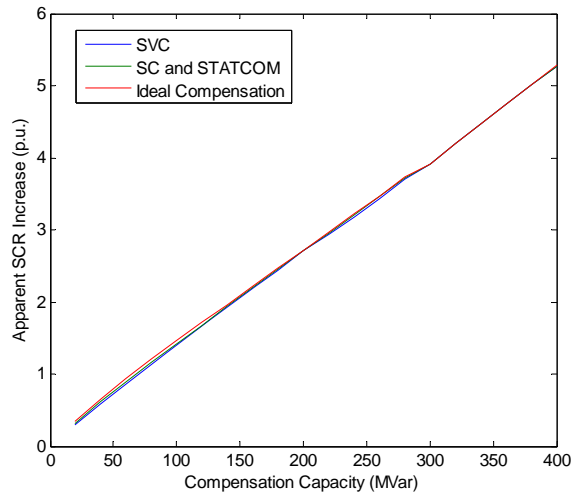


Figure 5. 4: Comparison of the ASCRI-M of different Reactive Power Compensators

5.4 Apparent Short Circuit Ratio Increase Based on the CFII

The concept and the implementation procedure of the CFII have been discussed in Section 4.5. The relationship between the CFII and the SCR can be obtained by changing SCR values and then conducting the simulations. Figure 5.5 demonstrates that the CFII increases almost linearly when the SCR varies from 1.5 to 4.5.

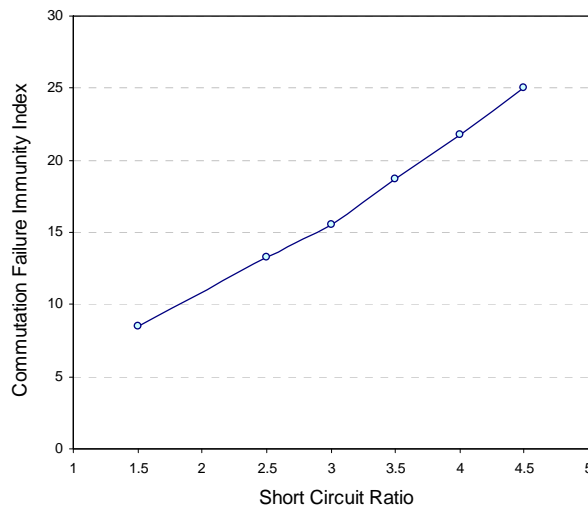
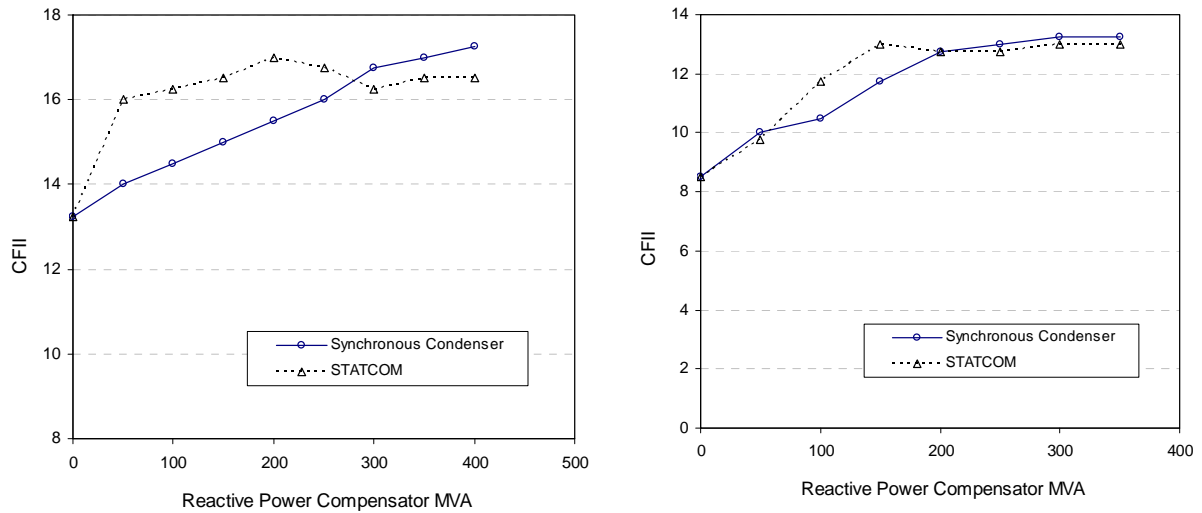


Figure 5. 5: Relationships between the CFII and the SCR for a System without Compensation

Further simulation studies were performed to examine the impact of SCs and STATCOMs of different sizes on the CFII in the CIGRE Benchmark system with the SCR at 1.5 and 2.5. The results are shown in Figure 5.6 (a) and (b).



(a) SCR = 2.5

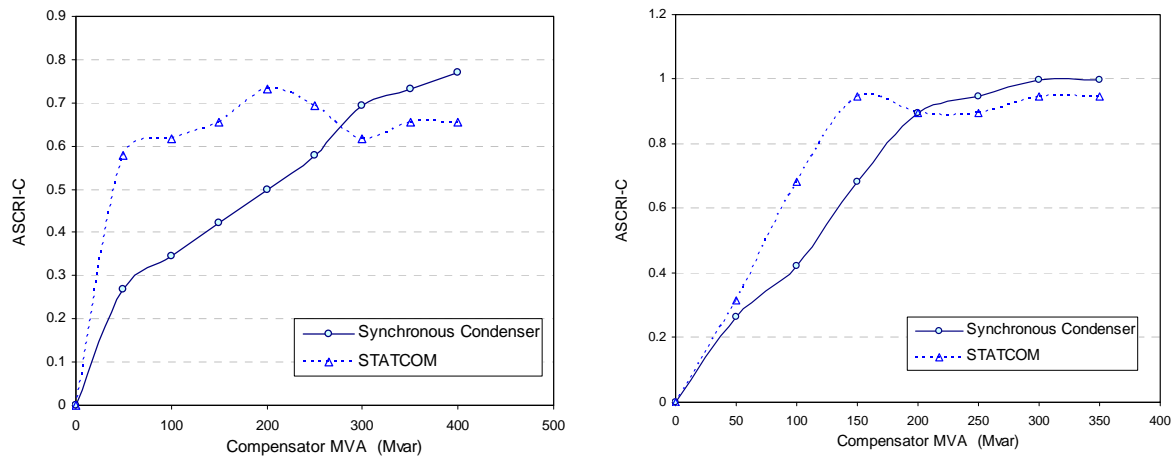
(b) SCR = 1.5

Figure 5. 6: Relationships between CFII and STATCOM Capacity

Figure 5.6(a) indicates that a relatively small-sized STATCOM can help to increase the CFII to about 16.0, but that its effects are saturated quickly. No matter how large a STATCOM is added, the CFII is around 16.0 to 17.0, which basically shows that its effects on the CFII are at a similar level. Figure 5.6(b) shows the results for a STATCOM that increases the CFII from 8.5 to 13.0 quickly, and then becomes saturated. For the SC, the results of the CFII are more linear with respect to the size increasing. Therefore, in both SCR situations, the STATCOM is stronger when small in size but a little weaker

when its size becomes large. This phenomenon indicates that the STATCOM behaves in a more nonlinear way than the SC.

The correlation between the SCR and compensator capacity can be found by combining the results in Figure 5.5 and Figure 5.6. Figure 5.7 shows the ASCRI in the two SCR levels based on the CFII. The results of ASCRI-C shown in Figure 5.7 describe the function of the reactive compensators to increase the ability to resist commutation failures. The ASCRI-C increases when the reactive power compensators are installed. The comparison in Figure 5.7 shows the STATCOM increases the ASCRI-C more quickly and the SC increases the ASCRI-C more linearly. The STATCOM works better than the SC against commutation failure when the capacity of the compensator is smaller. On the hand, the SC works better than the STATCOM against commutation failure when the capacity of the compensator is larger.



(a) SCR = 2.5

(b) SCR = 1.5

Figure 5. 7: Comparison of the ASCRI-C of different Reactive Power Compensators

5.5 Apparent Short Circuit Ratio Increase based on Fault Recovery Time

The ability to recover quickly from AC system faults is a typical requirement of an HVDC system. The acceptance performance test sometimes requires the transferring power P_{dc} to recover from a three-phase fault to a certain level within a certain time. In this section, we use the time from the fault clearance to P_{dc} coming back to 80% to measure the fault recovery performance, as in Figure 5.8.

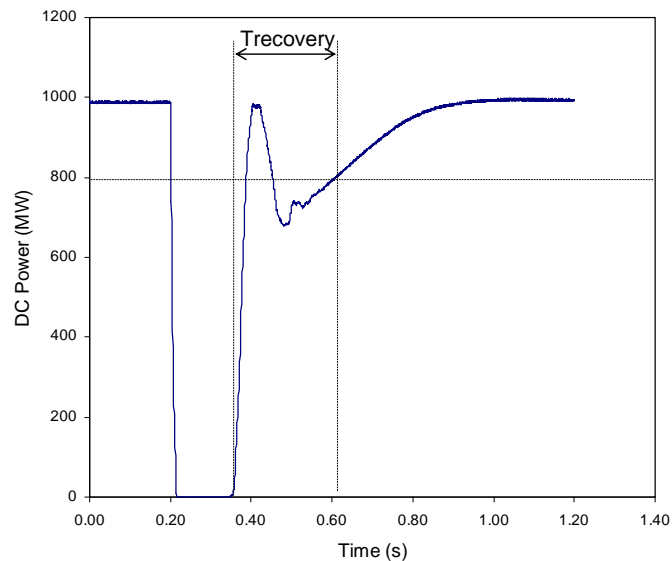


Figure 5. 8: Recovery Time from a Three-Phase Fault

It is commonly thought that a stronger system will have a faster fault-recovery time. In the CIGRE benchmark system, by varying the SCR at the inverter side different recovery times can be obtained, as shown in Figure 5.9. It is interesting to see that fault recovery time decreases when the SCR increases from 1.5 to 3.0, but then it stays the same

regardless of the further increase of the SCR. This indicates that there is a smallest fault recovery time for a certain system when its SCR is boosted to a certain large value. In this test case, the smallest fault recovery time is 0.1 seconds. In fact, when the system is strong enough, the second commutation failure will disappear. Therefore, as soon as the DC power recovers to 0.8 pu, it will never again swing back to below this level.

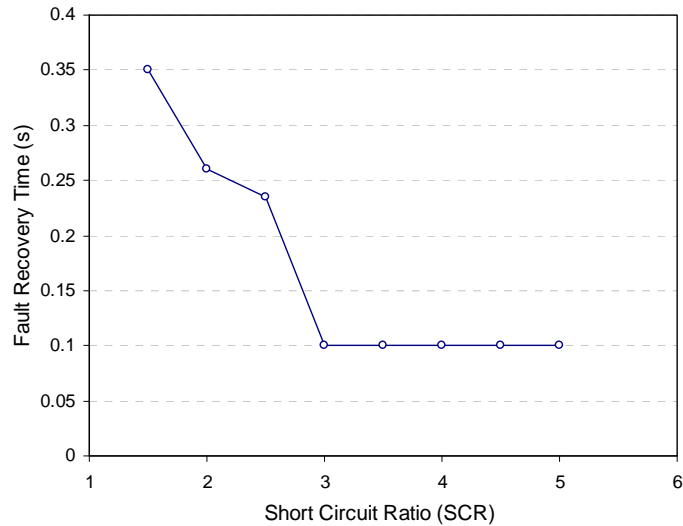


Figure 5. 9: Recovery Time and SCR for a System without Compensation

The reactive power compensators provide voltage support to the converter bus. It is natural to expect that the reactive compensators can reduce the recovery time of the HVDC system from AC system faults. This expectation was tested by adding an SC and a STATCOM to the CIGRE Benchmark system. Figure 5.10 demonstrates the change of recovery times that occurs with the increase of capacities of the SC and the STATCOM. The fault recovery time approaches the previously mentioned shortest value of 0.1 seconds when the compensators are larger than 250 MVA. This implies that the compensation does not have to be larger than this value to improve fault recovery time. Figure 5.10 also demonstrates that the SC is slightly stronger than the STATCOM in

improving the fault recovery time before the capacities of the compensators are large enough to achieve the best recovery time.

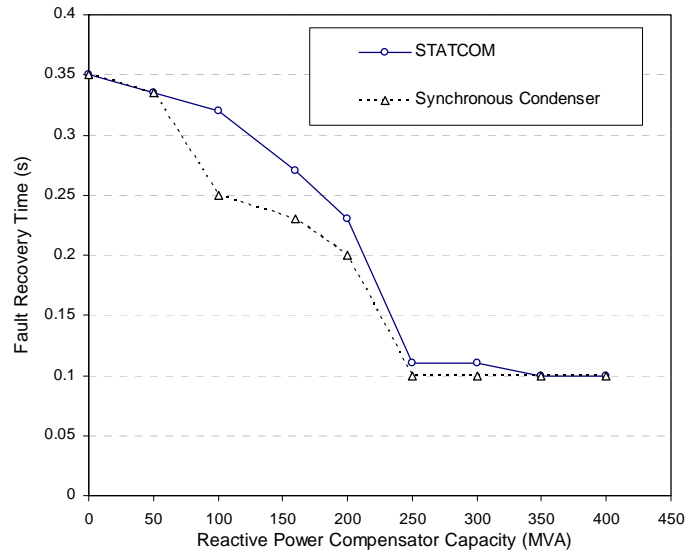


Figure 5. 10: Recovery Time and Reactive Power Compensator Capacity

Fault recovery time is an index that contains the information of how an HVDC system responds to faults in the transient period. It indicates the system strength regarding performance during the fault recovery. Given the relationship between the fault recovery time, SCR, and the capacities of the reactive power compensators, a new index, ASCRI-R, is proposed. ASCRI-R is defined as the equivalent SCR increase that brings the same fault recovery time change as the reactive power compensators. ASCRI-R indicates the contributions of the reactive power compensators in improving the performance of the HVDC system during fault recovery. The results of the ASCRI-R of the SC and the STATCOM in the CIGRE HVDC Benchmark system are shown in Figure 5.11. The new index ASCRI-R shows that both compensators can significantly increase the ASCRI-R up to about 1.5 and achieve the best fault recovery time. It shows the SC had slightly

better performance than the STATCOM when the capacity is lower; for instance, a 100 MVA SC gets 0.56 pu. of ASCRI-R while the same sized STATCOM gets 0.17 pu of ASCRI-R. However, the difference between the two types of compensators reduces along with the increase of their capacity. Finally, both of them can achieve 1.5 pu ASCRI-R.

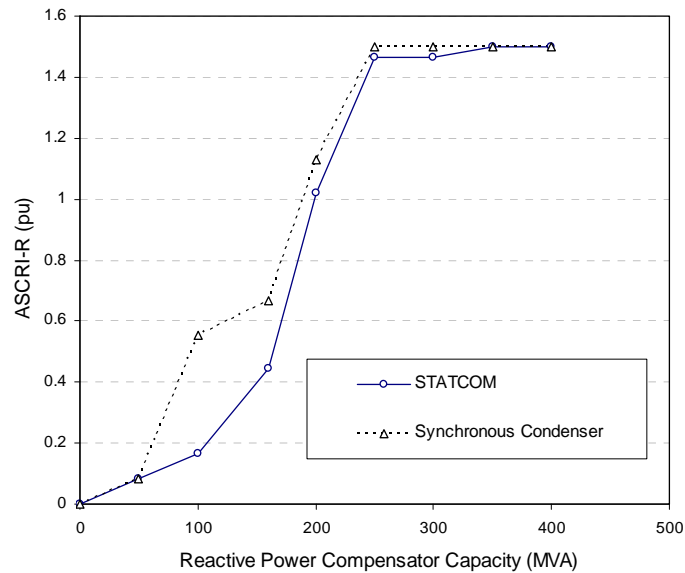


Figure 5. 11: ASCRI based on Fault Recovery Time

5.6 Apparent Short Circuit Ratio Increase based on TOV

The TOV was studied in Section 4.4. Among the typical disturbances studied, the DC permanent block caused severe and sustained TOV. Therefore, the DC permanent block was selected to examine the capability of reactive power compensators to suppress TOV.

The voltage peak value is a commonly used index to measure the problem of TOV. It is expected that the stronger AC system will have the lower TOV peak. Figure 5.12 shows the relationship between the AC system SCR and the TOV peak at the inverter bus after the DC is blocked. The sensitivity study of TOV was conducted by changing the size of the SC and the STATCOM connected to the inverter bus. Figure 5.13 shows the results of overvoltage controlled by reactive power compensators with different capacities.

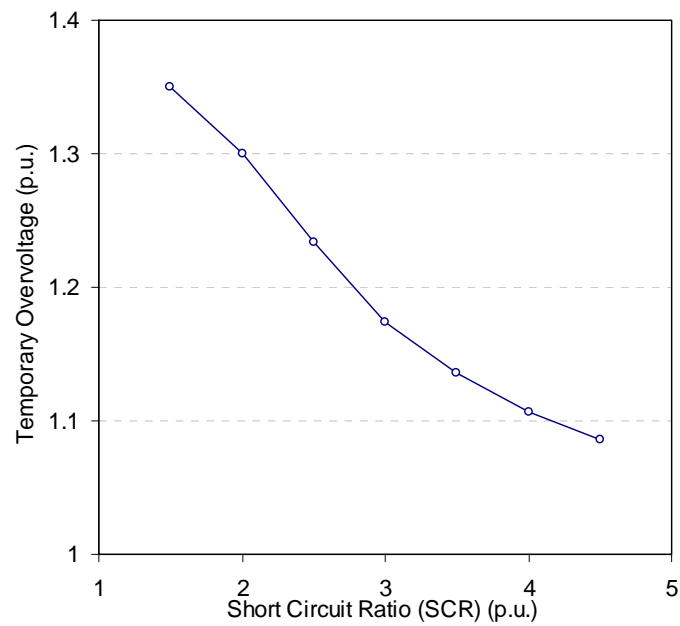


Figure 5. 12: TOV and SCR for a System without Compensation

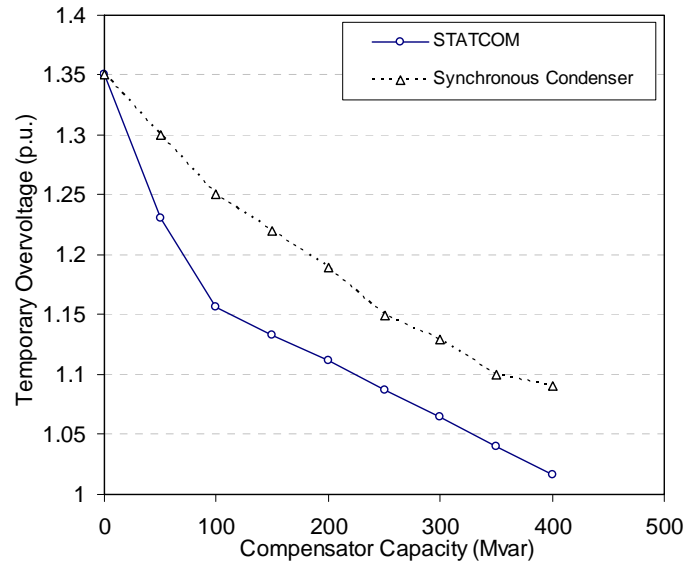


Figure 5.13: TOV and Reactive Power Compensator Capacity

Figure 5.13 shows the both compensators can effectively improve the ability of the AC bus to prevent TOV when the HVDC system is permanently blocked. From the point of view of the TOV, adding an SC or a STATCOM has same function as strengthening the AC system. In order to quantify the effects of the reactive power compensators in preventing TOV, we define a new index, ASCRI-T. ASCRI-T is the apparent SCR increase measured by the highest RMS value of the TOV. In other words, a stronger system with SCR being equal to existing SCR plus ASCRI-T will have the same level of TOV as the existing system with reactive compensators. The new index reflects the ultimate effect of the reactive compensator, such as an SC or a STATCOM, in increasing the ability to control the TOV. The ASCRI-T brought about by the SC and the STATCOM in the CIGRE Benchmark system are plotted in Figure 5.14.

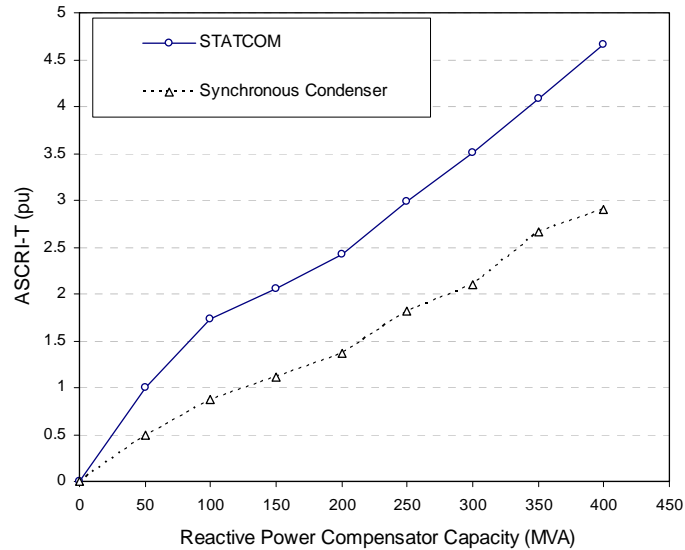


Figure 5. 14: TOV-based ASCRI

Figure 5.14 shows that both the SC and the STATCOM can significantly increase the apparent SCR. The STATCOM has an obvious advantage over the SC in increasing the ASCRI-T.

5.7 The Average ASCRI and Minimum ASCRI

The ASCRI has been evaluated by observing different system performances. Reactive power compensators may have different capabilities in enhancing system strength in different aspects. For example, it has been shown in Chapter 4 that a STATCOM is very powerful in controlling TOV but not as powerful in resisting commutation failures. It would be interesting to compare the different capabilities of the compensators for different aspects. Figure 5.15 and Figure 5.16 illustrate the comparison of the ASCRI-C, ASCRI-R, and ASCRI-T of the STATCOM and the SC in the CIGRE benchmark system respectively. Both figures show that the ASCRIs of different aspects are quite different.

The average of the three ASCRI indices is plotted in the same figure, which provides an approximate estimation of the average system strength increase brought about by the reactive power compensator. In the meantime, the minimum ASCRI is also plotted, which indicates a conservative estimation of system strength increase by the compensator.

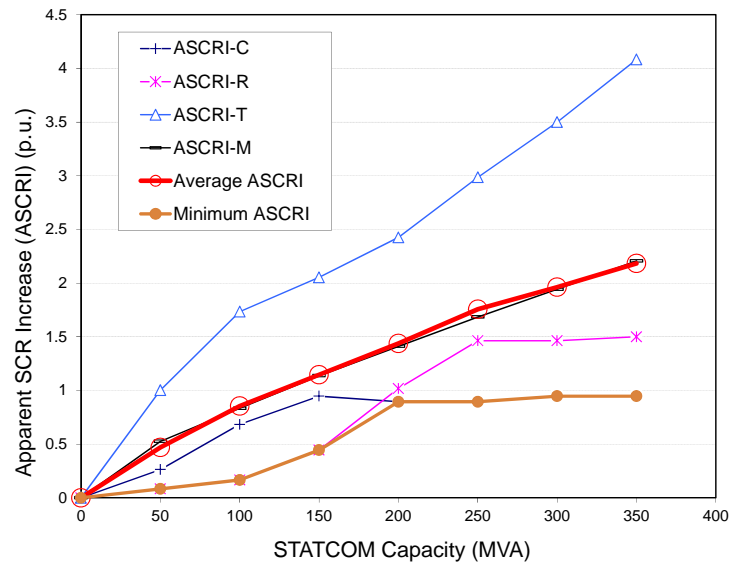


Figure 5. 15 Average ASCRI and Minimum ASCRI for a STATCOM

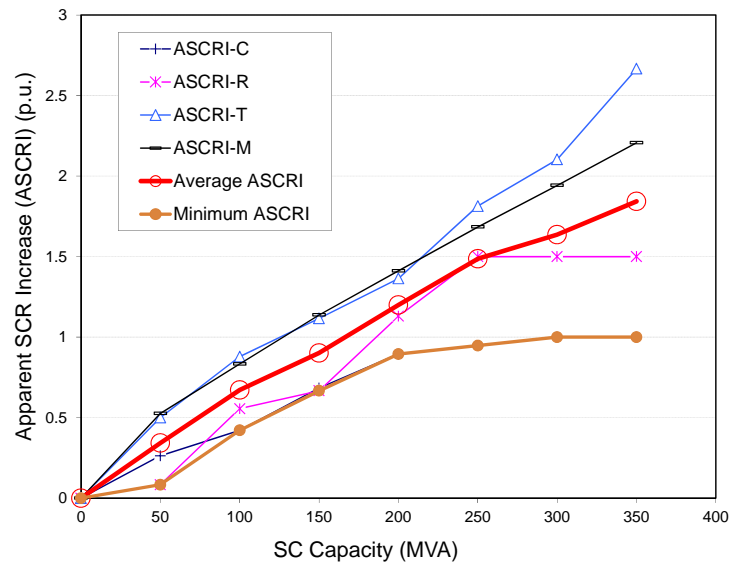


Figure 5. 16 Average ASCRI and Minimum ASCRI for a SC

5.8 Chapter Conclusions

SCR is a well-accepted index used to measure the strength of an AC/DC system. It is simple and has a very clear physical meaning. When a dynamic reactive power compensator is added on the converter bus, it provides extra voltage support but does not always add more short-circuit level support. It is no longer possible to measure the system strength by a simple and elegant index. In this chapter, a new index, Apparent Short Circuit Ratio Increase (ASCRI), was proposed. The new index was evaluated by the use of Maximum Available Power (MAP), Commutation Failure Immunity Index (CFII), Fault Recovery Time, and Temporary Over-Voltage (TOV), and was expanded as a series of indices that can measure system strength in different aspects: ASCRI-M, ASCRI-C, ASCRI-R, and ASCRI-T. Using these newly developed indices, the function of dynamic reactive compensations can be quantified by the apparent system strength. ASCRI opens a new methodology to define the system strength for AC/DC power systems with compensators at the converter bus.

The new index ASCRI was tested in the CIGRE Benchmark case with an SC and a STATCOM at the inverter bus. Those two different compensation options were compared regarding their ability to provide ASCRI for different situations and different capacities. Those intensive comparisons provided a great deal of insightful information that is not available in other conventional simulation studies.

This chapter made the following contributions:

- A new series of indices based on Apparent Short Circuits Ratio Increase (ASCRI) were proposed to quantify the system strength when dynamic reactive power compensators were connected to the converter bus.
- The contributions of SC and STATCOM to system strength were studied based on the new indices.

Chapter 6: Consideration of Inertia for Design of Reactive Power Compensation Schemes

6.1 Introduction

This chapter discusses the inertia of a synchronous condenser and its impact on power system stability, especially its impact on frequency stability.

As mentioned in Chapter 1, it has been debated whether the mechanical inertia of SCs provides additional frequency stability. There is concern that using a STATCOM may lead to insufficient inertia and cause transient or dynamic stability problems. In fact, the impact of the inertia of an SC depends on the mechanical energy stored in the rotor, which may improve the frequency dynamic during disturbances. It has been argued that the mechanical stored energy is not really required because an HVDC system already provides a large source of real power for this purpose. Most research on reactive compensation for HVDC systems focuses on the electrical strength and transient behavior of electrical variables; there are very few publications on the impact of inertia and associated mechanical dynamics.

In Chapter 2, we briefly examined the effects of an SC's inertia in a simple power system. It was shown by the simulation that the inertia made some difference in two scenarios:

during a permanent loss of power the load voltage declining speed with the SC was much slower than that with the STATCOM, and during a 3-cycle of power outage, the induction motor remained stable with the SC but became unstable with the STATCOM. Those two scenarios in the simple system at least indicated the inertia of the SC provided some benefit to system stability. Therefore, it is worth further investigation to find out whether the inertia of an SC can improve the performance of an AC/DC system. It would be interesting and important to know whether the frequency stability is a problem if a STATCOM is used as the reactive power compensator at the HVDC system.

It is necessary to model the details of generators to represent the frequency dynamics of the power system. Figure 6.1 illustrates an example AC/DC system in which the inverter-side system contains generators, loads, and a transmission network. The first part of this chapter will investigate the power-frequency characteristics of the AC/DC system. The purpose of this study is to examine the effects of the inertia of reactive power compensators on frequency stability. Then simulation studies will be conducted to show the effects in an example system. How to consider the inertia of an SC when designing reactive power compensation for AC/DC systems will then be discussed.

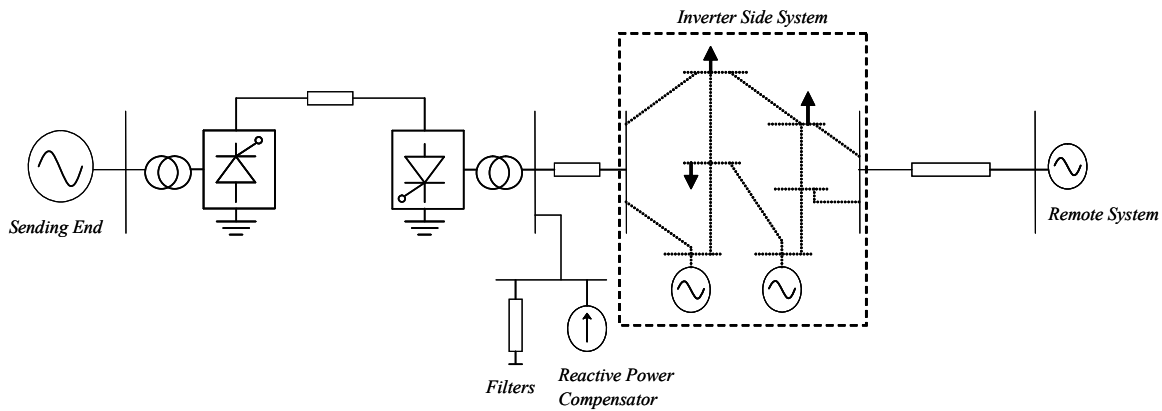


Figure 6. 1: Circuit of an AC/DC System with Detailed AC Network at the Inverter Side

6.2 Effects of Reactive Compensator Inertia on Frequency Stability

6.2.1 Inertia of Power Systems

Each turbine generator in an AC power system represents a large rotating mass. The inertia of the entire system is formed by adding together the inertia of all machines in the power system. The inertia plays an important role in system dynamics. It maintains the speed of the machines and the frequency of the system. Without sufficient inertia, the frequency of the power system will be hard to maintain during any power unbalance caused by faults or load changes. Generally, the inertia of a power system indicates its ability to keep the frequency in the desired range.

The per unit inertia constant H of an electrical machine can be defined as the kinetic energy in watt-seconds at rated speed divided by the rated MVA base.

By its physical meaning, the inertia constant H is given by:

$$H = \frac{\text{Stored Energy at Rated Speed in } MW \cdot S}{MVA \text{ Rating}} \quad (6-1)$$

Using ω_{om} to denote the rated angular velocity in mechanical radians per second, the inertia constant can be represented as:

$$H = \frac{1}{2} \frac{J\omega_{om}^2}{VA_{base}} \quad (6-2)$$

in which J is the combined moment of inertia of the generator and turbine.

According to [2], a typical steam turbine generator set may have an inertia constant H of 2.5 to 6.0 seconds based on the generator MVA rating. Hydraulic generators have a little less inertia constant H of about 2.0 to 4.0 seconds.

The average inertia constant of a multi-machine power system can be represented as:

$$H = \frac{\sum_{i=1}^n (H_i \cdot MVA_i)}{\sum_{i=1}^n MVA_i} \quad (6-3)$$

If the system inertia is converted to the base of the dc power rating, it gives the Effective Inertia Constant H_{dc} [5]:

$$H_{dc} = \frac{\sum_{i=1}^n H_i \cdot MVA_i}{MW \text{ Rating of The DC System}} \quad (6-4)$$

The physical meaning of H_{dc} is the energy stored in the generator rotors divided by the dc rating power. H_{dc} gives a measure of the inertia weakness of the system by relating the

change of generator speed to the temporary energy imbalance imposed any disturbances of dc block.

6.2.2 Frequency Deviation in Multi-Machine AC/DC Systems

The relationship [5] between change of machine frequency (Δf), mechanical power input (P_m), and electrical power output (P_e) for small changes of frequency can be represented by

$$\Delta f_i = \frac{(P_{mi} - P_{ei}) \cdot f_0 \cdot dt}{2H} \quad (6-5)$$

Where

f_0 is the system nominal frequency in Hz

H_i is the inertia constant of the machine in MW· S/MVA

P_{mi} is the machine mechanical power in per unit

P_{ei} is the machine electrical power in per unit

In multi-machine power systems, the frequency of the entire system is an average concept, which is defined as the frequency of the system's center of inertia (COI):

$$f = \frac{\sum_{i=1}^n (f_i \cdot H_i \cdot MVA_i)}{\sum_{i=1}^n (H_i \cdot MVA_i)} \quad (6-6)$$

The frequency deviation of COI is the average frequency deviation of all the machines:

$$\Delta f = \frac{\sum_{i=1}^n (\Delta f_i \cdot H_i \cdot MVA_i)}{\sum_{i=1}^n (H_i \cdot MVA_i)} \quad (6-6)$$

If we assume all the machines have identical frequency deviation:

$$\Delta f_i = \Delta f^* \quad (6-7)$$

The frequency of COI can be simplified as:

$$\Delta f = \Delta f^* \quad (6-8)$$

For general cases, the frequency deviation of a machine can be represented as:

$$\Delta f_i = \frac{\Delta P_i \cdot f_0 \cdot \Delta t}{2H_i} \quad (6-9)$$

In which ΔP_i is the active power mismatch of the i th machine, and Δt is the time the power mismatch lasts. If we assume ΔP is shared by all the machines in the system, we can obtain ΔP_i as:

$$\Delta P_i = \frac{\Delta P \cdot H_i \cdot MVA_i}{\sum_{i=1}^n (H_i \cdot MVA_i)} \quad (6-10)$$

If we per unitize ΔP_i based on MVA_i :

$$\Delta P_i^* = \frac{\Delta P \cdot H_i}{\sum_{i=1}^n (H_i \cdot MVA_i)} \quad (6-11)$$

Substitute (6-11) into (6-9) we obtain:

$$\Delta f_i = \frac{\Delta P \cdot f_0 \cdot \Delta t}{2 \sum_{i=1}^n (H_i \cdot MVA_i)} \quad (6-12)$$

It is noticed that Δf is not dependent on i , which indicates the frequency deviation is an average concept as long as we assume the power is shared by all the machines in the

system. Therefore, the mean frequency deviation of the entire system due to power unbalance ΔP can be written as:

$$\Delta f = \frac{\Delta P \cdot f_0 \cdot \Delta t}{2 \sum_{i=1}^n (H_i \cdot MVA_i)} \quad (6-13)$$

If the power unbalance is caused by DC power change or interruption, the frequency deviation of the system will be:

$$\Delta f = \frac{\Delta P_{dc} \cdot f_0 \cdot \Delta t}{2 \sum_{i=1}^n (H_i \cdot MVA_i)} \quad (6-14)$$

If we use per unit P_{dc}^* to replace P_{dc} , and consider (6-4), we can obtain:

$$\Delta f = \frac{\Delta P_{dc}^* \cdot f_0 \cdot \Delta t}{2 \sum_{i=1}^n (H_i \cdot MVA_i) / P_{dc}} = \frac{\Delta P_{dc}^* \cdot f_0 \cdot \Delta t}{2H_{dc}} \quad (6-15)$$

Equation (6-15) is the frequency deviation of the system caused by the DC power change.

6.2.3 Inertia Requirement of AC/DC Power Systems

6.2.3.1 Requirements of the Generator Capacity

If we assume the amount and duration of the DC power mismatch, and define a permissible frequency deviation, we can get the minimum required inertia of the system as:

$$H_{dc} = \frac{\Delta P_{dc}^* \cdot f_0 \cdot \Delta t}{2\Delta f} \quad (6-16)$$

As an example, we consider a fault at the sending end AC system of an HVDC link. If the typical maximum AC fault duration time is of the order of 100 ms, the recovery time of the DC link is 200 ms and the maximum permissible frequency decline is 0.05 p.u. The minimum required mechanical inertia of the system is

$$H_{dc \min} = \frac{1.0 \cdot (100 + 200) \cdot 10^{-3} \cdot 1.0}{2 \cdot 0.05} = 3MW \cdot S / MVA \quad (6-17)$$

Substitute (6-17) into (6-4) we obtain:

$$\frac{\sum_{i=1}^n (H_i \cdot MVA_i)}{MW \text{ Rating of The DC System}} > 3MW \cdot S / MVA = H_{dc \min} \quad (6-18)$$

As we mentioned previously [2], the typical value of H of the turbine generator is 2 to 6 seconds. So we can estimate the total system MVA as:

$$\frac{\sum_{i=1}^n (H_i \cdot MVA_i)}{P_{dc}} \geq \frac{2.0 \sum_{i=1}^n MVA_i}{P_{dc}} \geq 3.0 \quad (6-19)$$

Therefore, we have:

$$\sum_{i=1}^n MVA_i \geq 1.5P_{dc} \quad (6-20)$$

This means that if the generator MVA in the AC system is larger than 1.5 times the rated power of the DC link, the frequency deviation will be within the permissible range of 5% for the typical DC interruption mentioned above. It should be noticed that Equation (6-20) is a conservative approximation rather than a necessary condition. In the cases that H is larger than 2, the total generation capacity does not have to be as large as $1.5P_{dc}$. In fact,

the required total MVA of the generator installation of the AC system changes with the value of average H constants as in Figure 6.2.

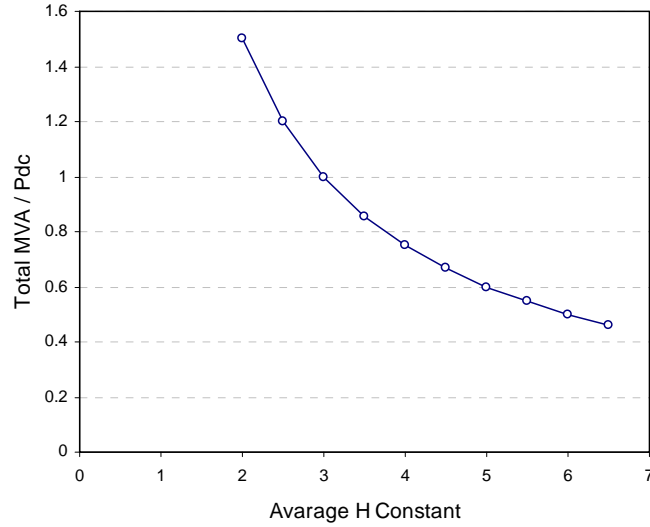


Figure 6. 2: The Relationship between Average H and Total MVA at the Sending End

6.2.3.2 The Requirement of Inertia at a Sending End

For those systems in which 100% power generation is sent out through the DC transmission, we have:

$$\sum_{i=1}^n (MVA_i \cdot \cos \varphi_i) = P_{dc} \quad (6-21)$$

Considering the filters at the converter bus, we can assume $\cos \varphi_i = 0.9$, and then the total generator MVA can be represented as:

$$\sum_{i=1}^n MVA_i = \frac{P_{dc}}{\cos \varphi_i} = \frac{P_{dc}}{0.9} \quad (6-22)$$

If the permissible frequency deviation remains the same as above, the inertia constant of the machine must be larger than a certain value in order to satisfy (6-18)

$$H_i \geq \frac{3.0}{0.9} \geq 3.3333 \quad (6-23)$$

If H_i is smaller than 3.3333, the frequency deviation is larger than the permissible frequency, for instance, if $H_i = 2.0$, we have:

$$\Delta f_i = \frac{1.0 \cdot 0.3 \cdot 1.0}{2 \cdot 2 \cdot 0.9} = 0.08333 \quad \text{or} \quad 8.333\% \quad (6-24)$$

The relationship between Δf and H_i is illustrated in Figure 6.3. If the sending end inertia cannot be reached beyond (6-23), then a frequency deviation larger than 5% has to be accepted at the rectifier side.

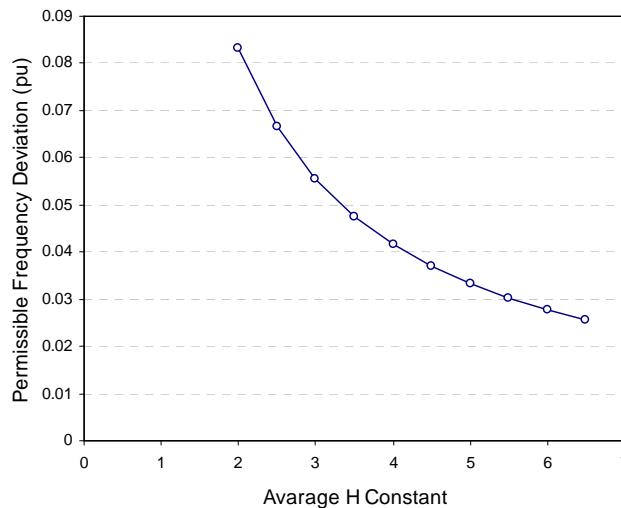


Figure 6. 3: The Relationship between Average H and Frequency Deviation

For the systems in which 100% generation is transferred out by HVDC link, which are referred to as collector systems, the restriction of frequency deviation is normally not strict because the sending end generators are only synchronized to each other and not to

any AC network. Because there is no AC load in these systems, sometimes the frequency deviation is permitted to be as high as over 10%. From Figure 6.3, we can see that even when the H is small, the frequency deviation is still within the permissible range of 10%. Therefore, the inertia and frequency stability should not be concerns for the sending end from which all generation is sent by HVDC links.

6.2.3.3 The Requirement of Inertia at a Receiving End

For the receiving end, let us examine the load rejections of an HVDC link. If we consider an interruption of the HVDC link, a fault duration of 100 ms, an HVDC link recovery time of 200 ms, and a maximum permissible frequency deviation of 0.05 pu, we have:

$$H_{dc\ min} = \frac{1.0 \cdot (100 + 200) \cdot 10^{-3} \cdot 1.0}{2 \cdot 0.05} = 3MW \cdot S / MVA \quad (6-25)$$

Similarly, we found the minimum system inertia to be:

$$\sum_{i=1}^n (H_i \cdot MVA_i) \geq 3.0P_{dc} \quad (6-26)$$

Equation (6-25) represents a criterion to evaluate the inertia of the inverter side AC system. We can further define margin K_m and relative margin K_p of the system inertia:

$$K_m = \sum_{i=1}^n (H_i \cdot MVA_i) - 3.0P_{dc} \quad (6-27)$$

And

$$K_p = \frac{\sum_{i=1}^n (H_i \cdot MVA_i) - 3.0P_{dc}}{3.0P_{dc}} \quad (6-28)$$

It should be noticed that not 100% of the energy stored in the generators' rotors can be used to retain the frequency because part of it must be consumed by the system loss in the transient process. A margin must be considered when we analyze the frequency deviation. It is reasonable to reserve a margin of 10 to 20% for K_p , as in (6-28).

The relationship between the H constants and the total generation MVA with a different margin K_p is shown in Figure 6.4. For a strong receiving end with a large number of generators, K_m and K_p will be large numbers. For a weak system with a small number of generators, they will be small positive numbers or even negative numbers. K_m reaches the minimum when no generator is installed in the receiving end, that is:

$$K_m = -3.0P_{dc} \quad (6-29)$$

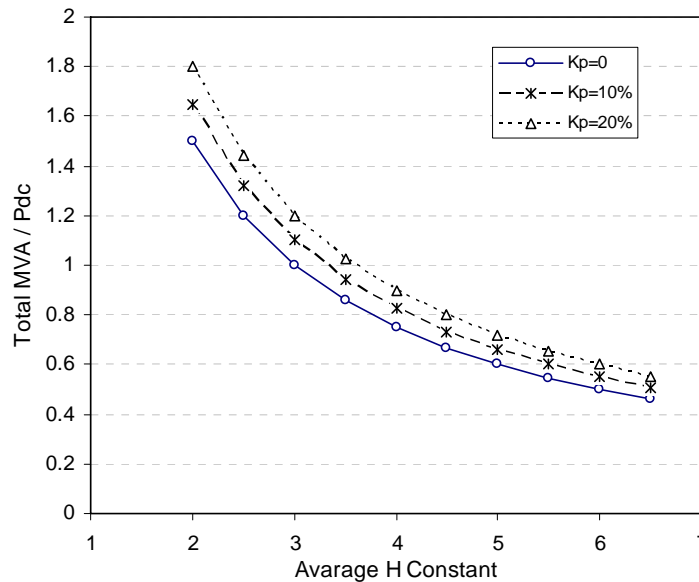


Figure 6. 4: Relationship between H Constants and Total MVA at the Receiving End

6.2.4 Effects of Synchronous Condensers on System Inertia

A synchronous condenser (SC) provides two basic functions: the transient reactance of the SC will be electrically in parallel with the AC system equivalent impedance, reducing the short-circuit impedance as seen from the converter station and thereby improving the SCR; and the inertia of the SC will act as a temporary energy storage device for the AC system.

An SC is usually installed at the inverter bus to support the voltage of the inverter bus and increase the strength of the receiving end system. We analyzed the inertia of the receiving end in the previous section. If equation (6-23) is not satisfied, the relative margin K_p will become a negative number. By adding a synchronous condenser, K_p can be improved as:

$$K_p = \frac{\sum_{i=1}^n (H_i \cdot MVA_i) + H_{sc} \cdot MVA_{sc} - 3.0P_{dc}}{3.0P_{dc}} \quad (6-30)$$

To have a positive margin of system inertia, the minimum value of compensated inertia should be:

$$H_{sc} \cdot MVA_{sc} = 3.0 \cdot (K_p + 1.0) \cdot P_{dc} - \sum_{i=1}^n (H_i \cdot MVA_i) \quad (6-31)$$

The conventional inertia of an SC is approximately 1.25 [2]. Therefore, the minimum MVA of the SC will approximately be:

$$MVA_{sc} = \frac{3.0 \cdot (K_p + 1.0) \cdot P_{dc} - \sum_{i=1}^n (H_i \cdot MVA_i)}{H_{sc}} = \frac{3.0 \cdot (K_p + 1.0) \cdot P_{dc} - \sum_{i=1}^n (H_i \cdot MVA_i)}{1.25} \quad (6-32)$$

It may be possible to reduce the minimum required rating of the generator by increasing its inertia constant; for example, by adding a fly wheel to the machine shaft.

For an island with zero power generation, the synchronous condenser becomes a must regarding inertia compensation. The specific inertia can be designed according to (6-32) as:

$$MVA_{sc} = \frac{3.0 \cdot (K_p + 1.0) \cdot P_{dc}}{H_{sc}} \quad (6-33)$$

Balance between the H constants and the MVA of an SC can be considered as (6-33) when designing the reactive power compensation for the receiving end with no generation.

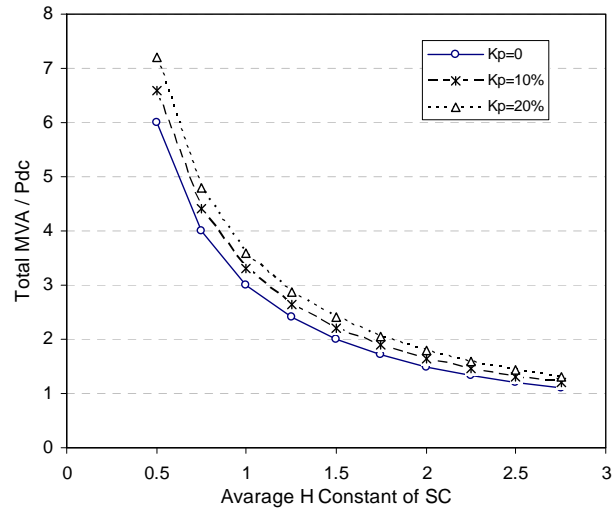


Figure 6. 5: Relationship between the H Constant and the MVA of a Synchronous Condenser

6.2.5 Selecting a Reactive Power Compensator Considering the Inertia

Combine (6-3), (6-4), and (6-16), and assume a general reactive power compensator instead of an SC, we can have the following equation:

$$H_{dc} = \frac{\Delta P_{dc}^* \cdot f_0 \cdot \Delta t}{2\Delta f} = \frac{\sum_{i=1}^n (H_i \cdot MVA_i) + H_{comp} \cdot MVA_{comp}}{P_{dc}} \quad (6-34)$$

Among the available compensators, only the SC physically has inertia; therefore we have:

$$H_{comp} = \begin{cases} H_{sc} & \text{for synchronous condenser} \\ 0 & \text{for other compensators} \end{cases} \quad (6-35)$$

By considering a margin of K_p , we can re-arrange (6-34) and obtain the following condition for reactive power compensation design with consideration of inertia:

$$\sum_{i=1}^n (H_i \cdot MVA_i) + H_{comp} \cdot MVA_{comp} - \frac{\Delta P_{dc}^* \cdot f_0 \cdot \Delta t}{2\Delta f} \cdot (K_p + 1.0) \cdot P_{dc} > 0 \quad (6-36)$$

We consider the worst case situation in designing the compensator, which is the entire DC link being blocked; in this case, $\Delta P_{dc} = 1.0$. The per unit value f_0 is 1.0, and the permissible frequency deviation Δf is usually 5%. With those assumptions we can simplify (6-36) into:

$$\sum_{i=1}^n (H_i \cdot MVA_i) + H_{comp} \cdot MVA_{comp} - 10\Delta t \cdot (K_p + 1.0) \cdot P_{dc} > 0 \quad (6-37)$$

If there is no generation in the inverter side AC system, a synchronous condenser must be used and its size should be chosen according to:

$$MVA_{sc} > \frac{10\Delta t \cdot (K_p + 1.0) \cdot P_{dc}}{H_{sc}} \quad (6-38)$$

If there is generation and

$$\sum_{i=1}^n (H_i \cdot MVA_i) - 10\Delta t \cdot (K_p + 1.0) \cdot P_{dc} > 0 \quad (6-39)$$

the inertia is sufficient and it is not a restriction in selecting reactive power compensators. The selection of an SC or a STATCOM will be dependent on the technical or economic conditions other than the inertia. For example, as shown in Section 4.4, the STATCOM is better at regulating voltage.

If there are some generations, but the inertia is not sufficient,

$$\sum_{i=1}^n (H_i \cdot MVA_i) - 10\Delta t \cdot (K_p + 1.0) \cdot P_{dc} < 0 \quad (6-40)$$

We need to consider the inertia, an SC should be chosen and its capacity should satisfy the following condition:

$$MVA_{sc} > \frac{10\Delta t \cdot (K_p + 1.0) \cdot P_{dc} - \sum_{i=1}^n (H_i \cdot MVA_i)}{H_{sc}} \quad (6-41)$$

6.3 Simulation Studies

6.3.1 Simulation Case

6.3.1.1 Circuit Configuration

This section shows the impact of inertia on system stability. Thus, the test system should be able to reflect the system angle stability. A test system as in Figure 6.6 was designed for this purpose. A back-to-back HVDC system rated at 60 kV and 200 MW is used to connect two AC systems. The rectifier side is represented by a voltage source. The inverter side transmits 200 MW of power through a 20 km 345 kV line to a load center. The total load of the load center is about 400 MW, of which 200 MW is supplied by the HVDC power and the rest by a local generator. The load center also connects a remote power grid through a 370 km 345 kV transmission line. There is no power flow on that line in the normal operating condition. An SC and a STATCOM are installed at the inverter bus. Both of the compensators are rated at 100 Mvar.

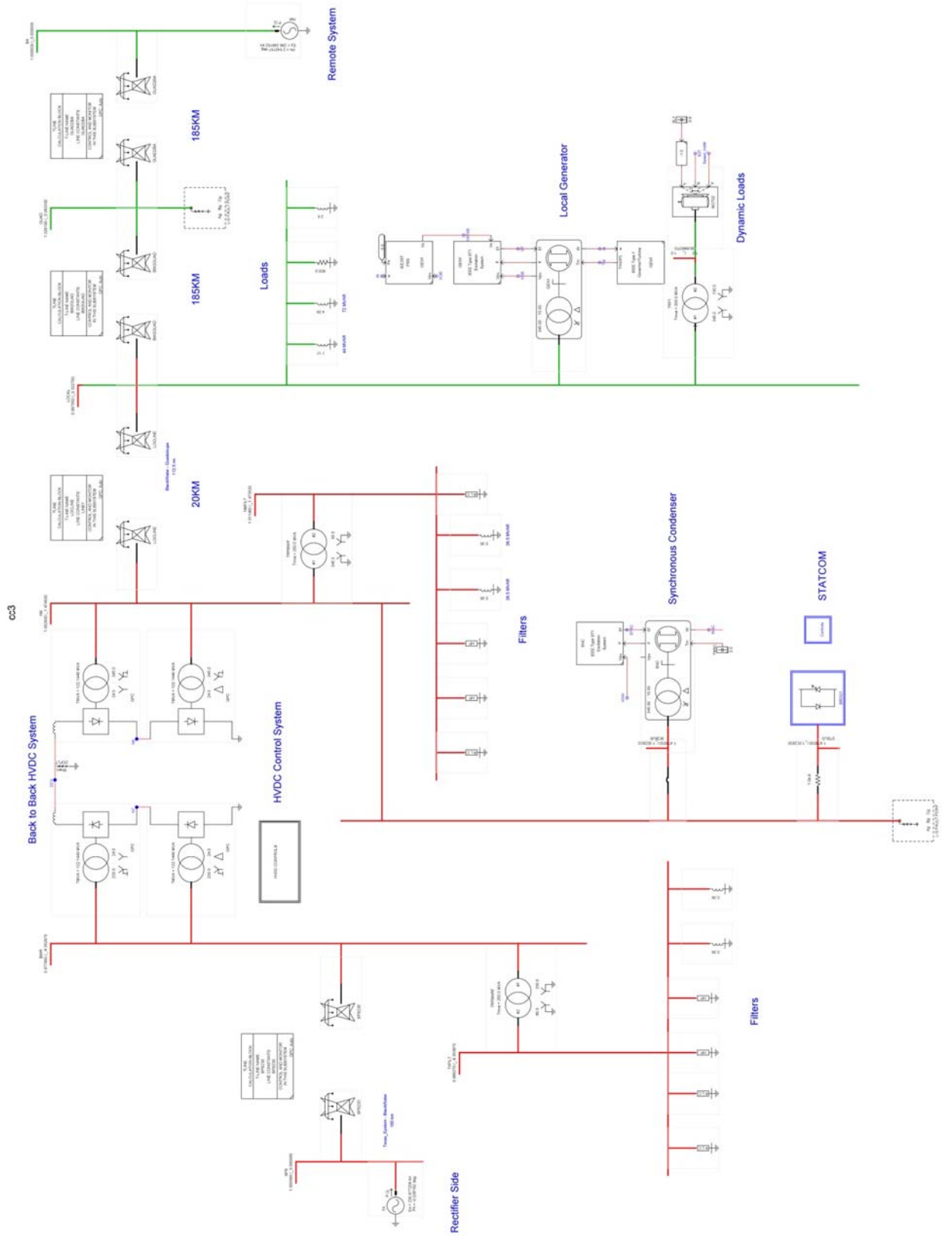


Figure 6. 6: Test Case to Show the Impact of Inertia

6.3.1.2 Frequency Change Due to a DC Block

The first test on the simulation case was undertaken to show the frequency dynamic under a DC block. In the simulation case, the H constant of the generator was set to 3.0 while the H constant of the SC was set to 2.0. The speed responses of the generator with an SC and a STATCOM are shown in Figure 6.7.

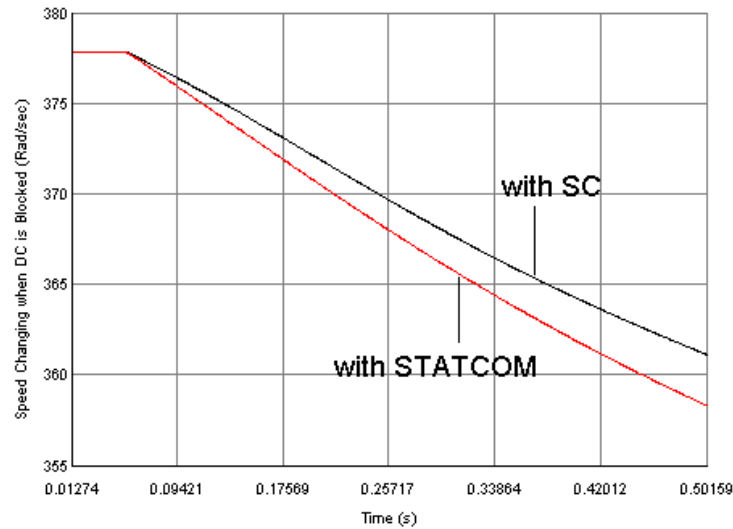


Figure 6. 7: Speed Changing when the DC is Blocked

The generator speed decline is slower with the SC. This is because the energy stored in the rotor of the SC is released at the moment of DC block, which helps to retain the rotating speed. If we measure the decline of the rotating speed of the generator during 0.3 seconds from the fault starting time, the results are 12.11 rad/sec with the SC and 14.30 rad/sec with the STATCOM. The H_{dc} can be calculated theoretically and can be measured numerically as follows:

The theoretically calculated H_{dc} for the case with an SC according to (6-34) is:

$$H_{dc} = \frac{\sum_{i=1}^n (H_i \cdot MVA_i) + H_{comp} \cdot MVA_{comp}}{P_{dc}} = \frac{3.0 \cdot 300 + 2.0 \cdot 100}{200} = 5.5 MW \cdot S / MVA \quad (6-44)$$

The measured H_{dc} from simulation can be calculated according to (6-34):

$$H_{dc} = \frac{\Delta P_{dc}^* \cdot f_0 \cdot \Delta t}{2\Delta f} = \frac{1.0 \cdot 1.0 \cdot 0.3}{2.0 \cdot (12.119/377)} = 4.67 MW \cdot S / MVA \quad (6-45)$$

As discussed in the previous section, part of the stored energy in the rotor will be consumed by loss, which causes the difference between the theoretical and numerical results of H_{dc} . We should introduce a margin factor K_p to assure the sufficient estimation of the inertia. According to (6-36), we can calculate the minimum K_p as:

$$K_p = \frac{\sum_{i=1}^n (H_i \cdot MVA_i) + H_{comp} \cdot MVA_{comp}}{P_{dc} \cdot \frac{\Delta P_{dc}^* \cdot f_0 \cdot \Delta t}{2\Delta f}} - 1.0 = 17.8\% \quad (6-46)$$

For the case with a STATCOM, the theoretical H_{dc} is:

$$H_{dc} = \frac{\sum_{i=1}^n (H_i \cdot MVA_i)}{P_{dc}} = \frac{3.0 \cdot 300}{200} = 4.5 MW \cdot S / MVA \quad (6-47)$$

From an analysis of the simulation results, it is:

$$H_{dc} = \frac{\Delta P_{dc}^* \cdot f_0 \cdot \Delta t}{2\Delta f} = \frac{1.0 \cdot 1.0 \cdot 0.3}{2.0 \cdot (14.301/377)} = 3.97 MW \cdot S / MVA \quad (6-48)$$

The minimum K_p can be calculated as:

$$K_p = \frac{\sum_{i=1}^n (H_i \cdot MVA_i)}{P_{dc} \cdot \frac{\Delta P_{dc}^* \cdot f_0 \cdot \Delta t}{2\Delta f}} - 1.0 = 13.9\% \quad (6-49)$$

The above results verified that it is reasonable to assume the margin factor K_p to be 10 - 20%.

6.3.2 Simulation Study Results

In order to investigate the effects of inertia on system stability, the H constants of the generator were purposely changed to mimic the scenarios of different system inertias. For both the high and low inertia, simulation studies were carried out to demonstrate the performance of the SC and the STATCOM. Many types of scenarios were studied, but only the following disturbances are discussed here:

1. Rectifier side three-phase fault
2. Inverter side close-in three-phase fault
3. Inverter remote three-phase fault
4. DC block

Many variables were monitored. However, due to space limitations, only the following variables are discussed here:

- (a) DC transfer power
- (b) AC RMS voltage
- (c) Rotating speed of inverter side generator
- (d) Swing angle of inverter side generator

DC power and AC voltage were plotted to show the performances associated with temporary overvoltage, AC voltage recovery and DC power recovery. It should be noted that the generator speed and swing angle can demonstrate the effects of inertia on frequency stability and rotor angle stability.

6.3.2.1 System Performance with High System Inertia

6.3.2.1.1 Rectifier Side Three-Phase Fault

A high inertia situation was modelled by setting the H constant of the generator to 4.7. Figure 6.8 shows the results when a 0.1 second three-phase fault occurred at the rectifier side. The recovery time of the DC power was almost the same for the STATCOM and the SC, as shown in Figure 6.8(a), while the AC voltage recovery with the STATCOM was apparently more smoothly regulated to its set point than with the SC, as shown in Figure 6.8(b). The oscillations of the generator speed and angle are very close. Figure 6.8(c) and Figure 6.8(d) demonstrate slightly less oscillation for the STATCOM and slightly faster decay for the SC.

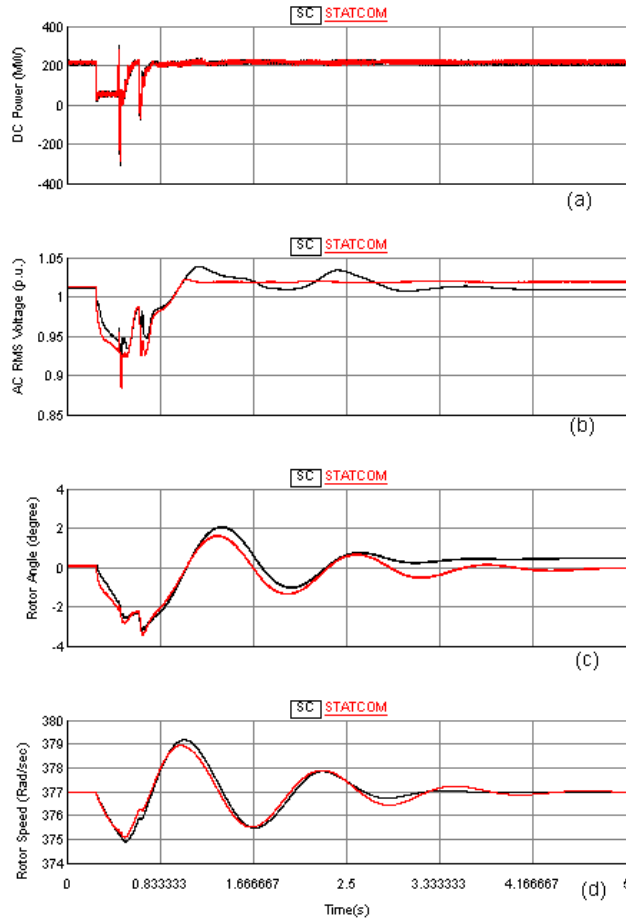


Figure 6. 8: Rectifier Side Fault with High Inertia

6.3.2.1.2 Inverter Side Close-in Three-Phase Fault

Figure 6.9 shows the results when a 0.1 second three-phase fault occurred at the inverter bus. Both the SC and the STATCOM worked well. The recovery times of the DC power and the AC voltage with the STATCOM are slightly shorter than with the SC, as shown in Figure 6.9(a) and (b). Figure 6.9(b) shows that the voltage control is smoother and faster with the STATCOM. The oscillations of the generator speed and angle are similar

for both compensators, as shown in Figure 6.9(c) and (d). Again, the oscillation decay is slightly faster with the SC.

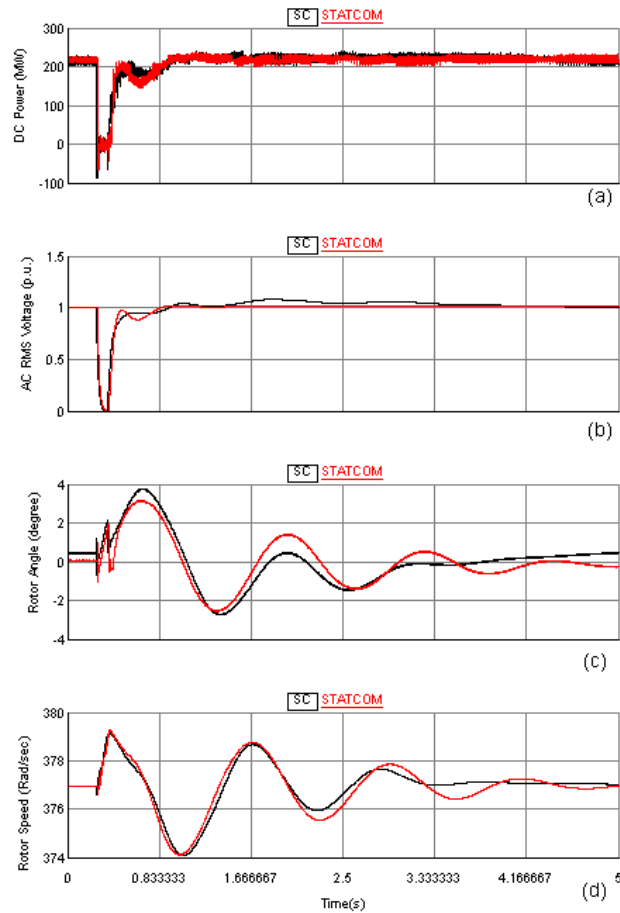


Figure 6. 9: Inverter Side Close-in Fault with High Inertia

6.3.2.1.3 Inverter Side Remote Three-Phase Fault

The remote three-phase fault was modelled by applying a 0.1 second voltage dip of 50% at the bus 370 km from the inverter side load centre under investigation. This models the situation of influence by disturbances in the remote power network. Although these faults

are normally less severe for the stability of the studied area, the possibility of having these faults is much higher. Figure 6.10 shows the results of a remote fault. Although both the SC and the STATCOM work well, the response of the rotor angles and rotor speed shown in Figure 6. 10 (c) and (d) have lower amplitude with the SC. This is to be expected due to the larger inertia. The SC also appears to have more damping.

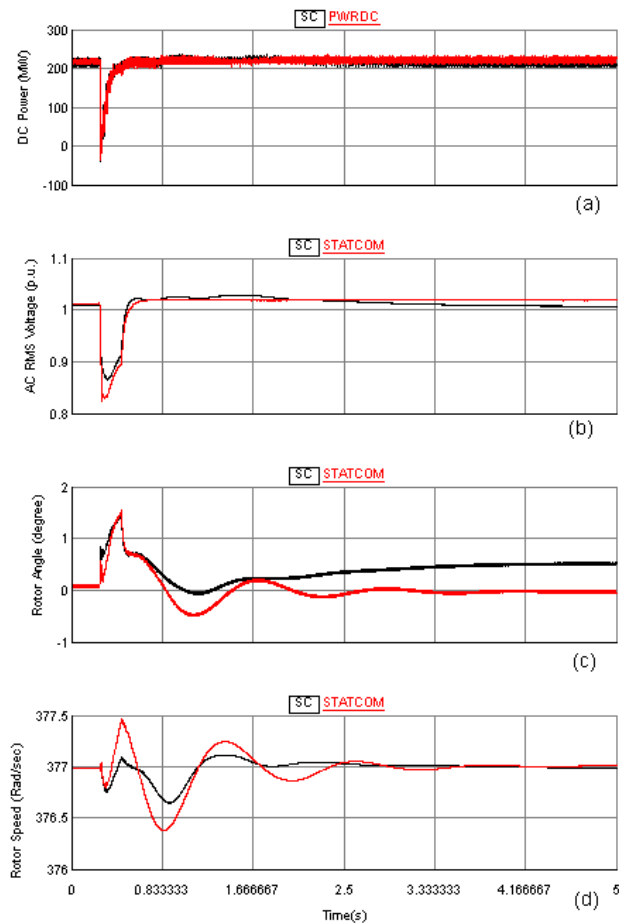


Figure 6. 10: Inverter Side Remote Fault with High Inertia

6.3.2.1.4 DC Permanent Block

Figure 6.11 shows the results when the HVDC converters are blocked. Although the generator becomes unstable, as shown in Figure 6.11(c) and (d), the bus voltage can be effectively controlled by both of the compensators. Figure 6.11(b) shows the STATCOM has significantly greater capability to control the TOV than the SC. With the SC, the RMS bus voltage reaches about 1.2 p.u. With the STATCOM, it only reaches about 1.05 p.u.

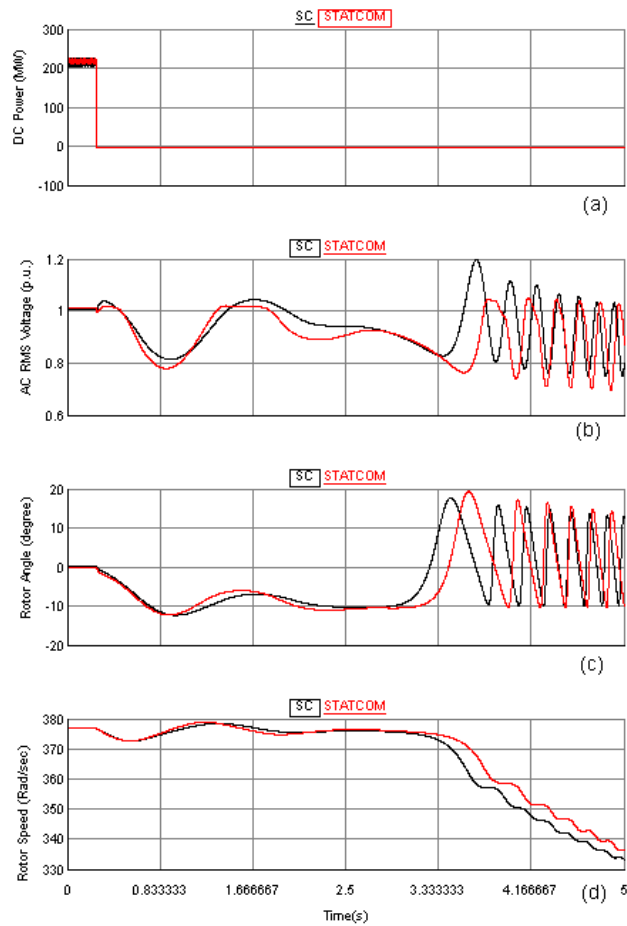


Figure 6. 11: DC Block with High Inertia

6.3.2.2 System Performance with Low System Inertia

6.3.2.2.1 Rectifier Side Three-Phase Fault

The low inertia situation can be modelled by setting the H constant of the generator to 3.0. Figure 6.12 shows the results when a 0.1 second three-phase fault occurred at the rectifier side. Figure 6.12(a) shows the STATCOM has better recovery of the DC power and the AC voltage. The DC experienced one more commutation failure with the SC. The oscillations of generator angle and speed are plotted in Figure 6.12(c) and (d), which show the SC brings about slightly smaller amplitude and higher damping.

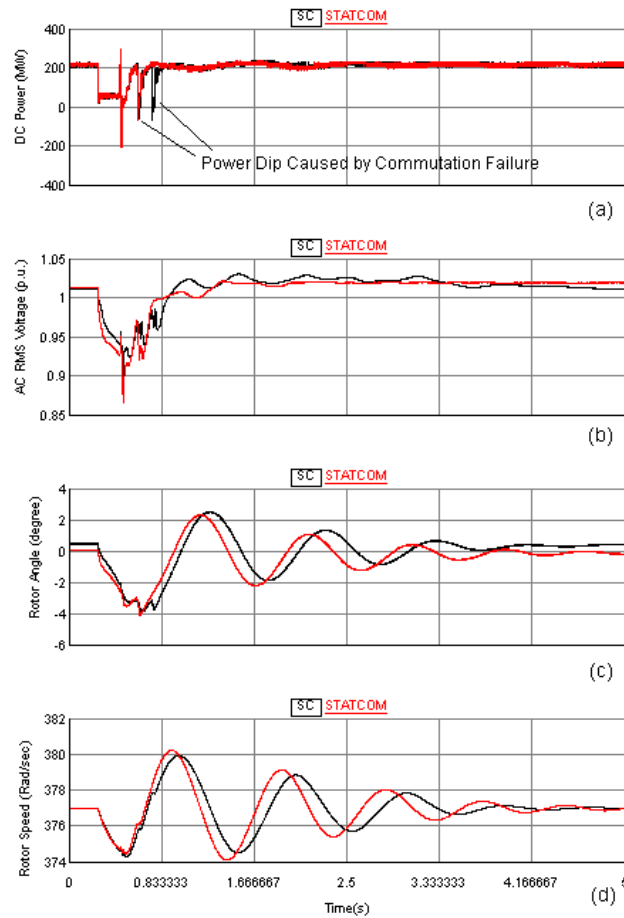


Figure 6.12: Rectifier Side Fault with Low Inertia

6.3.2.2.2 Inverter Side Close-in Three-Phase Fault

Figure 6.13 shows the results when a 0.1 second three-phase fault occurred at the inverter bus. A close-in three-phase fault is a severe disturbance. The SC demonstrated obviously better performance. Figure 6.13(a) shows the DC power recovers very successfully with the SC but fails to recover with the STATCOM. It is shown in Figure 6.13(a), that when the STATCOM was used, the DC system experienced repeated commutation failures and the DC power could not be stably restored. Due to the DC power interruptions, the generator oscillations increased and the system underwent dynamic instability, as shown in Figure 6.13(c) and (d). Figure 6.13 (a) and (b) demonstrate that the SC brought about a very fast recovery of the DC power and the AC voltage and that the oscillations of the generator speed and angle decays and system settled down to stable operation successfully, as shown in Figure 6.13(c) and (d). The results demonstrate two issues regarding stable operation of an AC/DC system with lower inertia. One issue is the interaction between the DC recovery and the generator oscillation. These processes affect each other: the DC recovery failure causes more power unbalance and tends to increase the generator oscillation, and the generator oscillation brings voltage fluctuation and causes more difficulties for DC recovery. The other issue the results demonstrate is that a severe fault tends to cause problems in an AC/DC system with lower inertia.

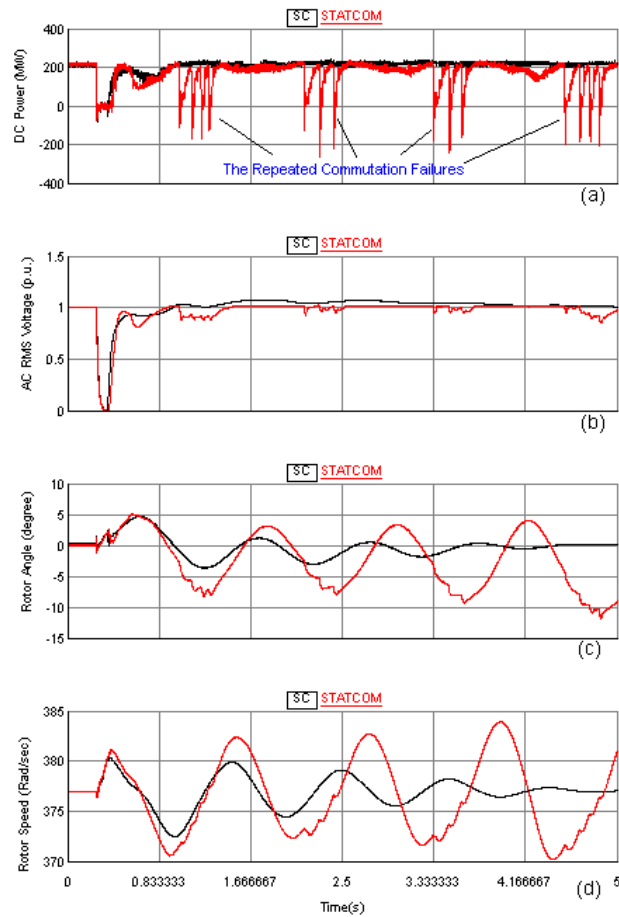


Figure 6.13: Inverter Side Close-in Fault with Low Inertia

The fault clearing time was changed and further studies were conducted. Figure 6.14 shows the results when the fault clearing time is 11 cycles. This is the critical clearing time when the SC is used. The results demonstrate that the SC can bring DC recovery from faults after several commutation failures. When a STATCOM is used, the generator becomes unstable at the first swing instead of experiencing gradually increased oscillation, as shown in Figure 6.14(c) and (d). Both Figure 6.13 and 6.14 reveal that the low inertia may become a problem when the system experiences severe disturbances.

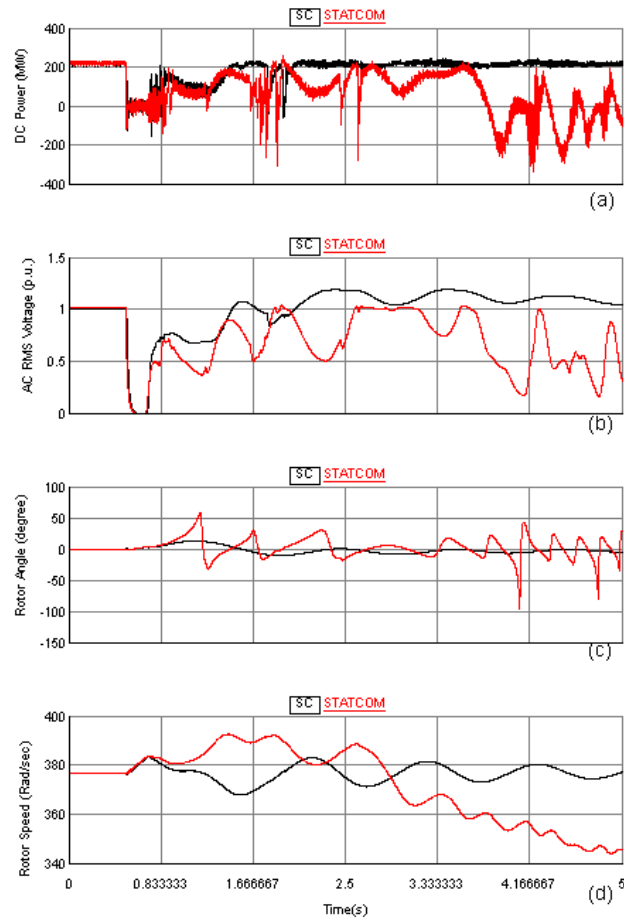


Figure 6. 14: Inverter Side Close-in Fault with Slow Clearing

6.3.2.2.3 Inverter Side Remote Three-Phase Fault

Figure 6.15 shows the results of a remote fault. The oscillation with the SC is a little smaller than it is with the STATCOM; however, both compensators work well during the disturbance. This is to be expected because the remote fault is very light, which does not cause any large impact on the DC and generator hundreds of kilometers away. The responses of generator angle and speed in Figure 6.15(c) and (d) still indicate that the SC has slightly better capability in reducing and damping the oscillations.

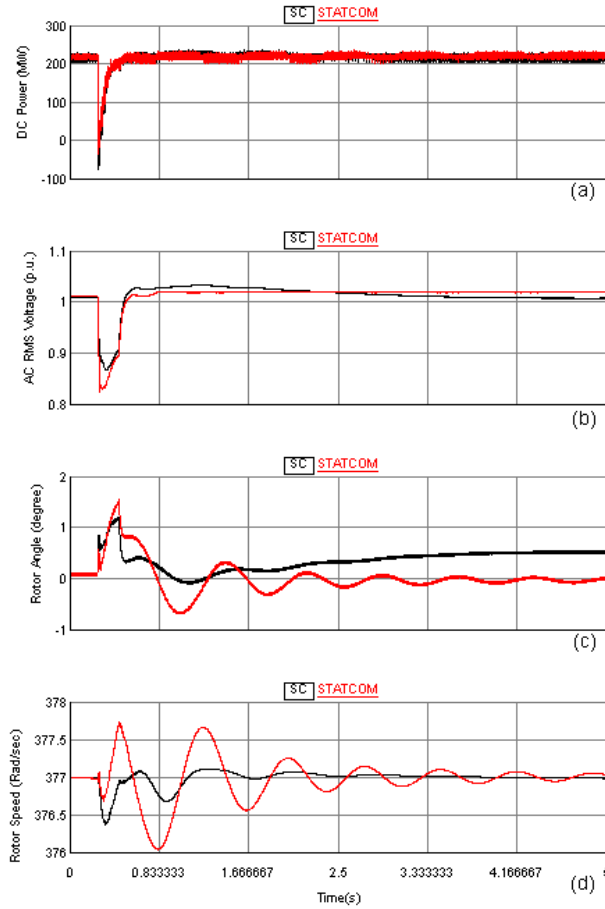


Figure 6. 15: Inverter Side Remote Fault with Low Inertia

6.3.2.2.4 DC Permanent Block

Figure 6.16 shows the inverter bus when the HVDC converters are blocked. The results are very similar to Figure 6.11. The generator becomes unstable due to the large power mismatch caused by the DC block. However, with the SC and the STATCOM, at least the TOV at the inverter bus is effectively controlled. Figure 6.16(c) demonstrates that the

STATCOM has greater capability to control the TOV than the SC, no matter what the inertia is.

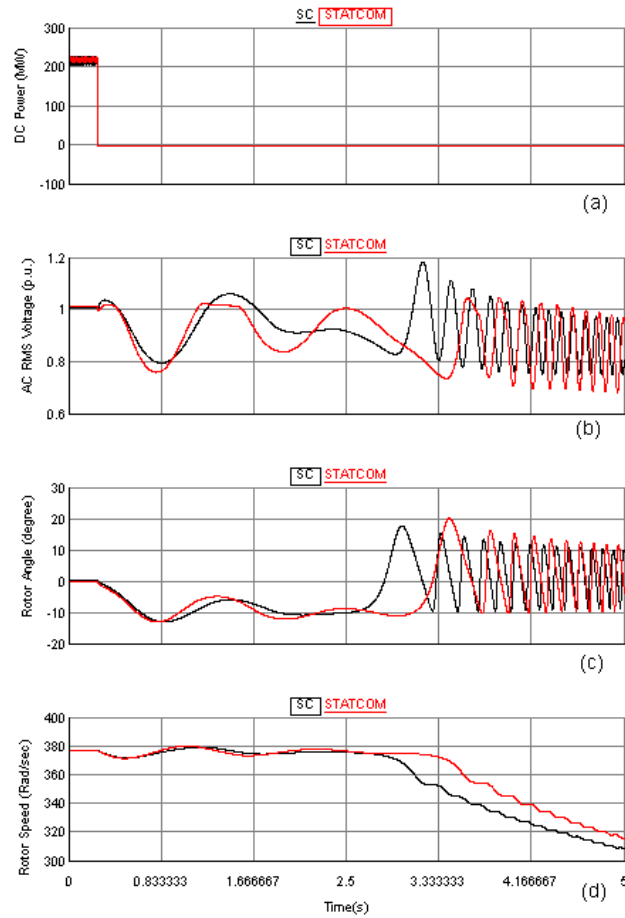


Figure 6.16: DC Block with Low Inertia

6.3.3 Discussion of the Simulation Results

6.3.3.1 Summary of the Simulation Results

The results in Figures 6.8 to 6.16 demonstrate the performances of the SC and the STATCOM during various disturbances for different system inertia levels. The results show that the STATCOM has better or equal performance than the SC for all

disturbances when the system inertia is high. When the system inertia is low, the STATCOM works well for most of the disturbances except the inverter close-in three-phase fault. This indicates the inertia can be critical for system stability during some severe disturbances.

The results also show that the STATCOM is significantly better than the SC in controlling the TOV during DC block even when the inertia is low. This can be explained by the faster response of the STATCOM. The STATCOM is based on fast-switching power electronics devices. It has much faster response during system disturbances. There is no doubt that the STATCOM is superior in fast voltage control.

6.3.3.2 Frequency Stability Versus Rotor Angle Stability

The research in this chapter was motivated by concerns regarding the effects of inertia on frequency stability. The concept of frequency stability refers to the ability of a power system to maintain its frequency after severe system upsets [63]. It is normally the significant imbalance between the generation and the load that causes the frequency instability. The frequency instability is likely caused by the power system being split into islands by faults and the power not being able to be balanced in certain islands. The solution to the frequency stability problem can be generation reserve and under-frequency load shedding [59], [60], [61], [62].

When the DC system is blocked, it may cause a significant power shortage for the inverter side. If the DC cannot be recovered, load shedding or reserve generation must be used to balance the power shortage and avoid frequency instability. The small amount of energy stored in the SC rotor is not likely having a significant impact on the frequency stability in such a situation. If the DC can be recovered, then it is a temporary DC block and the energy stored in the SC rotor may have an effect.

However, the frequency stability and the rotor angle stability are developing simultaneously at the moment of DC temporary block. The two processes interact with each other and may eventually lead to system collapse. In some cases, it is hard to distinguish whether the system instability is caused by a frequency stability problem or a rotor angle stability problem.

6.3.3.3 Power-Angle Characteristic of Inverter Side System

The power imbalance caused by dc block can be illustrated by the power-angle curve and the equal area criterion. In order to analyze the rotor angle stability and frequency stability of AC/DC power system, we derived the power-angle characteristic of the inverter side generator as follows.

The example circuit of the inverter side power system is shown as in Figure 6.17. It is a simplified system, which assumes only one generator is operating at the inverter side.

The generator and the HVDC together supply the power to the local load center, and connect the remote infinite system through a transmission line. It should be noted that system in Figure 6.17 is the simplest configuration for a power system in which the rotor dynamics can be represented.

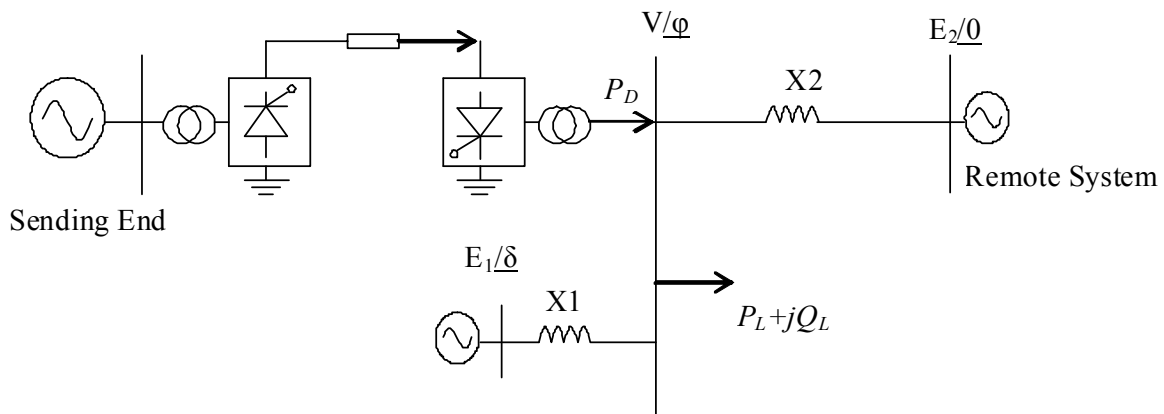


Figure 6.17 Inverter Side Power System

For simplicity, we assume the HVDC system filters and reactive compensation balance the reactive consumption of the converter station, so the reactive power exchange between the AC and HVDC at the inverter bus is zero at the normal operation condition. Assuming the voltage magnitudes of the generator bus and the infinite bus are given as E_1 and E_2 , and the impedances between the load center to generator and infinite bus are X_1 and X_2 respectively, the purpose now is to derive the formula of power output P_G of the local generator as a function of generator rotor angle δ with respect to the angle of the remote infinite bus as:

$$P_G = f(\delta) \quad (6-50)$$

P_G can be represented with the traditional power angle relationship as:

$$P_G = \frac{E_1 V}{X_1} \sin(\delta - \varphi) \quad (6-51)$$

In order to obtain equation (6-50), voltage magnitude V and angle φ of the load bus in equation (6-51) need to be eliminated. The following 2 load flow equations can be used to solve these 2 unknowns.

$$\frac{E_1 V}{X_1} \sin(\delta - \varphi) - \frac{V E_2}{X_2} \sin(\varphi) + P_D - P_L = 0 \quad (6-52)$$

$$\frac{E_1 V}{X_1} \cos(\delta - \varphi) - \frac{V^2}{X_1} - \left(\frac{V E_2}{X_2} \sin(\varphi) - \frac{V^2}{X_2} \right) - Q_L = 0 \quad (6-53)$$

In which P_D is the power supplied by the HVDC system and $P_L + jQ_L$ is the load connected to the load center bus. Unfortunately it is not possible to get a simple analytical solution of equations (6-52) and (6-53). However, we can use MathCAD to solve the equations and obtain the numerical solution of P-Angle characteristic curve. Assuming the parameters and operation conditions in Table 6.1, the P-delta curves when HVDC system is on and off are solved and demonstrated in Figure 6.18.

Table 6. 1 Parameters and Operation Conditions

	Value in Per Unit
P_D	0.6
P_L	1.0
Q_L	0.0
E_1	1.0
E_2	1.0
X_1	0.5
X_2	0.5

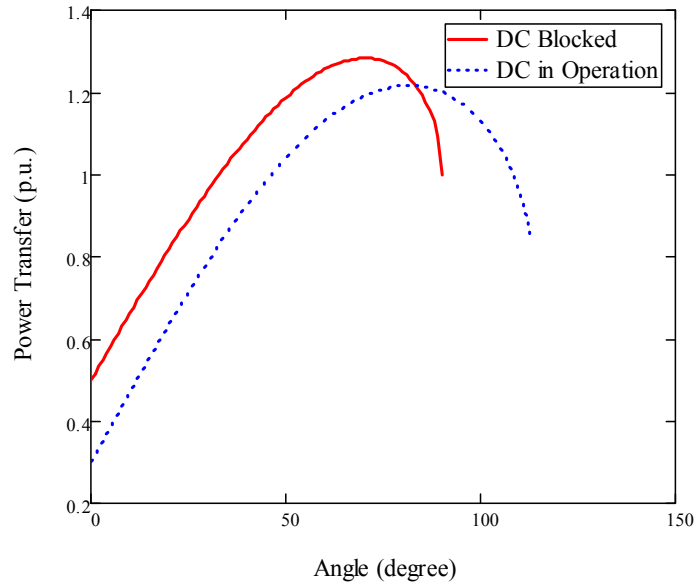


Figure 6.18 P-delta Characteristic of AC/DC Power Systems

Figure 6.18 shows that the P-delta curve is shifted up when the HVDC is blocked. This is because the power shortage caused by the HVDC blocking has to be shared by the remaining generators. In this case, the local generator and the remote infinite bus are taking the power mismatch together. At the moment of HVDC blocking, the electromagnetic torque imposed on the generator rotor will be larger than the mechanical torque, which will cause the deceleration of the generator.

It appears counterintuitive that even with power import from the inverter, the resulting P-Angle curve is below that with the inverter disconnected. This is because as the inverter import real power, it absorbs reactive power which reduces the commutating busbar voltage, thereby limiting the maximum power transfer to either the local machine (E_1/δ) or the remote system (E_2/δ) (see Figure 6.17).

6.3.3.4 Analysis of Rectifier Side Faults

Now let us use the derived P-delta characteristic curves and Equal Area Criterion to analyze the stability issues in the AC/DC system. Figure 6.19 and Figure 6.20 show the power-angle characteristics for rectifier side faults and inverter side faults, respectively. It is assumed there is only one generator at the inverter side, as in the system in Figure 6.17. This example system is useful to explain the concepts in spite of its simple configuration. In fact, the analysis below can also be extended to a multi-machine system by sharing the unbalance power due to a DC block among all the generators in the system. There are two P-delta curves in Figure 6.19 and Figure 6.20 that represent the power-angle curves when the DC is operating and when it is blocked.

Figure 6.19 shows the power angle curve of the generator at the inverter side when the DC is interrupted by a rectifier side fault. In Figure 6.19, the operating point jumps from A to B when the DC is blocked and the mechanical power is less than the electromagnetic power, so the angle starts to decrease from B to C. Then the DC recovers and the operating point jumps from C to D. The generator starts to accelerate and the angle will swing back. If the DC fails to recover, the power shortage cannot be balanced and the system will go toward frequency collapse. It can be noticed that the decelerating area is sufficient as even negative angle swings are possible to increase the decelerating area. So there is no risk of rotor angle stability for this type of fault. The concern here is that over-deceleration could cause frequency collapse. The risk of over-deceleration depends on the duration of the DC block. As long as the DC can recover before the frequency goes too

far and frequency instability occurs, the system will be safe. The effect of additional inertia here is the prevention of large frequency deviation in the inverter side system and the avoidance of unnecessary load shedding. Therefore, the risk of a DC temporary block due to a rectifier side fault is more likely to be frequency instability rather than rotor angle instability. Disturbances other than faults at the inverter side will have similar consequences.

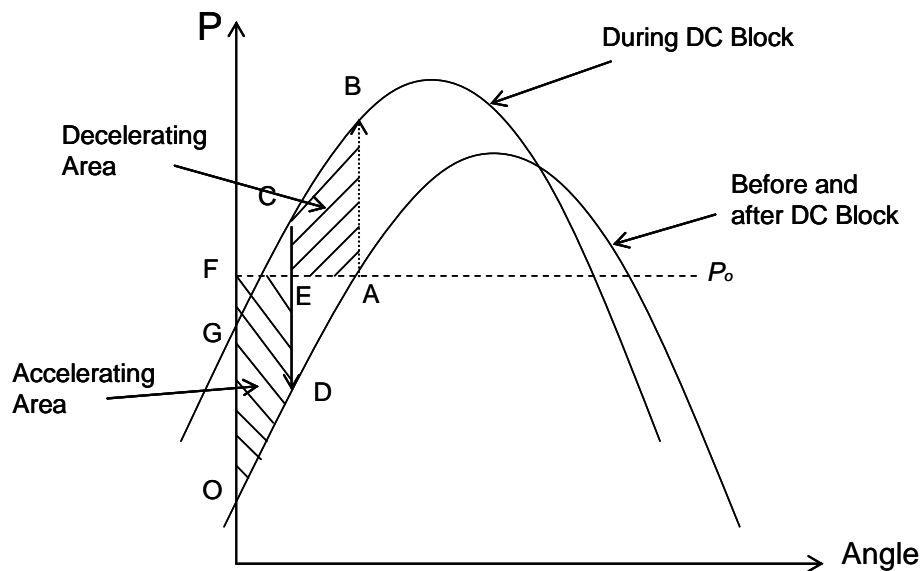


Figure 6. 19 Equal Area Criterion for a Sending End Fault

6.3.3.5 Analysis of Inverter Side Faults

An inverter side fault is a little different than a rectifier side fault. In Figure 6.20, the operating point jumps from A to B when the fault occurs and the DC is blocked. The first action of the generator is acceleration rather than deceleration during rectifier faults. This phenomenon can be verified by the simulation results in this chapter. Figures 6.8 to 6.16 show the rotor angle increased and then decreased following inverter side faults, but that it decreased and then increased following rectifier side faults. Then the generator will

rapidly move from B to C as no power can be sent out. At C, the fault is cleared but the DC is still blocked and the operating point will jump from C to E. The generator then starts to decelerate. At F, the DC recovers and the operating point jumps to J. If the decelerating area is sufficient, the system will settle down at a stable operating point. Otherwise, the operation point will pass G and then start to go to rotor angle instability. The rotor angle instability will certainly harm the DC recovery, and it may finally block the DC and result in system frequency collapse. However, the direct consequence of the inverter side fault is the risk of rotor angle instability. If the rotor angle is stable, as long as the DC can recover, the entire system will be stable. Therefore, inverter side faults can potentially cause rotor angle instability, which brings about frequency instability. The effects of SC inertia on system stability are to help to maintain the frequency, and as such, to improve rotor angle stability.

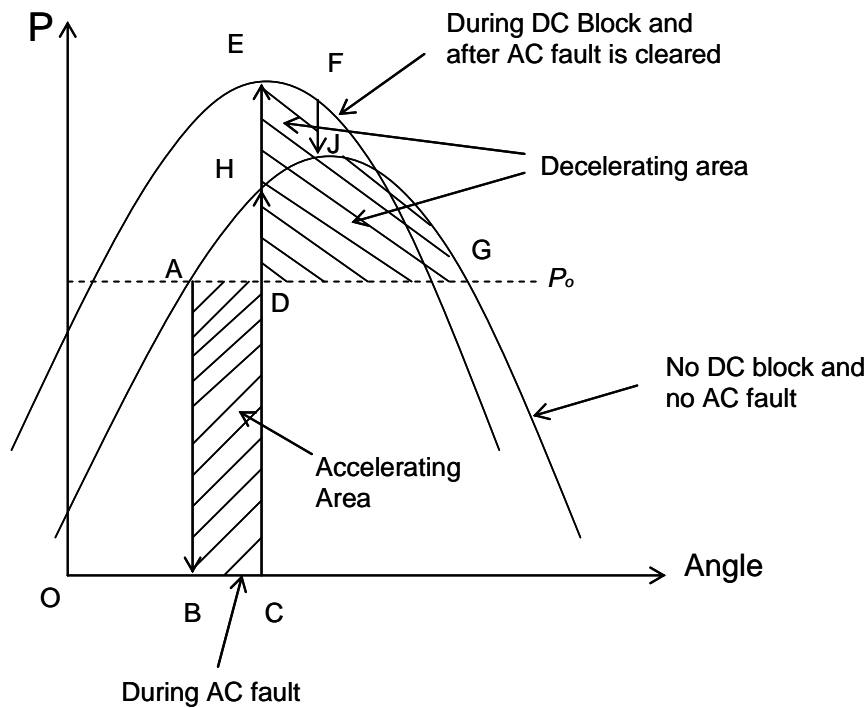


Figure 6. 20: Equal Area Criterion for a Receiving End Fault

6.4 Guideline on Considering Inertia in Designing Reactive Power Compensation

For frequency stability we can use the results obtained in Section 6.2 to examine the inertia of the entire power system and follow the procedure in Section 6.2.5 to choose the proper reactive power compensator for the HVDC system. If we assume K_p to be 20%, DC power interruption to be 0.3 seconds, and the permissive frequency excursion to be 5%, we can get the minimum required Effective Inertia Constant H_{dc} as:

$$H_{dc} = \frac{\Delta P_{dc}^* \cdot f_0 \cdot \Delta t}{2\Delta f} (1 + K_p) = \frac{1.0 \cdot 1.0 \cdot 0.3}{2 \cdot 0.05} (1 + K_p) = 3.6 \quad (6-54)$$

If the system inertia is lower than 3.6, it is recommended to use an SC to add some addition inertia.

However, equation (6-54) is a criterion only for frequency stability, which cannot guarantee rotor angle stability. In fact, equation (6-54) is derived with frequency deviation in mind. As discussed in the previous section, the lower inertia may also result in rotor angle stability rather than frequency stability following a fault. The interaction between generator rotor angle stability and DC recovery could be very complicated. The loss of stability could be either transient instability or dynamic stability. The simulation results in Figure 6.14 is more like a dynamic stability problem in which slowly diverging oscillations of the generator and repeated commutation failures of the HVDC system are developing and interacting simultaneously. Such a process could be highly nonlinear due to the repeated interruptions of the DC power by commutation failures. It would be an elegant solution if we could give an analytical estimation of the critical inertia as in

equation (6-54). Unfortunately, it seems to be impossible to get such a direct solution. In this example, we demonstrated that the dynamic instability occurred when the H_{dc} was 4.5, a value higher than the critical value of 3.6 required for frequency stability. It should be noted that the critical inertia of 3.6 presented in equation (6-54) can only be used for the purpose of addressing the frequency stability issue. In order to ensure the rotor angle stability, detailed simulation studies must be carried out when designing the reactive power compensators for an HVDC system.

6.5 Chapter Conclusions

The analytical and simulation studies in this chapter lead to the following conclusions:

- The effects of the inertia of SCs on power system frequency dynamics were analyzed and guidelines to select compensators were proposed.
- A simulation case was designed to demonstrate the stability problem in AC/DC power systems. Simulation studies were conducted to investigate the impact of SC inertia on power system stability.
- The simulation results showed the STATCOM has better performance than the SC in most cases, but only the SC can stabilize the system with a lower inertia during an inverter side close-in three phase fault. This indicates the inertia should be carefully considered in the design of reactive power compensation for HVDC converters.
- It is recommended that the procedure in Section 6.2.5 be followed to examine the system inertia and choose a proper reactive power compensator for HVDC systems.

- The investigation demonstrated that in a low inertia power system the frequency stability and the rotor angle stability interact with each other during the transients of DC blocking. For rectifier side faults, the frequency instability is likely happening before the rotor angle instability. For inverter side faults, the rotor angle instability develops before the frequency instability. The effect of additional inertia is the prevention of significant frequency excursion and the improvement of both frequency stability and rotor angle stability.
- The interaction between generator rotor angle stability and DC recovery could be very complicated. The critical inertia of 3.6 presented in (6-54) can only be used as a reference for frequency stability. The estimation of rotor angle stability requires detailed simulation studies.

This chapter made the following contributions:

- Investigated the impact of inertia on the dynamic behavior of the receiving end system. The studies showed that the inverter side system may lose stability during severe faults when the inertia of the system is low.
- The power angle curve of AC/DC power system is introduced and used to analyze the system stability for faults at rectifier side and inverter side. It explained that the rectifier side faults tend to cause frequency stability and the inverter side faults tend to cause rotor angle stability.
- Proposed a guideline to consider the inertia for designing dynamic reactive power compensations for HVDC systems.

Chapter 7: Conclusions and Future Work

This thesis systematically investigated reactive power compensation for HVDC systems using both steady state and transient analyses. The potential application of STATCOMs for reactive power compensation at HVDC terminals was demonstrated. The concept of system strength was expanded by proposing the new index of Apparent Short Circuits Ratio (ASCRI). The contribution of Synchronous Condenser and Static Synchronous Compensator to system strength was quantified by ASCRI. The impact of the inertia on reactive power compensator design was investigated.

7.1 The Main Contributions of This Thesis

The main contributions of this thesis are listed as following:

- The analytical relationship between the voltage stability maximum power transfer and the size of reactive power compensator in a simple ac transmission system was derived.
- In a simple ac power system, the impact of reactive power compensator inertia on system stability was revealed by EMT simulation. It was demonstrated that only the SC could help the motor to recovery from temporary islanding operation in case no other generators are available in the isolated power network.

- The reactive power requirement of the HVDC converter station as a function of ac bus voltage was derived.
- The algorithm to calculate the Maximum Power Curve (MPC) and Maximum Available Power (MAP) to including the contribution of dynamic reactive power compensation was developed and the validation of the proposed algorithm was performed by EMT simulation.
- The performance of the SC and the STATCOM in reducing commutation failure susceptibility of HVDC systems was compared based on EMT simulation study. The results showed that the capabilities of the SC and the STATCOM in preventing commutation failure are very similar.
- A new series of indices based on Apparent Short Circuits Ratio Increase (ASCRI) were proposed to quantify the system strength when dynamic reactive power compensators are connected to the converter bus. The contributions of SC and STATCOM to system strength were studied based on the new indices.
- The impact of inertia on the dynamic behavior of the receiving end system was investigated. The studies showed that the inverter side system may lose stability during severe faults when the inertia of the system is low.
- The power angle curve of AC/DC power system is introduced and used to analyze the system stability for faults at rectifier side and inverter side. It explained that the rectifier side faults tend to cause frequency stability and the inverter side faults tend to cause rotor angle stability.
- A guideline to consider the inertia for designing dynamic reactive power compensations for HVDC systems was proposed.

7.2 Conclusions

The conclusions of the thesis can be summarized as the following:

7.2.1 Comparison of Dynamic Reactive Power Compensators in Simple AC Systems

- The capability of reactive power compensation to enhance voltage stability in a simple system was examined. The work shows that maximum power on the PV curve will increase when reactive power compensation is installed. The relationship between the amount of reactive power compensation and the increase of maximum power was obtained.
- The impact of reactive power compensation upon angle stability was examined using analytical methods. By installing a reactive power compensator at the mid-point of a transmission line, the angle stability of the transmission system can be significantly improved. The analytical form of the power and angle equations that considers mid-point compensation was derived.
- The performances of reactive power compensators during transients in a simple AC system were studied using EMT simulation. The results showed that the STATCOM offers the best performance in most cases, however, only SC offers a successful recovery from temporary islanding operation.

7.2.2 Steady State Analysis of Reactive Power Compensations for HVDC systems

- Steady state analysis of reactive power compensation at an HVDC converter bus was conducted. The voltage dependences of the HVDC converters at various control modes were studied. An algorithm to calculate the maximum available power (MAP) when reactive power compensation was proposed.
- The voltage dependency of the HVDC converter was derived by analytical method. The results show how HVDC converters impact the AC system voltage stability as a dynamic load. The analysis shows that, considering the filters and capacitor, the total reactive power consumption increases and the converter station becomes more inductive as voltage drops. This is an unfavorable effect as far as voltage stability is concerned.
- An algorithm to calculate the MAP considering the reactive power compensation was developed and implemented in MATLAB. The algorithm can precisely represent the steady state behavior of a HVDC system including the reactive power compensator at the converter bus. The validation of the algorithm was conducted by EMT digital simulation.

7.2.3 Transient State Analysis of Reactive Power Compensations for HVDC systems

- The transient performances of reactive power compensation options for HVDC Systems were studied. The performances of an SC and a STATCOM were

intensively studied and compared based on EMT simulation on PSCAD. The simulation studies included detailed comparisons of three major transient performances: fault recovery time, Temporary Overvoltage (TOV), and Commutation Failure Immunity Index (CFII).

- The simulation results showed both the SC and the STATCOM could improve the performance of the HVDC system in the dc power recovery from faults and to avoid commutation failure. However, the performances of the two compensators are very close.
- Both compensators can effectively suppress the temporary overvoltage upon dc blocking. However, the STATCOM has significant better performance than the SC in TOV control.

7.2.4 The Concept of System Strength when Dynamic Reactive Power Compensators are connected to Converter Bus

- The problem of how to quantify the system strength when reactive compensators are connected to the converter bus was investigated. A new series of indices were developed based on Apparent Short Circuit Ratio Increase (ASCRI). The indices include the ASCRI-M based on MAP, ASCRI-C based on CFII, ASCRI-R based on fault recovery time, and ASCRI-T based on TOV.
- As examples, the SC and STATCOM were tested and further compared using the new indices. In further comparisons, the performances of the STATCOM and the SC are similar.

7.2.5 Consideration of Inertia for Design of Reactive Power Compensations

- The inertia and its impact on the frequency stability of an AC/DC system were discussed. The requirement of minimum effective inertia constant for frequency stability in multi-machine AC/DC power system was obtained. Analytical studies were conducted to show how to consider the system inertia when designing reactive power compensation for HVDC systems.
- A simulation case was set up to study the dynamic performance of reactive power compensators in HVDC systems. The case extended the existing research in modelling the inverter side AC system with more details by adding a generator and some dynamic loads in the inverter side system. Such a simulation case can be used to study the frequency deviation or angle swing of power systems when reactive power compensators are used.
- The effects of “inertia” were investigated by purposely changing the inertia of the receiving end system. It was demonstrated that STATCOMs are better than or equal to SCs in improving the performance of the entire AC/DC power system in most of the cases in which the inertia was sufficient or the fault was not very severe.
- The investigation also showed that the inverter side system may lose stability during severe faults when the inertia of the system is not sufficient. It was confirmed that an SC can help to stabilize the system in those low-inertia circumstances, while a STATCOM cannot. This finding indicates that the

inertia of the system should be considered when designing the reactive power compensation. The SC should be recommended if the inertia is not sufficient.

- The power angle curve of AC/DC power system was derived based on MATCAD, which explained the power mismatch and its sharing among generators when the HVDC system is blocked. With the proposed Power angle curves, the stability issues caused by various faults were analyzed with Equal Area Criterion. Based on this approach, it was found that the rectifier side faults tend to cause frequency stability and the inverter side faults tend to cause rotor angle stability.
- A guideline for designing dynamic reactive power compensation was proposed. It is recommended that a STATCOM be used when the inverter side system has sufficient inertia. When the system does not have sufficient inertia, an SC should be used to enhance the frequency stability and the rotor angle stability.

7.3 Future Work

The concept, methodologies and indices developed in this thesis have great potential to be applied in designing and analyzing reactive power compensations in AC/DC power systems. Based on the findings of this thesis, the following topics are recommended for further research.

1. Attempt to use STATCOM with energy storage to improve the performance of existing HVDC systems. As shown in this thesis, one drawback of a STATCOM is that it does not have the ability to supply or absorb real power. With the

addition energy storage, the STATCOM can supply real power as well as reactive power to support frequency and voltage of the AC/DC power system. A STATCOM with energy storage is hopeful to have the advantages of both an SC and a STATCOM. Therefore, it is potentially possible that it could provide superior performance. It would be interesting to see the exact performance of such a new device. The indices ASCRI can be applied to evaluate the contribution of STATCOM with energy storage to system strength.

2. The ASCRI can be used to evaluate the contributions to system strength by other reactive power compensators. The potential contribution to system strength by SVC, super conductor based synchronous condenser and UPFC can be evaluated based on ASCRI;
3. Renewable energy generations are becoming more and more popular in today's power system. The system inertia is likely reduced as the penetration level of renewable energy generations is increase. How to improve the frequency stability of a power system with large amount of renewable generations is becoming a concern for power system engineers. The concept and methodology about minimum system inertia and inertia compensation can be tried to analyze and resolve the frequency stability problem brought by the renewable energy generations.
4. This thesis focused on the reactive power compensation for HVDC systems. In real large power system, the HVDC links are normally embedded in a large ac network. The reactive power compensation and control of the entire power system

- need to be considered together. It would be interesting to investigate the reactive power coordination control for AC/DC power systems.
5. Voltage Source Inverter (VSC) based HVDC technology is becoming more and more popular today. The VSC HVDC converter station can regulate reactive power and voltage by itself. However, the frequency stability is still a problem if the system inertia is low. The problem will be more predominate if the VSC HVDC is used to supply power to an island system without other generation. It would be interesting to investigate whether the synchronous condenser needs be used to enhance the frequency stability in this circumstance.
 6. This thesis mainly investigates the performance of SC and STATCOM as reactive power compensation devices in HVDC systems. Further research can be done with similar methods to examine the performance of combinations of different reactive power compensation devices, such as 50% SVC and 50% STATCOM, or 50% fixed capacitor and 50% SC, etc. Together with the restriction of economic assessment, an optimal solution might be found with a proper combination of various reactive power compensators to achieve an optimal technical performance with minimum cost.
 7. The low frequency load shedding is the last possible countermeasure to prevent the power system frequency instability. In the case the system inertia is low, a predefined load shedding list can be created based on the agreement between the utility companies and customers, which is called as customer driven interruptive load shedding. As a future work, the coordination between the design of a

reactive power compensator and the customer driven interruptive load shedding can be studied to enhance the power system frequency stability.

REFERENCES

- [1] N. G. Hingorani., Laszio Gyugyi, “Understanding FACTS: Concept and Technology of Flexible AC Transmission Systems”, New York, 1999
- [2] P. Kundur, “Power System Stability and Control”, *McGraw-Hill, 1994*
- [3] T. J. Miller, “Reactive Power Control in Electric Systems”, John Wiley & Sons, Nov. 1982.
- [4] C. Taylor, “Power System Voltage Stability”, *McGraw-Hill, 1994*
- [5] “IEEE Guide for Planning DC Links Terminating at AC Locations Having Low Short – Circuit Capacities”, IEEE Std 1204-1997
- [6] P.C.S. Krishnayya, R.J. Piwko, et al, “DC Transmission Terminating at Low Short Circuit Ratio Location”, *IEEE Transactions on Power Delivery, Vol. 1, No. 3, July 1986, pp308-318.*
- [7] C. V. Thio, J. B. Davies, and K. L. Kent, "Commutation Failures in HVDC Transmission Systems", *IEEE Trans. Power Delivery, volume. 11, no. 2, April 1996.*
- [8] A. Gavrilovic,, “AC/DC System Strength As Indicated By Short Circuit Ratios”, *AC/DC Conference,1991*
- [9] C. Schauder and H. Mehta, “Vector Analysis and Control of Advanced Static Compensators”, *IEE Proc. –C, Vol. 140, No.4, July 1993, pp.299-306*
- [10] A.E. Hammad, “Comparing the Voltage Control Capabilities of Present and Guture Var Compensating Techniques in Transmission Systems”, *IEEE Trans. on Power Delivery, Vol.11, No. 1, January 1996, pp 475-484.*
- [11] E. Larsen, et al, “ Benefits of GTO-Based Compensation Systems For Electric Utility Applications”, *IEEE Trans. on Power Delivery, Vol 7, No. 4, Oct. 1992, pp 2056-2064*
- [12] S. Teleke, T. Abdulahovic, et al, “Dynamic Performance Comparison of Synchronous Condenser and SVC”, *IEEE Transactions on Power Delivery, Vol. 23, No. 3, July 2008, pp 1606-1612.*
- [13] S. Nyati, R. Atmuri, et al, “Comparison of Voltage Control Devices at HVDC Converter Stations Connected to Weak AC Systems”, *IEEE Transactions on Power Delivery, Vol. 3, No. 2, April 1988, pp 684-693.*
- [14] O.B. Nayak, A.M. Gole, et al, “Dynamic Performance of Static and Synchronous Compensators at An HVDC Inverter Bus in A Very Weak AC System”, *IEEE Transactions on Power Delivery, Vol. 9, No. 3, April 1994, pp 1350-1358.*
- [15] O.B. Nayak, “Dynamic Performance of Static and Synchronous Compensators at An HVDC Inverter Bus in A Very Weak AC System”, Ph.D. Thesis, The University of Manitoba, 1993.
- [16] R. W. Menzies and Y. Zhuang, “ Advanced Static Compensation Using A Multilevel GTO Thyristor Inverter”, *IEEE Transactions on Power Delivery, Vol. 10, No. 2, April 1995, pp. 732-738.*
- [17] Y. Zhuang, R.W. Menzies, et al. “Dynamic Performance of A STATCON At The HVDC Inverter Feeding A Very Weak AC System”, *IEEE Transactions on Power Delivery, Vol. 11, No. 2, April 1996, pp958-964.*

- [18] Y. Zhuang, "Investigation of The Multilevel GTO Inverter as An Advanced Static Compensator", Ph.D. Thesis, The University of Manitoba, 1996.
- [19] HVDC Handbook, EPRI USA
- [20] C.V. Thio and J.B. Davies, "New Synchronous Compensators For The Nelson River HVDC System – Planning Requirements and Specification", *IEEE Transactions on Power Delivery*, Vol. 6, No. 2, April 1991, pp922-928.
- [21] I. T. Fernando, K. L. Kent, et al, "Parameters For Panning And Evaluation of Multi-Infeed HVdc Schemes", *Cigre OSAKA 2007*, pp326-339.
- [22] O.B. Nayak, A.m. Gole, et al, "Steady State Stability of HVDC Systems", *IEEE Transactions on Power Delivery*, Vol. 10, No. 4, October 1995, pp 2054-2060.
- [23] The IEEE Special Stability Controls Working Group and The Dynamic Performance and Modeling of DC Systems Joint Working Group, "HVDC Controls for System Dynamic Performance", *IEEE Transaction on Power Systems*, Vol. 6, No. 2, May 1991, pp743-752.
- [24] H.H. Happ and K.A. Wirgau, "Static and Dynamic Var Compensation in System Planning", *IEEE Transactions on Power Apparatus and Systems*, Vol. PAS 97, No. 5, Sept/Oct 1978, pp1564-1578.
- [25] D. H. A. Lee, G. Andersson, "Impact of Dynamic System Modelling on The Power System Stability of HVDC Systems", *IEEE Transactions on Power Delivery*, Vol. 14, No. 4, October 1999, pp 1427-1437.
- [26] D. H. A. Lee, G. Andersson, "Nonlinear Dynamics In HVDC Systems", *IEEE Transactions on Power Delivery*, Vol. 14, No. 4, October 1999, pp 1417-1436.
- [27] D. H. A. Lee, G. Andersson, "Influence of Load Characteristics on The Power/Voltage Stability of HVDC Systems", *IEEE Transactions on Power Delivery*, Vol. 13, No. 4, October 1998, pp 1437-1444.
- [28] C. A. Cañizares, M. Pozzi, S. Corsi, and E. Uzunovic, "STATCOM Modeling for Voltage and Angle Stability Studies," *International Journal of Electrical Power & Energy Systems*, Vol. 25, No. 6, June 2003, pp. 431-441.
- [29] N. Mithulananthan, C. A. Cañizares, J. Reeve, and G. J. Rogers, "Comparison of PSSS, SVC and STATCOM Controllers for Damping Power System Oscillations," *IEEE Transactions on Power Systems*, Vol. 18, No. 2, May 2003, pp. 786-792.
- [30] C. A. Cañizares and Z. T. Faur, "Analysis of SVC and TCSC Controllers in Voltage Collapse," *IEEE Transactions on Power Systems*, Vol. 14, No. 1, February 1999, pp. 158-165.
- [31] C. A. Cañizares, "Conditions for Saddle-Node Bifurcations in AC/DC Power Systems," *International Journal of Electrical Power & Energy Systems*, Vol. 17, No. 1, 1995, pp. 61-68.
- [32] C. A. Cañizares and F. L. Alvarado, "Point of Collapse and Continuation Methods for Large AC/DC Systems," *IEEE Transactions on Power Systems*, Vol. 8, No. 1, February 1993, pp. 1-8.
- [33] C. A. Cañizares, F. L. Alvarado, C. L. DeMarco, I. Dobson, and W. F. Long, "Point of Collapse Methods Applied to AC/DC Power Systems," *IEEE Transactions on Power Systems*, Vol. 7, No. 2, May 1992, pp. 673-683.

- [34] X.R. Xie, Q. R. Jiang, "The Theory and Application of FACTS", Tsinghua University Publish House, 2005, Beijing.
- [35] R.W. Menzies, "Static Compensation", Course Notes, The University of Manitoba, 2002.
- [36] A.M. Gole, "HVDC Transmission I", Course Notes, The University of Manitoba, 2002.
- [37] D.A. Woodford, "HVDC Transmission", Notes, Manitoba HVDC Research Centre, 1998.
- [38] J.D. Ainsworth, A. Gavrilovic, et al, "Static and Synchronous Compensators for HVDC Transmission Converters Connected Weak AC Systems", CIGRE
- [39] J. Reeve and E. Uzunovic, "Study of Power Transfer Capability of DC Systems Incorporating AC Loads and A Parallel AC Line", IEEE Transactions on Power Delivery, Vol. 12, No. 1, January 1997, pp426-434.
- [40] A.E. Hammad, "Stability and Control of HVDC and AC Transmissions in Parallel", IEEE Transactions on Power Delivery, Vol. 14, No. 4, November 1999, pp1545-1554.
- [41] A.E. Hammad, J. Gagnon, et al, "Improving The Dynamic Performance of A Complex AC/DC System by HVDC Control Modification", IEEE Transactions on Power Delivery, Vol. 5, No. 4, November 1990, pp1934-1943.
- [42] A.E. Hammad, M. Z. El-Sadek, "Prevention of Transient Voltage Instabilities due to Induction Motor Loads By Static Var Compensators", IEEE Transactions on Power Systems, Vol. 4, No. 3, August 1989, pp1182-1190.
- [43] A.E. Hammad, W. Kuhn, "A Computation Algorithm for Assessing Voltage Stability at AC/DC Interactions", IEEE Transactions on Power Systems, Vol. 1, No. 1, February 1986, pp209-215.
- [44] "On Voltage and Power Stability in AC/DC Systems", Final Report, CIGRE WG14.05, June 13, 2002.
- [45] Sladiana Elez, "Power Voltage Instability in An HVDC Link Connected to A Weak AC System", Thesis of Master of Science, The University of Manitoba, May 1996.
- [46] G. Andersson, G. Liss, "Improving Voltage Stability in Power Systems with HVDC Converters", IEE International Conference on Advances in Power System Control, Operation and Management, November 1991, Hong Kong, pp698-703.
- [47] T. Smed, G. Andersson, et al, "A New Approach to AC/DC Power Flow", IEEE Transactions on Power Systems, Vol. 6, No. 3, August 1991, pp1238-1244.
- [48] T. Smed, G. Andersson, "Utilising HVDC to Damp Power Oscillation", IEEE Transactions on Power Delivery, Vol. 8, No. 2, April 1993, pp620-627.
- [49] B. Franken, G. Andersson, "Analysis of HVDC Converters Connected to Weak AC Systems", IEEE Transactions on Power Systems, Vol. 5, No. 1, February 1990, pp235-242.
- [50] S.R. Aumuri, J. Chand, et al, "Evaluating Interaction Between High Speed Power System Controllers", IEEE WESCANEX '95 Proceedings, pp270-275.
- [51] L.X. Bui, V.K. Sood, et al, "Dynamic Interactions Between HVDC Systems Connected to AC Buses", IEEE Transactions on Power Delivery, Vol. 6, No. 1, January 1991, pp223-229.
- [52] E. Rahimi, S. Filizadeh, A.M. Gole, "Commutation Failure Analysis in HVDC Systems Using Advanced Multiple-Run Method", IPST'05, Montreal, Canada, June 2005, Paper No. IPST05-160

- [53] E. Rahimi, A.M. Gole, J.B. Davis, I.T. Fernando and K. L. Kent, "Commutation Failure Analysis in Multi-infeed HVDC Systems", IEEE Transactions on Power Delivery, Vol. 26, No. 1, January 2011, pp378-384.
- [54] M. Szechtman, et al, "First Benchmark Model for HVDC Control Studies", Electra, Vol. 135, April 1991, pp 55-73.
- [55] E. W. Kimbark, "Direct Current Transmission", Volume1, John Wiley & Sons, 1971.
- [56] J. Dixon, L. Moran, J. Rodriguex and R. Domke, "Reactive Power Compensation Technologies: State-of-the-Art Review", Proceeding of the IEEE, Vol. 93, No. 12, December 2005, pp2144-2164.
- [57] L. A. S Pilotto, M. Szechtman and A. E. Hammad, "Transient AC Voltage Related Phenomena for HVDC Schemes Connected to Weak AC Systems", IEEE Transactions on Power Delivery, Vol. 7, No. 3, July 1992, pp1396-1404.
- [58] R. Adapa and J. Reeve, "A New Approach to Dynamic Analysis of AC Network Incorporating Detailing of DC Systems. Part II: Applications to Interaction of DC and Weak AC Systems", IEEE Transactions on Power Delivery, Vol. 3, No. 4, July 1988, pp2012-2019.
- [59] Y. Han, Y. Min, S. Hong, "A Co-Frequency Dynamic Equivalence Method for Power-Frequency Dynamics Simulation in Multi-Machine Power Systems", IEE International Conference on Advances in Power System Control, Operation and Management, November 1991, Hong Kong, pp877-882.
- [60] Y. Min, Y. Han, "A Co-Frequency Dynamic Equivalence Approach for Calculation of Power System Frequency Dynamics", The Proceedings of CSEE, Vol. 11, No. 2, March 1991, pp29-36
- [61] Y. Min, S. Hong, Y. Han, Y. Gao and Y. Wang, "Analysis of Power-Frequency Dynamics and Designing of Under Frequency Load Shedding Scheme in Large Scale Multi-Machine Power Systems", IEE International Conference on Advances in Power System Control, Operation and Management, November 1991, Hong Kong, pp871-876.
- [62] Z. Han, "Power System Stability", China Electric Power Publish House, Beijing 1995.
- [63] IEEE/CIGRE Joint Task Force on Stability Terms and Definitions, "Definition and Classification of Power System Stability", IEEE Transactions on Power Systems, Vol. 19, No. 2, May 2004, pp 1387-1401.
- [64] A. M. Gole, V. K. Sood, "A Static Compensator Model for Use with Electromagnetic Transients Simulation Programs", IEEE Transactions on Power Delivery, Vol. 5, No. 3, July 1990, pp1398-1407.